OPTIMAL VERTICAL PLANE BOOSTER GUIDANCE INCLUDING PITCH DYNAMICS

by

William Michael Waldron

Dissertation submitted to the Faculty of the
Virginia Polytechnic Institute and State University
in partial fulfillment of the requirements for the degree of

DOCTOR OF PHILOSOPHY

in

Aerospace Engineering

APPROVED:

E. M. Cliff, Chairman

F. H. Lutze

W. C. Durham

M. R. Anderson

H. H. Robertshaw

April, 1996

Blacksburg, Virginia

Key Words: Optimization, Singular Perturbation, Trajectory

OPTIMAL VERTICAL PLANE BOOSTER GUIDANCE INCLUDING PITCH DYNAMICS

by

William Michael Waldron

Committee Chairman: Eugene M. Cliff

Aerospace Engineering

(ABSTRACT)

The problem of vertical plane booster guidance including pitch dynamics for a two stage launch vehicle is investigated using Singular Perturbation Theory and Neighboring Optimal Control. In this investigation a point mass model is extended to include the rotational dynamics through the ideas of Singular Perturbation Theory. The equations of motion of the vehicle are formulated in a manner such that the singular perturbation parameter arises naturally from the problem and is not forced into the equations. Once an optimal solution to a point mass model is obtained, corrections are added which encompass the rotational dynamics of the vehicle and provide an inner-loop feedback control structure. Neighboring Optimal Control is then used to obtain an outer-loop guidance law to meet the prescribed terminal conditions. Results are presented for the point mass model and feedback law trajectories. The singular perturbation parameter is then varied to show its effect on the feedback solutions.

ACKNOWLEDGMENTS

I wish to acknowledge and thank my advisor Dr. Eugene Cliff for his support, guidance, and patience which allowed me to complete this work. I would also like to thank Drs. Lutze, Durham, Anderson, and Robertshaw for serving on my examination committee.

I also wish to acknowledge my numerous teachers, professors, and coworkers who, over the years, enabled me to increase my knowledge of science and engineering and thus undertake this endeavor.

Most of all I would like to thank my family and friends who gave their support and encouragement. I especially would like to thank my wife and daughter, who have made numerous sacrifices in their lives to allow me the time to work on my research.

TABLE OF CONTENTS

1.0 INTRODUCTION

Motivation

Artificial satellites have been in use for forty years, yet the process of getting a payload into orbit takes an enormous amount of fuel and is still very expensive. Efficient guidance is crucial in aeronautical problems in general but especially so in orbit insertion problems. For a typical launch vehicle, a savings of just one percent in fuel may lead to a doubling of the allowable payload mass. This importance of efficient guidance is the motivation for this work.

Historical Background

The history of optimization of rocket trajectories can be traced back to the Goddard problem. This problem, posed by Goddard in 1919[1], involves finding the thrust profile to maximize the final attitude of a sounding rocket. Only vertical motion is considered and the forces include an inverse squared gravitational field, atmospheric drag and propulsive thrust. With the development of optimal control theory it was shown by Tsien and Evans[2] that the optimal thrust profile consisted of a full thrust or boost phase, a sustain phase, and a zero thrust or coast phase of flight. The sustain phase called a singular arc results from the control, thrust, appearing linearly in the equations of motion. Variations of this problem have been studied, such as the investigation of constraining the time of flight and the effect of variations in the drag law by Tsiotras and Kelley[2,3], and the investigation of a dynamic pressure limit by Seywald and Cliff[1].

In 1952, Hibbs formulated as a problem in variational calculus, the complementary problem, that of horizontal flight of a missile.[4] In this problem, an optimal control formulation was used to obtain the thrust profile to achieve either maximum range or the maximum velocity at a given range. Hibbs reported that to obtain maximum range the

optimum profile was an impulsive burn, sustain phase, and coast phase. The vehicle vertical and rotational degrees of freedom were not considered and the vehicle lift was set equal to the weight to keep the altitude constant. In 1956, Cicala and Miele, extended the horizontal flight problem to remove restrictions imposed by Hibbs on the shape of the drag polar and imposed limits on the burn rate of the fuel and the maximum lift coefficient.[5]

The next logical step was to combine the vertical and horizontal flight problems into that of a two-dimensional problem in the vertical plane. An example of vertical plane optimization is given by Bryson and Ross.[6] In this example, a point mass model is used to determine the thrust profile which will propel a rocket to a specified location using the least amount of fuel. Bryson and Ross used a flat earth model with constant gravitational acceleration, a general drag law, zero aerodynamic lift and the thrust aligned with the flight path angle. The results obtained showed an initial impulse burn followed by a sustain phase and then a coast phase to the terminal point. Another example of vertical plane optimization can be found in Bryson and Ho[7] where the thrust angle is now the control. This problem is modeled with a constant gravitational acceleration and exoatmospheric conditions. With the thrust given to produce a constant acceleration, the optimal control law obtained is referred to as the "bilinear tangent law" which is still used in exoatmospheric applications.

We wish to build on the vertical plane problem with the inclusion of pitch dynamics. Cliff[8] used a singular perturbation approach to include the pitch dynamics and develop a pitch-loop controller for exoatmospheric flight over a flat Earth with constant gravitational acceleration. Bushong[9] investigated a problem similar to that which will be presented in this dissertation. Bushong used two different vehicles, an exoatmospheric missile and a horizontal takeoff single stage to orbit vehicle, as examples for his vertical plane analysis. A singular perturbation approach was used to develop the pitch-loop

controller while linear quadratic regulator techniques were used to provide path guidance. Both Cliff and Bushong imposed a singular perturbation parameter in order to obtain order reduction in the problem.

This investigation will extend the previous work to that of a vertical takeoff two stage vehicle in an inverse squared gravitation field using a round Earth model. The system equations will be formulated in a manner such that the singular perturbation parameter will arise naturally to obtain order reduction. With a two stage vehicle, the pitch dynamics about staging will also be investigated. The path guidance will be obtained using neighboring optimal control. The application of these techniques will provide more accurate analysis than provided by a point mass model.

Organization of Dissertation

In this dissertation it will be shown how Singular Perturbation Theory and Neighboring Optimal Control can be used to obtain an optimal reference trajectory of a reduced order problem and calculate control gains which account for the rigid body dynamics of the vehicle. Using the calculated control gains, near-optimal trajectories can be simulated which include the vehicle rigid body dynamics. These trajectories can be used in performance studies and sensitivity analysis.

In Chapter 2, a description of the optimization problem will be given. A mathematical description will be presented which models the launch vehicle and the boundary conditions for the problem. A brief discussion will also be presented on methods of obtaining a solution to the optimization problem.

Chapter 3 is used to introduce the use of Singular Perturbation Theory and the ideas of differing time scales within the system dynamics. The system equations are then normalized based on the different time scales. From this normalization a singular

perturbation parameter is derived which will be used to obtain a reduced order, point mass model, from the full model which includes pitch dynamics. Next the necessary conditions for optimality are presented for the point mass model. These necessary conditions are then applied to our example problem and obtaining a solution is discussed. In Chapter 4, the solution to this reduced order, point mass model, is presented.

Chapter 5 begins the process of incorporating the pitch dynamics into the reference trajectory. The terms "outer" and "inner" problem are introduced and corrections to the point mass model are discussed using the singular perturbation idea of *stretched time*. A method of calculating feedback gains for the inner loop, or pitch dynamics, is presented based on stability of the linearized inner problem. Using the calculated feedback gains boundary layer corrections are presented which account for the pitch dynamics of the vehicle.

The ideas of neighboring optimal control are introduced in Chapter 6. A method is presented to calculate an outer loop, or guidance, feedback structure to account for perturbations in the trajectory in a near optimal manner. The neighboring optimal control gains are calculated and presented.

Chapter 7 begins by summarizing the control structure formulated in Chapters 5 and 6. The implementation of this control structure is then discussed and the resulting feedback trajectory is compared with that obtained from the point mass model. Next the effects of perturbations in the initial conditions are presented. The angle of attack at staging constraint, which is lost in the point mass model, is imposed to investigate the effects of pitch dynamics on the trajectory. The singular perturbation parameter is then varied by changing the pitch moment of inertia of the vehicle to investigate its effect on the resulting pitch dynamics and the comparison between the feedback trajectory and the point mass model solution.

Chapter 8 then presents some conclusions and discussed some possible areas of future work.

2.0 DESCRIPTION OF OPTIMIZATION PROBLEM

Orbital insertion problems are commonly studied with a mathematical model that describes the translational motion of the booster's center of mass, a so-called point mass model. Our primary goal is to extend the analysis to account for the rotational motions, at least approximately. The mathematical model is extended so that the point mass model can be readily distilled from it. The resulting optimal control problem is analyzed using Singular Perturbation Theory to account for the rotational dynamics. We combine the Singular Perturbation analysis with ideas of Neighboring Optimal Control to produce a feedback implementation.

In order to illustrate these ideas an orbital insertion example problem will be used. This example will investigate the launch trajectory of a vehicle into a specified orbit with the goal of using the least amount of fuel. The vehicle modeled is patterned after vehicles designed for NASA's Advanced Launch System (ALS) program.[10] This vehicle is a two stage vehicle using solid rocket boosters during the first stage of flight with the vehicle core continuing for the second stage. In order to simplify the dynamics a non-rotating spherical Earth model is used. A pitch plane model can then be used to represent a vehicle launch in the direction of the desired orbit. This simplification allows the optimization techniques to be illustrated without an excessively complex model.

2.1 Mathematical Description

In order to express the problem mathematically, variables must be defined that describe the vehicle and its trajectory. The first variables that must be defined are the state variables as listed in Table 2.1 and illustrated in Figure 2.1

Table 2.1 State Variable Definitions

variable	definition
r	distance from the center of the Earth to vehicle center of mass
ϕ	downrange angle
V	velocity magnitude of the vehicle
γ	velocity path angle measured from local horizontal
m	vehicle mass
θ	vehicle pitch angle measured from local horizontal
q	vehicle inertial pitch rate

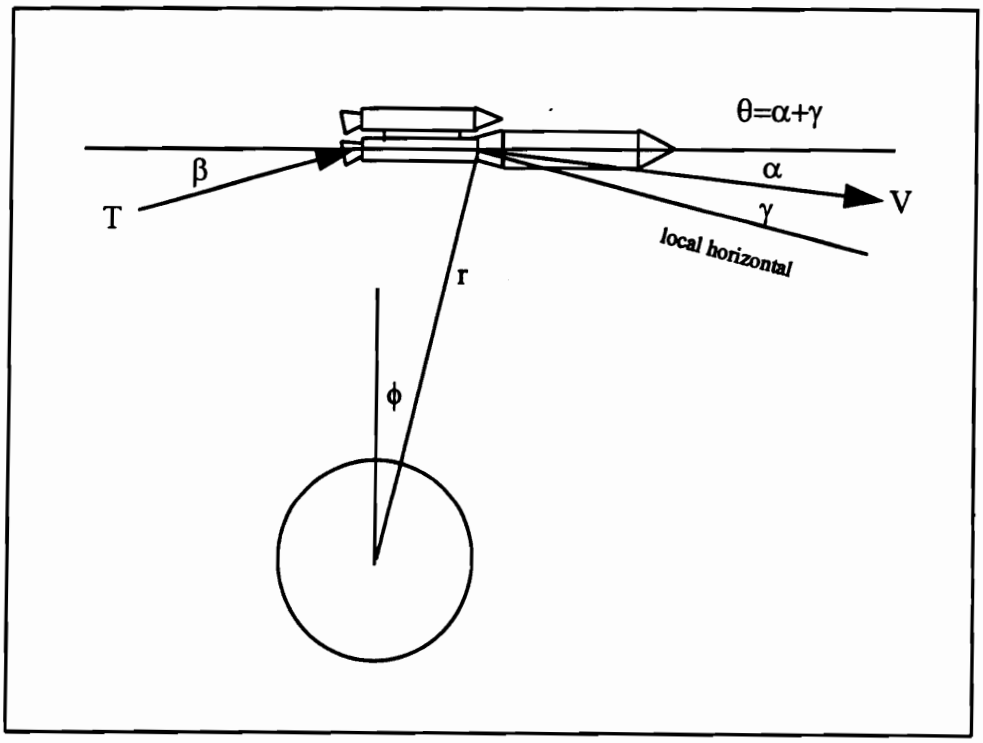

Figure 2.1: Illustration of State Variables

The vehicle is controlled by directing its thrust at an angle relative to the body axis of the vehicle. The thrust is produced by ten engines during the first stage of flight and three engines after staging. Each engine is modeled as having identical vacuum thrust which is

a function of altitude only. Note that the engines are not throttled during flight. The control variable, β, is the angle that the total thrust vector makes with the vehicle body axis defined such that a positive β causes a nose down or negative pitch acceleration, $\dot{q}$.

State Differential Equations

The dynamic system that describes the launch vehicle can be expressed as;

$$\dot{x} = f(x, u, t)$$

where x represents the state variables, u represents the control variables, and f is an expression of the equations of motion. The dynamic system equations for this problem are given by Equation 2.1.

$$\frac{dr}{dt} = V \cdot \sin\gamma \tag{2.1a}$$

$$\frac{d\phi}{dt} = \frac{V \cdot \cos\gamma}{r} \tag{2.1b}$$

$$\frac{dv}{dt} = \frac{T \cdot \cos(\theta - \gamma + \beta) - D}{m} - g \cdot \sin\gamma \tag{2.1c}$$

$$\frac{d\gamma}{dt} = \frac{T \cdot \sin(\theta - \gamma + \beta) + L}{m \cdot V} + \left(\frac{V}{r} - \frac{g}{V}\right) \cdot \cos\gamma \tag{2.1d}$$

$$\frac{dm}{dt} = -\frac{T_{vac}}{c} \tag{2.1e}$$

$$\frac{d\theta}{dt} = q + \frac{V \cdot \cos\gamma}{r} \tag{2.1f}$$

$$\frac{dq}{dt} = \frac{M - T \cdot \ell \cdot \sin\beta}{I_{yy}} \tag{2.1g}$$

The variables D, L, and M represent the aerodynamic drag, lift, and pitching moment on the vehicle and are based on NASA data for the Advanced Launch System.[10,11] These aerodynamic forces and moments are expressed by the relations.

$$L = \bar{q} \cdot S \cdot C_L(M,\alpha)$$

$$D = \bar{q} \cdot S \cdot C_D(M,\alpha)$$

$$M = \bar{q} \cdot S \cdot \bar{c} \cdot C_M(M,\alpha)$$

The dynamic pressure, $\bar{q}$, is a function of atmospheric density and velocity, and S and $\bar{c}$ are geometric parameters of the vehicle. The aerodynamic coefficients C_L, C_D, C_M are provided by a surface fit of tabular data given as a function of Mach number, M, and angle of attack, α. The variable T_{vac} is the thrust of the vehicle engines under vacuum conditions. Each engine is modeled as having a constant vacuum-thrust of 2,585,880 N. The variable c is the engine exhaust velocity with respect to the body, c = 4217 m/s and ℓ is the moment arm from point where the net thrust acts on the vehicle to the vehicle center of mass. Appendix A provides details on the atmospheric, aerodynamic, and engine models used in this problem.

The acceleration due to gravity term, g, follows an inverse squared gravitational law such that $g = g_0 \cdot \left(\frac{Re}{r}\right)^2$ where g_0 is the acceleration due to gravity at a distance from the center of the Earth equal to the radius of the Earth, Re. For this example, $g_0 = 9.807\ m/s^2$ and Re = 6,377,940 m.

The vehicle pitch moment of inertia, I_{yy}, is modeled as a linear function of the vehicle mass;

$$I_{yy} = A \cdot \frac{m}{m_t} + B$$

where m is the instantaneous mass, m_t is the total mass with a full fuel load and

$$A = 5.47844 \times 10^8\ kg \cdot m^2$$

$$B = 2.62200 \times 10^6\ kg \cdot m^2$$

The instantaneous mass should not decrease to zero since the vehicle is comprised of a physical structure in addition to the fuel.

Initial Conditions

The initial conditions, x_o, for the state variables are known at the time t_0.

$$r_o = 6{,}378{,}833 \text{ m}$$

$$\phi_o = 0.0 \text{ degrees}$$

$$V_o = 118.63 \text{ m/s}$$

$$\gamma_o = 78.0 \text{ degrees}$$

$$m_o = 1{,}569{,}340.69 \text{ kg}$$

$$\theta_o = 78.0 \text{ degrees}$$

$$q_o = -\frac{V_o \cdot \cos\gamma_o}{r_o} \cong 3.866626369 \times 10^{-6} \text{ rad/s}$$

The initial condition corresponds to a vehicle that has just left the launch pad. Starting the model shortly after the vehicle has left the pad avoids the singularity in the differential equation for the state variable γ when the velocity is zero.

Staging Conditions

Information on the vehicle staging is also known. For this investigation, vehicle staging is a function of mass only. When the vehicle reaches a known mass, m_s^-, part of the first stage separates resulting in a change in mass of Δm_s and a reduction in the number of engines from ten to three.

$$m_s^- = 936{,}518 \text{ kg}$$

$$\Delta m_s = 98{,}582 \text{ kg}$$

The condition that the angle of attack goes to zero at staging is also imposed by forcing the equality of γ and θ. This condition adds realism such that high aerodynamic loads are

avoided during staging. Meeting this condition can have a significant effect on the launch trajectory which is part of the motivation for this work.

Terminal Conditions

The goal of the launch is to place the vehicle into an orbit of specified size and shape; defined by a semi-major axis, **a**, and an orbit eccentricity, **e**. The semi-major axis and orbit eccentricity can be expressed in Equation 2.2 where μ is a gravitational constant.

$$a = \left(\frac{2}{r} - \frac{V^2}{\mu}\right)^{-1} \tag{2.2a}$$

$$e^2 = \frac{1}{\mu}\cos^2\gamma \cdot \left(\frac{V^4 r^2}{\mu} - 2V^2 r\right) + 1 \tag{2.2b}$$

The desired terminal conditions for the trajectory are a specified semi-major axis, a_f, and orbit eccentricity, e_f.

$$a_f = 1.0334 \text{ Re}$$

$$e_f = 0.98354 \text{ x } 10^{-2}$$

These are the same end conditions used by Seywald and Cliff[11] and result in approximately a 148km x 277km (80nm x 150nm) orbit.

2.2 Computational Procedures

The task is now to use the equations presented in order to find the control history $\beta(t)$ which will propagate the initial state values, x_o, using the state differential equations and meeting specified point conditions while using the least amount of fuel. This formulation results in a problem of optimal open loop control.[7]

Methods of Finding Solutions

The methods for finding optimal solutions are generally divided into two categories; direct methods and indirect methods.[12] Modern direct methods transcribe the problem of determining the *infinite dimensional* control function u(t) into finding a *finite*

dimensional parameterization; i.e. $u^N(t;q) = q_1 \cdot u_1(t) + \cdots + q_N \cdot u_N(t)$. There are several ways of performing this transcription; by parameterizing only the controls, by parameterizing both the states and controls, and by parameterizing only the states. Examples of direct methods are the *Program to Optimize Simulation Trajectories* (POST) and the *Optimal Trajectories by Implicit Simulation* (OTIS) software.

Indirect methods make use of a theory of necessary conditions and/or sufficient conditions which are based on the problem's measure of performance and constraints to characterize a solution. In a finite dimensional setting the usual necessary conditions lead to a system of algebraic equations. For optimal control problems, such as the problem we are considering, the necessary conditions lead to a multipoint boundary value problem.

For this work, we choose the indirect method because of its greater precision. Later we will use this formulation to find feedback gains $\frac{\partial u}{\partial x}$ by a finite difference method. Thus we need a high accuracy in computing the control. The parameterization methods do not give this accuracy.[12]

Accounting for Rigid Body Dynamics

In order to more thoroughly investigate the effects of the vehicle dynamics on the launch performance of a vehicle, the rigid body dynamics need to be taken into account. These dynamics may have a significant effect on control use while leaving the launch pad and near staging.

In order to include the rigid body dynamics the orbital insertion problem will be addressed as follows. First the equations of motion including rigid body dynamics will be described. Using ideas of differing time scales the problem will be reduced to a "point mass" problem with rotational equilibrium imposed. This simplified problem will then

be solved for a reference trajectory. Corrections for the rigid body dynamics will then be added to the solution through the use of a feedback control structure which flies the vehicle along the reference trajectory. Chapter 3 describes how this process is implemented using the ideas of Singular Perturbation Theory.

3.0 ORBITAL INSERTION OPTIMIZATION PROBLEM

3.1 Introduction of Singular Perturbation Theory

In order to obtain an optimal reference trajectory we need to first outline the optimization problem. In this chapter a generic two stage orbital insertion problem will be discussed. Singular Perturbation Theory will be introduced and will provide a motivation in the method of normalizing the equations of motion. The resulting singular perturbation structure will then be used in conjunction with necessary conditions for an optimal solution to develop a multiple point boundary value problem for the reference trajectory.

Time Scaling

In order to facilitate the solution of the optimization problem, a simplification of the problem will be imposed. This simplification is accomplished by taking advantage of some of the physical properties of the dynamic system. By looking at the behavior of the state elements with respect to time it can be seen that some of the state elements have faster dynamics than the others. Intuitively, if the rate of a given state is directly coupled to a powerful control then such a state will change more rapidly than a state without such control coupling. For example, a one degree change in pitch attitude can be affected much faster than a one degree change in range angle. For our problem, these fast responding elements, which will be referred to as *fast* state elements, are the vehicle inertial pitch rate, q, and the vehicle pitch orientation, θ. The remaining elements, which will be referred to as *slow* state elements, are the radius, r, the downrange angle, ϕ, the vehicle velocity, V, the flight path angle, γ, and the vehicle mass, m. These two groups of state elements can be thought of as evolving in two different time scales.[13]

In the time scale of the *fast* state elements, the *slow* state elements can be thought of as frozen; while in the time scale of the *slow* state elements, the *fast* state elements can be

thought of as changing instantaneously. These ideas will be used to separate the full optimization problem into two parts in order to facilitate a solution.[13] The practice of separating variables into different time scales is commonly used in engineering problems. For example, when investigating the range performance of an aircraft, the rotational dynamics of the aircraft are usually assumed to occur instantaneously and handled by imposing equilibrium conditions. Likewise, in investigating controllability or agility of an aircraft the aircraft mass is typically held constant during a maneuver.

Normalization

In order to mathematically distinguish between the *slow* and *fast* state elements, normalization of the problem is carried out. This normalization is intended to transform the state and control variables into dimensionless quantities with magnitude on the order of unity. The variables used to describe our problem are listed in Table 3-1.

Table 3-1: Variable Definitions

Variable	Definition
r	distance from the center of the Earth to vehicle center of mass
ϕ	downrange angle
V	velocity magnitude of the vehicle
γ	velocity path angle measured from local horizontal
m	vehicle mass
θ	vehicle pitch angle measured from local horizontal
q	vehicle inertial pitch rate
β	angle of the thrust vector w.r.t. vehicle body axis
α	vehicle angle of attack
T	thrust magnitude at current flight conditions
T_{vac}	thrust magnitude if at vacuum flight conditions
ℓ	distance from point at which thrust acts to center of mass
c	exhaust velocity with respect to vehicle
D	aerodynamic drag at current flight condition
L	aerodynamic lift at current flight condition
M	aerodynamic pitch moment at current flight condition
g	acceleration due to gravity
I_{yy}	vehicle pitch moment of inertia

The normalization of the state variables will take place in two stages. First the *slow* state elements and their differential equations will be normalized followed by the normalization of the *fast* state elements and their differential equations.

The differential equations for the *slow* state elements were given by Equations 2.1a - 2.1e and are repeated here.

$$\frac{dr}{dt} = V \cdot \sin\gamma$$

$$\frac{d\phi}{dt} = \frac{V \cdot \cos\gamma}{r}$$

$$\frac{dv}{dt} = \frac{T \cdot \cos(\theta - \gamma + \beta) - D}{m} - g \cdot \sin\gamma$$

$$\frac{d\gamma}{dt} = \frac{T \cdot \sin(\theta - \gamma + \beta) + L}{m \cdot V} + \left(\frac{V}{r} - \frac{g}{V}\right) \cdot \cos\gamma$$

$$\frac{dm}{dt} = -\frac{T_{vac}}{c}$$

where the gravitational acceleration is modeled as $g = g_0 \cdot \left(\frac{Re}{r}\right)^2 = \frac{\mu}{r^2}$.

The following scale factors are used to normalize these state elements.

Scale Factor	Formula	Physical Definition
length	$\bar{r} = Re$	radius of the Earth
acceleration	$\bar{a} = g_0$	acceleration due to gravity at the surface of the Earth
mass	$\bar{m} = m_t$	total vehicle mass with full fuel load

These three scale factors can be combined to form the additional scale factors below.

Scale Factor	Formula	Physical Definition
velocity	$\bar{V} = \sqrt{\bar{r} \cdot \bar{a}}$	velocity of a vehicle in a circular orbit of radius Re
time	$\bar{t} = \sqrt{\bar{r}/\bar{a}}$	time for vehicle to sweep out one radian of a circular orbit of radius Re
force	$\bar{f} = \bar{m} \cdot \bar{a}$	weight of a vehicle with total mass m_t at the surface of the Earth

Note that the variables that represent angular measurements are not scaled since they are in radians.

Using the above scale factors the state differential equations are normalized resulting in the Equations 3.1a - 3.1e.

$$\frac{dr}{dt} = V \cdot \sin\gamma \tag{3.1a}$$

$$\frac{d\phi}{dt} = \frac{V \cdot \cos\gamma}{r} \tag{3.1b}$$

$$\frac{dV}{dt} = \frac{T \cdot \cos(\theta - \gamma + \beta) - D}{m} - \frac{\sin\gamma}{r^2} \tag{3.1c}$$

$$\frac{d\gamma}{dt} = \frac{T \cdot \sin(\theta - \gamma + \beta) + L}{m \cdot V} + \left(\frac{V}{r} - \frac{1}{V \cdot r^2}\right) \cdot \cos\gamma \tag{3.1d}$$

$$\frac{dm}{dt} = -\frac{T_{vac}}{c} \tag{3.1e}$$

Throughout the remainder of this text variables in italics will represent normalized variables. The variable "*t*" represents a normalized time for the *slow* state elements.

$$t = \frac{\mathrm{t}}{\bar{\mathrm{t}}}.$$

The time scale $\bar{\mathrm{t}}$ is approximately 806 seconds.

The next step is to extend our model to include the *fast* state elements which describe the vehicle pitch dynamics. These dynamics are described through the state variables θ, the vehicle pitch orientation with respect to the local horizontal where $\theta = \alpha + \gamma$; and q, the pitch rate in inertial space. The differential equations for these state elements were given by Equation 2.1f - 2.1g and are repeated here.

$$\frac{\mathrm{d}\theta}{\mathrm{dt}} = \mathrm{q} + \frac{\mathrm{V}}{\mathrm{r}}\cos\gamma$$

$$\frac{\mathrm{dq}}{\mathrm{dt}} = \frac{\mathrm{M} - \mathrm{T} \cdot \ell \cdot \sin\beta}{\mathrm{I}_{yy}}$$

These equations will be normalized as follows. The pitch rate equation is rewritten as,

$$\frac{dq}{dt} = \frac{M_{ref}}{I_{yy_{ref}}} \cdot \left[\frac{\frac{M}{M_{ref}} - \frac{T \cdot \ell}{M_{ref}} \sin\beta}{\frac{I_{yy}}{I_{yy_{ref}}}} \right]$$

where M_{ref} and $I_{yy_{ref}}$ are reference values such that M_{ref} is the moment imposed on the vehicle by all ten engines deflected at an angle of one degree in vacuum conditions and $I_{yy_{ref}}$ is the moment of inertia of the vehicle with a full fuel load. These terms are chosen for normalizing such that $\frac{T \cdot \ell}{M_{ref}}$, and $\frac{I_{yy}}{I_{yy_{ref}}}$ are on the order of unity. The term $\frac{M_{ref}}{I_{yy_{ref}}}$ has the units of pitch acceleration and will be used to define a pitch time scale τ_p.

$$\tau_p = \sqrt{\frac{I_{yy_{ref}}}{M_{ref}}} .$$

For our problem τ_p is approximately 6 seconds.

Using this expression, the pitch rate equation can be rewritten as

$$\tau_p^{\,2} \frac{dq}{dt} = \frac{1}{I_{yy}} \cdot \left[\frac{M}{M_{ref}} - \frac{T \cdot \ell \cdot \sin\beta}{M_{ref}} \right]$$

where I_{yy} is the normalized pitch moment of inertia, $I_{yy} = \frac{I_{yy}}{I_{yy_{ref}}}$.

Returning to the differential equation for θ and multiply both sides of the equation by τ_p.

$$\tau_p \frac{d\theta}{dt} = \tau_p q + \tau_p \frac{V}{r} \cdot \cos\gamma$$

Multiplying the left hand side by $\frac{n_0}{n_0}$ where n_0 is the reciprocal of the time scale used for the *slow* state elements $n_0 = 1/t$, and noting that $\frac{V}{r} = n_0 \frac{V}{r}$, we obtain;

$$(n_0\tau_p)\frac{d\theta}{d(n_0 t)} = \tau_p q + (n_0\tau_p)\frac{V}{r}\cos\gamma \ .$$

Now defining $(n_0\tau_p)$ as the dimensionless parameter ε, $(n_0 t)$ as a normalized time t (note that this t is the same normalized time as for the *slow* state elements), and $(\tau_p q)$ as the normalized pitch rate q, the normalized differential equation for the pitch attitude shown in Equation 3.1f is obtained.

$$\varepsilon\frac{d\theta}{dt} = q + \varepsilon\frac{V}{r}\cos\gamma \ . \tag{3.1f}$$

Now returning to the pitch rate differential equation

$$\tau_p{}^2\frac{dq}{dt} = \frac{1}{I_{yy}}\cdot\left[\frac{M}{M_{ref}} - \frac{T\cdot\ell\cdot\sin\beta}{M_{ref}}\right]$$

Multiplying the left hand side by $\frac{n_0}{n_0}$.

$$(n_0\tau_p)\frac{d(\tau_p q)}{d(n_0 t)} = \frac{1}{I_{yy}}\cdot\left[\frac{M}{M_{ref}} - \frac{T\cdot\ell\cdot\sin\beta}{M_{ref}}\right]$$

Substituting in the variables q, t, and ε, Equation 3.1g is obtained.

$$\varepsilon\frac{dq}{dt} = \frac{1}{I_{yy}}\cdot\left[\frac{M}{M_{ref}} - \frac{T\cdot\ell\cdot\sin\beta}{M_{ref}}\right] \tag{3.1g}$$

Although the expression on the right hand side produces a normalized quantity, the variables are dimensional with the exception of I_{yy} and β. It is also important to note that the parameter ε has a physical definition, given by Equation 3.2, and is the ratio of the pitch time scale to original time scale.

$$\varepsilon = \sqrt{\frac{I_{yy_{ref}}}{M_{ref}}} \Big/ \sqrt{\frac{Re}{g_0}} \tag{3.2}$$

With a value for the original time scale of approximately 806 seconds and the value of the pitch time scale of about 6 seconds, the parameter ε has a value of approximately 0.0075.

Singular Perturbation Parameter

Now that we have obtained normalized differential equations for both the *slow* and *fast* elements of the state vector, we can apply the idea of time scaling to reduce the order of our problem. If x represents the *slow* elements of the state vector and y represents the *fast* elements, the state differential equations can be represented by the system

$$\dot{x}(t) = f(x, y, u)$$
$$\varepsilon\dot{y}(t) = g(x, y, u, \varepsilon)$$

The functions f and g are the right hand side of the normalized differential equations developed in the previous subsection.

The system is now in standard Singular Perturbation form[13,14] and the parameter ε can be considered a singular perturbation parameter. Note that this parameter was a "natural" part of the dynamic system and was not arbitrarily added. Also note that the parameter appears on both the right and left side of the differential equations. If we let this parameter go to zero the differential equations for the *fast* elements of the state vector become algebraic path constraints and the associated state vector elements become "control-like". The "reduced order" system can be expressed as

$$\dot{x}(t) = f(x, y, u)$$
$$g(x, y, u, 0) = 0$$

In letting ε go to zero, we are making the assumption that the control history obtained in the solution of our problem with ε=0 is close to the solution that would be obtained if ε had its natural value.[13,15] We will solve for the control with ε=0 to obtain the "zeroth order" solution to our reduced problem which we designate $u^{o}(t)$. After obtaining this

solution, we will make adjustments to our approximation. These adjustments will be discussed in Chapter 5.

3.2 Defining the Reduced Order Problem

Necessary Conditions for Optimality

Now that we have described the problem to be solved, we need to investigate the necessary conditions for optimality. In this section the necessary conditions will be presented for our problem with $\varepsilon=0$. More detailed developments are also available.[1,2,3,4]

Given $x(t_0) = x_0$ and the system of equations;

$$\dot{x}(t) = f(x,y,u)$$

$$g(x,y,u,0) = 0$$

where $x \in R^n$, $y \in R^m$, and $u \in R^k$. The point conditions which are to be enforced are described by the equations,

$$\psi(x_0, x_s^-, x_s^+, x_f) = 0$$

These equations describe the initial, staging, or terminal conditions imposed on the vehicle state, x. Note that ψ must formally include point conditions across staging such as

$$\psi_i = x_{i_s}^- - x_{i_s}^+ = 0$$

which enforces state variable continuity across staging if it is required.

The performance index to be minimized can be described as a function of the *slow* state elements at terminal time,

$$J^0 = \phi(x_f).$$

We can then define two scalar functions;

$$\Phi(x_0, x_s^-, x_s^+, x_f, \upsilon) = \phi(x_f) + \upsilon^T \cdot \psi(x_0, x_s^-, x_s^+, x_f)$$

$$H(\lambda_x, \lambda_y, x, y, u) = \lambda_x{}^T \cdot f(x, y, u) + \lambda_y{}^T \cdot g(x, y, u, 0)$$

where υ is a vector of constant multipliers, and $\lambda_x{}^T$ and $\lambda_y{}^T$ are n and m element time varying vectors of multipliers. The scalar function H is the Hamiltonian function.

Now we can present the necessary conditions for the case of ε=0. It can be shown that if (x,y,u) is optimal then there is a set of multipliers corresponding to the state variables x, called costate or adjoint variables, which obey Equation 3-3.[7,16]

$$\dot{\lambda}_x{}^T = -\frac{\partial H}{\partial x} = -\lambda_x{}^T \cdot \frac{\partial f}{\partial x} - \lambda_y{}^T \cdot \frac{\partial g}{\partial x} \tag{3.3}$$

In addition, the following $(m+k)$ conditions shown in Equations 3.4 and 3.5 must hold throughout the trajectory. Notice that the *fast* state elements, y, are now treated as controls.

$$\frac{\partial H}{\partial y} = \lambda_x{}^T \cdot \frac{\partial f}{\partial y} + \lambda_y{}^T \cdot \frac{\partial g}{\partial y} = 0 \tag{3.4}$$

$$\frac{\partial H}{\partial u} = \lambda_x{}^T \cdot \frac{\partial f}{\partial u} + \lambda_y{}^T \cdot \frac{\partial g}{\partial u} = 0 \tag{3.5}$$

Point conditions on the costate variables can also be determined at each boundary point described by the function ψ. For our problem, these transversality conditions result in $4n$ point conditions on the costate variables as shown in Equations 3.6a - 3.6d.

$$\lambda_x{}^T(t_0) = -\frac{\partial \Phi}{\partial x_0} = -\upsilon^T \cdot \frac{\partial \psi}{\partial x_0} \tag{3.6a}$$

$$\lambda_x{}^T(t_s^-) = \frac{\partial \Phi}{\partial x_s^-} = \upsilon^T \cdot \frac{\partial \psi}{\partial x_s^-} \tag{3.6b}$$

$$\lambda_x{}^T(t_s^+) = -\frac{\partial \Phi}{\partial x_s^+} = -\upsilon^T \cdot \frac{\partial \psi}{\partial x_s^+} \tag{3.6c}$$

$$\lambda_x{}^T(t_f) = \frac{\partial \Phi}{\partial x_f} = \frac{\partial \phi}{\partial x_f} + \upsilon^T \cdot \frac{\partial \psi}{\partial x_f} \tag{3.6d}$$

It can also be shown that since the point conditions at staging are not explicit functions of time, the Hamiltonian is a constant across the staging condition,

$$H(t_s^-) - H(t_s^+) = 0$$

and since the terminal conditions are not an explicit function of time,[7,16]

$$H(t_f) = 0 .$$

Application to Orbit Insertion Problem

The necessary conditions, Equations 3.3 - 3.6, will now be applied to our problem where the nonlinear differential equations are given by Equations 3.1a-3.1g, the point constraints are mathematically expressed as;

$$\psi_1 = r(t_o) - r_o = 0 \qquad \psi_2 = \phi(t_o) - \phi_o = 0$$

$$\psi_3 = V(t_o) - V_o = 0 \qquad \psi_4 = \gamma(t_o) - \gamma_o = 0$$

$$\psi_5 = m(t_o) - m_o = 0 \qquad \psi_6 = r(t_s^-) - r(t_s^+) = 0$$

$$\psi_7 = \phi(t_s^-) - \phi(t_s^+) = 0 \qquad \psi_8 = V(t_s^-) - V(t_s^+) = 0$$

$$\psi_9 = \gamma(t_s^-) - \gamma(t_s^+) = 0 \qquad \psi_{10} = m(t_s^-) - m_s^- = 0$$

$$\psi_{11} = (m(t_s^-) - \Delta m_s) - m(t_s^+) = 0$$

$$\psi_{12} = \left[\frac{2}{r(t_f)} - V^2(t_f) - \frac{1}{a}\right] = 0$$

$$\psi_{13} = \left[\cos^2\gamma(t_f) \cdot (V^4(t_f) \cdot r^2(t_f) - 2 \cdot V^2(t_f) \cdot r(t_f)) + (1 - e^2)\right] = 0$$

and the performance index to be minimized is

$$J^0 = -m(t_f) .$$

Note that the angle of attack constraint at staging, $\alpha(t_s) = \theta(t_s) - \gamma(t_s) = 0$, can not be imposed in the reduced order problem because the pitch angle θ is now a control. This

constraint will be re-imposed when adjustments to the reduced order problem reference trajectory are provided in Chapter 5.

Costate Differential Equations

By evaluating Equation 3.3, where the functions f are given by the state differential Equations 3.1a - 3.1e, the functions g are given by the Equations 3.1f - 3.1g, the costate differential equations are obtained.

$$\dot{\lambda}_r = \lambda_\phi \cdot \left[\frac{V \cdot \cos\gamma}{r^2}\right] - \lambda_V \cdot \left[\frac{T_r \cdot \cos(\theta - \gamma + \beta) - D_r}{m} + \frac{2\sin\gamma}{r^3}\right]$$
$$-\lambda_\gamma \cdot \left[\frac{T_r \cdot \sin(\theta - \gamma + \beta) + L_r}{m \cdot V} + \left(-\frac{V}{r^2} + \frac{2}{V \cdot r^3}\right) \cdot \cos\gamma\right]$$
$$-\lambda_q \cdot \left[\frac{\mathrm{M}_r - \mathrm{T}_r \cdot \ell \cdot \sin\beta}{I_{yy} \cdot \mathrm{M}_{\mathrm{ref}}}\right]$$

$$\dot{\lambda}_\phi = 0$$

$$\dot{\lambda}_V = -\lambda_r \cdot [\sin\gamma] - \lambda_\phi \cdot \left[\frac{\cos\gamma}{r}\right] + \lambda_V \cdot \left[\frac{D_V}{m}\right]$$
$$+\lambda_\gamma \cdot \left[\frac{T \cdot \sin(\theta - \gamma + \eta) + L}{m \cdot V^2} - \frac{L_V}{m \cdot V} - \left(\frac{1}{r} + \frac{1}{V^2 \cdot r^2}\right) \cdot \cos\gamma\right]$$
$$-\lambda_q \cdot \left[\frac{\mathrm{M}_V}{I_{yy} \cdot \mathrm{M}_{\mathrm{ref}}}\right]$$

$$\dot{\lambda}_\gamma = -\lambda_r \cdot [V \cdot \cos\gamma] + \lambda_\phi \cdot \left[\frac{V \cdot \sin\gamma}{r}\right] - \lambda_V \cdot \left[\frac{T \cdot \sin(\theta - \gamma + \beta) - D_\gamma}{m} - \frac{\cos\gamma}{r^2}\right]$$
$$+\lambda_\gamma \cdot \left[\frac{T \cdot \cos(\theta - \gamma + \beta) - L_\gamma}{m \cdot V} + \left(\frac{V}{r} - \frac{1}{V \cdot r^2}\right) \cdot \sin\gamma\right] - \lambda_q \cdot \left[\frac{\mathrm{M}_\gamma}{I_{yy} \cdot \mathrm{M}_{\mathrm{ref}}}\right]$$

$$\dot{\lambda}_m = \lambda_V \cdot \left[\frac{T \cdot \cos(\theta - \gamma + \beta) - D}{m^2}\right] + \lambda_\gamma \cdot \left[\frac{T \cdot \sin(\theta - \gamma + \beta) + L}{m^2 \cdot V}\right]$$
$$+\lambda_q \cdot \left[I_{yy_m} \cdot \left(\frac{\mathrm{M} - \mathrm{T} \cdot \ell \cdot \sin\beta}{I_{yy}^{\ 2} \cdot \mathrm{M}_{\mathrm{ref}}}\right)\right]$$

Control Calculations

By evaluating Equation 3.4 and 3.5 where the functions f and g are given by the state differential equations 3.1a - 3.1g, the necessary conditions involving our "control" variables, θ, q, and β, are obtained.

$$\frac{\partial H}{\partial \theta} = -\lambda_V \cdot \left[\frac{T \cdot \sin(\theta - \gamma + \beta) + D_\theta}{m}\right] + \lambda_\gamma \cdot \left[\frac{T \cdot \cos(\theta - \gamma + \beta) + L_\theta}{m \cdot V}\right] + \lambda_q \cdot \left[\frac{\mathrm{M}_\theta}{I_{yy} \cdot \mathrm{M}_{\mathrm{ref}}}\right] = 0$$

$$\frac{\partial H}{\partial q} = \lambda_\theta + \lambda_q \cdot \left[\frac{\mathrm{M}_q}{I_{yy} \cdot \mathrm{M}_{\mathrm{ref}}}\right] = 0$$

$$\frac{\partial H}{\partial \beta} = -\lambda_V \cdot \left[\frac{T \cdot \sin(\theta - \gamma + \beta)}{m}\right] + \lambda_\gamma \cdot \left[\frac{T \cdot \cos(\theta - \gamma + \beta)}{m \cdot V}\right] - \lambda_q \cdot \left[\frac{\mathrm{T} \cdot \ell \cdot \cos\beta}{I_{yy} \cdot \mathrm{M}_{\mathrm{ref}}}\right] = 0$$

Point Conditions

Evaluating Equation 3.6 for our example problem will provide information on the value of the costate variables at specific points in the trajectory. Table 3.2 shows the value of the costate variables at t_0, t_s^-, and t_s^+ as a function of the unknown multipliers υ_i.

Table 3.2: Reduced Model Costate Values at t_0, t_s^-, and t_s^+

	t_0	t_s^-	t_s^+
λ_r	$-\upsilon_1$	υ_6	υ_6
λ_ϕ	$-\upsilon_2$	υ_7	υ_7
λ_V	$-\upsilon_3$	υ_8	υ_8
λ_γ	$-\upsilon_4$	υ_9	υ_9
λ_m	$-\upsilon_5$	$\upsilon_{10}+\upsilon_{11}$	υ_{11}

Although Table 3.2 does not provide specific values for the costates at the specified times it does imply certain relations among the costates. For example, while the specific values of the costates just before and just after staging are not given, Table 3.2 shows that λ_r,

λ_ϕ, λ_V, and λ_γ are continuous across staging while the costate λ_m jumps by the unknown value υ_{10}. On the other hand, it can be seen that all the costate variables at time t_0 are free parameters in the optimization.

Expressions for the values of the costate variables at terminal time, t_f, are also given by Equation 3.6. The resulting conditions, called transversality conditions[7], involve the state values at terminal time due to the point constraints ψ_{12} and ψ_{13} that specify the semi-major axis and the orbit eccentricity at final time.

$$\lambda_r(t_f) = \upsilon_{12} \cdot \left[-\frac{2}{r^2(t_f)} \right] + \upsilon_{13} \cdot \left[\cos^2 \gamma(t_f) \cdot \left(2 \cdot V^4(t_f) \cdot r(t_f) - 2 \cdot V^2(t_f) \right) \right.$$

$$\lambda_\phi(t_f) = 0$$

$$\lambda_V(t_f) = \upsilon_{12} \cdot \left[-2 \cdot V(t_f) \right] + \upsilon_{13} \cdot \left[\cos^2 \gamma(t_f) \cdot \left(4 \cdot V^3(t_f) \cdot r^2(t_f) - 4 \cdot V(t_f) \cdot r(t_f) \right) \right.$$

$$\lambda_\gamma(t_f) = \upsilon_{13} \cdot \left[-2 \cdot \cos\gamma(t_f) \sin\gamma(t_f) \cdot \left(V^4(t_f) \cdot r^2(t_f) - 2 \cdot V^2(t_f) \cdot r(t_f) \right) \right.$$

$$\lambda_m(t_f) = -1$$

In addition, the point conditions on the Hamiltonian are;

$$H(t_s^-) - H(t_s^+) = 0$$

$$H(t_f) = 0 .$$

3.3 Obtaining a Solution

Summary of Problem

We now must solve the boundary value problem posed by the previously obtained state and costate differential equations as well as the point conditions and control equations. The problem of obtaining a solution reduces to finding the initial costate values λ_{r_o}, λ_{V_o}, λ_{γ_o}, and λ_{m_o} (λ_{ϕ_o}=0 since λ_{ϕ_f} is zero and λ_ϕ is a constant); the constant multipliers υ_{12} and

υ_{13} that appear in the transversality conditions; the change in λ_m at staging, υ_{10}; and the final time t_f. These eight unknowns are solved for by using the four transversality conditions on λ_{r_f}, λ_{V_f}, λ_{γ_f}, and λ_{m_f} ; the two end conditions on the semi-major axis and orbit eccentricity; and the conditions that the Hamiltonian is constant across staging and is equal to zero at time t_f.

The process of obtaining a solution involves starting with the given values for the states, x_0, and the initial estimates for the costates, λ_{x_0}, and integrating these values forward in time throughout the trajectory using the state and costate differential equations. When staging time is reached (staging time can be precalculated from the known initial mass, the specified mass at staging, and the known mass flow rate), the mass is decreased by a known amount and the costate λ_m is changed by the estimate $\Delta\lambda_m$ which is one of the unknowns. The integration of the trajectory is then continued to the estimated final time t_f.

The residuals are then calculated by computing: the change in the Hamiltonian at staging, the final value of the Hamiltonian, the errors in the achieved semi-major axis and orbital eccentricity, and the difference between the final values of the costates obtained via the transversality. A root finding method is then used to update the estimate of the unknowns and to drive the residuals to zero.

Control Calculations

To integrate the vehicle trajectory from initial to final time, the values of the controls must be calculated along the trajectory. The controls are computed from the necessary conditions expressed in Equations 3.4 and 3.5 in conjunction with the algebraic constraints $g(x,y,u,0)=0$. To summarize, the equations

$$\frac{\partial H}{\partial \theta} = -\lambda_V \cdot \left[\frac{T \cdot \sin(\theta - \gamma + \beta) + D_\theta}{m}\right] + \lambda_\gamma \cdot \left[\frac{T \cdot \cos(\theta - \gamma + \beta) + L_\theta}{m \cdot V}\right] + \lambda_q \cdot \left[\frac{M_\theta}{I_{yy} \cdot M_{ref}}\right] = 0$$

$$\frac{\partial H}{\partial q} = \lambda_\theta + \lambda_q \cdot \left[\frac{M_q}{I_{yy} \cdot M_{ref}}\right] = 0$$

$$\frac{\partial H}{\partial \beta} = -\lambda_V \cdot \left[\frac{T \cdot \sin(\theta - \gamma + \beta)}{m}\right] + \lambda_\gamma \cdot \left[\frac{T \cdot \cos(\theta - \gamma + \beta)}{m \cdot V}\right] - \lambda_q \cdot \left[\frac{T \cdot \ell \cdot \cos\beta}{I_{yy} \cdot M_{ref}}\right] = 0$$

$$g_1 = q = 0$$

$$g_2 = \frac{M - T \cdot \ell \cdot \sin\beta}{I_{yy} \cdot M_{ref}} = 0$$

must be solved for β, θ, q, λ_θ, and λ_q at every point along the trajectory.

First $g_1 = q = 0$ is solved for q=0. Next, $\frac{\partial H}{\partial \beta} = 0$, $\frac{\partial H}{\partial \theta} = 0$, and $g_2 = 0$ are solved by numerical iteration for β, θ, and λ_q. For the initial estimate of β, θ, and λ_q at each point in the trajectory the values obtained at the previous trajectory point are used. The equation $\frac{\partial H}{\partial q} = 0$ is then solved for λ_θ.

Numerical Difficulties

Upon attempting to integrate the vehicle trajectory, numerical difficulties are encountered. Due to the Hamiltonian structure of the problem, the eigenvalues of the linearized system will be symmetric about the imaginary as well as the real axes.[11] This means that if the some variables are stable as we integrate forward in time (forward time stable), the other variables will be forward time unstable. These unstable elements cause problems while integrating the system. If the initial values are not close to the solution, then these variables will diverge during the integration and cause a numerical overflow.

In order to work around this stability problem the technique of multiple shooting is employed. This technique involves splitting the trajectory into several arcs and integrating each arc separately. This splitting procedure is accomplished by estimating the values of the states and costates at the beginning of each additional arc which increases the number of unknowns in the root finding problem. In turn, the additional equations are obtained to force continuity of the states and costates between arcs. Since each arc is shorter than the original trajectory, the integration has less time to diverge. This procedure increases the size of the root finding but also increases the "basin of attraction" for the algorithm. For the simulation software used to obtain a solution to our problem, two arcs were used before vehicle staging and three arcs were used after staging. This resulted in an increase from eight unknowns to forty unknowns.

Optimality Claims

Classical theory provides four necessary conditions for optimality: the Euler-Lagrange, Legendre-Clebsch, Weierstrass, and Jacobi conditions. All of these conditions are necessary in order for a solution to be a local minimum, and strengthened forms of these conditions are sufficient to ensure that a solution is a local minimum. The Euler-Lagrange conditions; $\dot{\lambda}^T = -H_x$, $H_u = 0$, and transversality, are satisfied by the fact that we used these conditions to compute our solution. The Legendre-Clebsch condition, $H_{uu} \geq 0$ along the trajectory, has been computed and found to be satisfied. The Weierstrass condition is satisfied because we have, in fact, imposed the minimum principle with controls allowed to vary over their allowed bounds. The fourth condition, that of Jacobi, states that a local minimizer can not have any conjugate points, and this condition has not been considered. Thus no formal claim to optimality can be made for this work.

4.0 SOLUTION TO POINT MASS PROBLEM

The solution to the reduced order (point mass) orbital insertion problem was carried out as described in the previous chapters. This solution was numerically obtained by solving the multi-point boundary value problem using multiple shooting techniques and the quasi-Newton root finding algorithm, HBRD, obtained from the Naval Surface Warfare Center/Dahlgren Division (NSWC/DD) math library. The solution was obtained using FORTRAN code on a 90 MHz Pentium PC with a computation time of approximately three to five minutes. The unknowns were solved to a relative error of $1x10^{-11}$. Each trajectory run took approximately one second to complete with forty-one trajectory runs needed per iteration. The integration scheme used was the variable order, variable step Adams predictor-corrector algorithm, ODE, also from the NSWC/DD math library. When difficulties were encountered obtaining a solution, the cause was usually the integration of the unstable system elements. Increasing the number of multiple shooting arcs tamed these instabilities so that convergence was achieved.

Figures 4.1 through 4.5 show the vehicle states obtained for the point mass optimal trajectory. Figure 4.1 shows the altitude of the vehicle above the Earth's surface. The actual state element, the radius, can be obtained by adding the reference Earth radius, Re., to the plotted altitude. The knee in Figures 4.3 and 4.4 and the discontinuity in Figure 4.5 are caused by staging which occurs at approximately 103 seconds. Recall that at staging part of the vehicle mass is thrown away and the number of engines are reduced from ten to three.

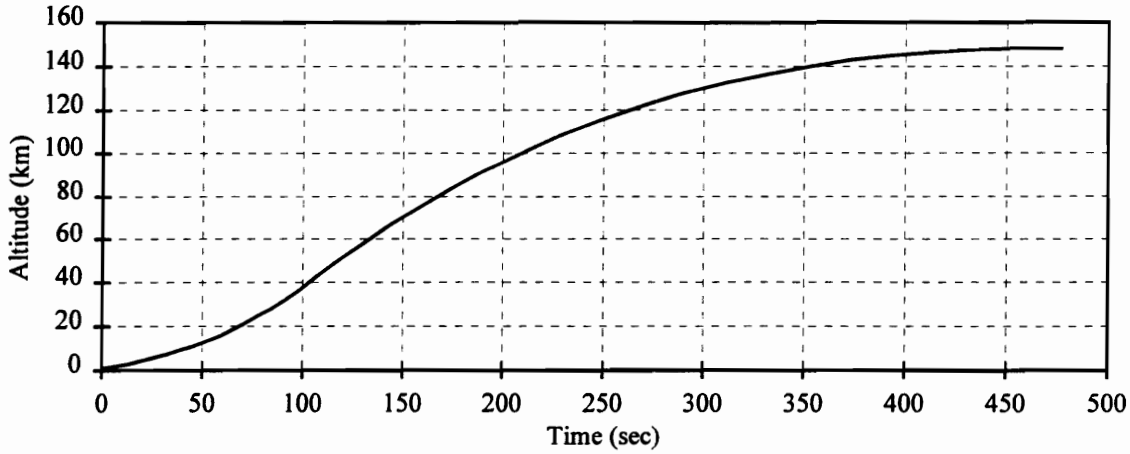

Figure 4.1: Point Mass Solution - Altitude History

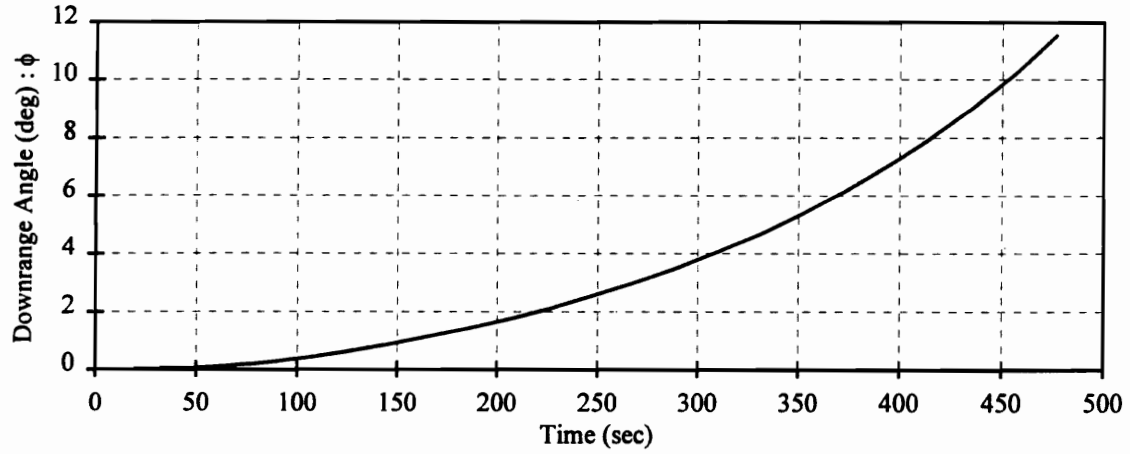

Figure 4.2: Point Mass Solution - Downrange Angle History

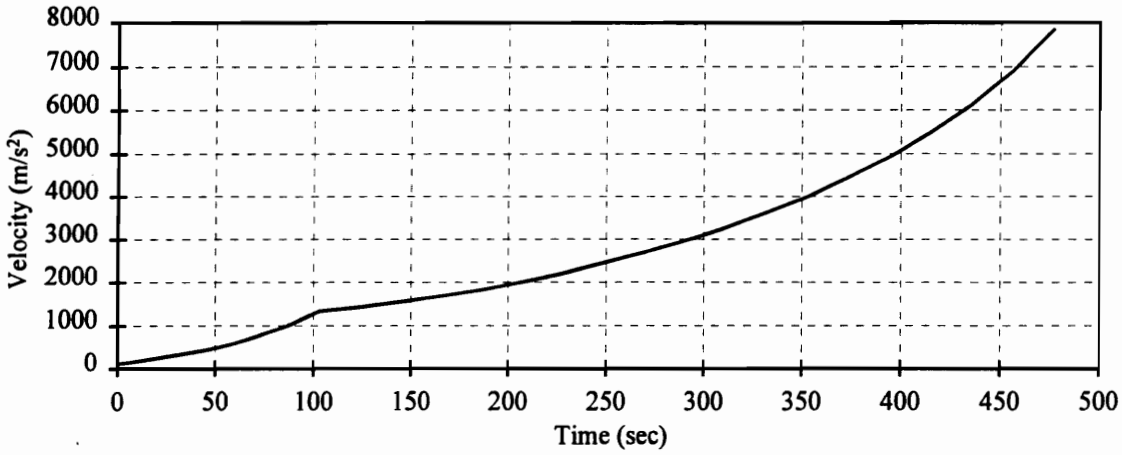

Figure 4.3: Point Mass Solution - Velocity History

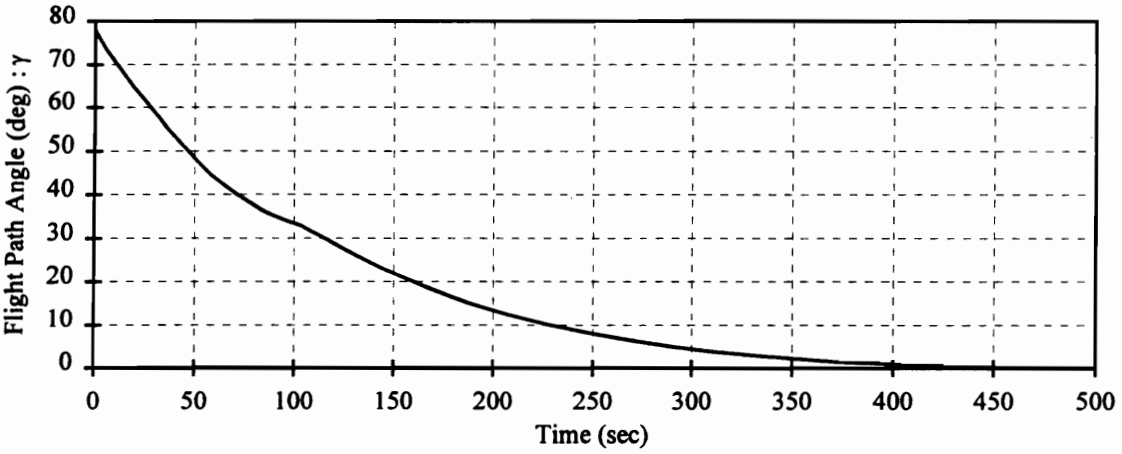

Figure 4.4: Point Mass Solution - Flight Path Angle History

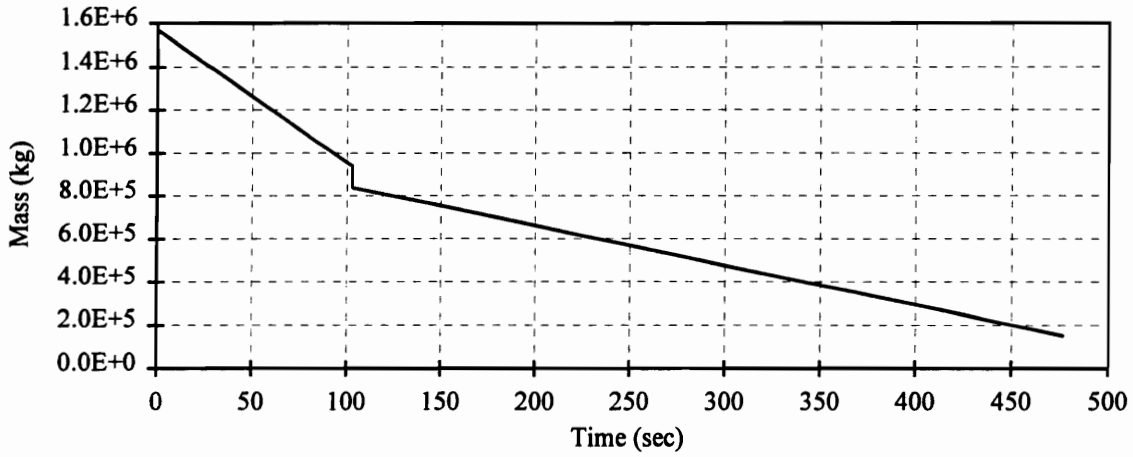

Figure 4.5: Point Mass Solution - Mass History

Figures 4.6 and 4.7 show the controls for the point mass reference trajectory. Although difficult to see in Figure 4.6, there is a discontinuity in the pitch angle, θ, at staging. This discontinuity in the pitch orientation is physically impossible and will be corrected for in Chapter 5 where the pitch dynamics are included. Figure 4.7 shows the gimbal angle, β, throughout the trajectory. The maximum deflection is approximately 2.2 degrees and occurs in the first stage of flight. A discontinuity in the gimbal angle is seen at staging and then the gimbal angle tends to zero during most of the second stage of flight. This is due to the optimization aligning the thrust with the vehicle body axis. If this alignment is not done, a moment will be present on the vehicle that will violate the algebraic constraint on the pitch rate.

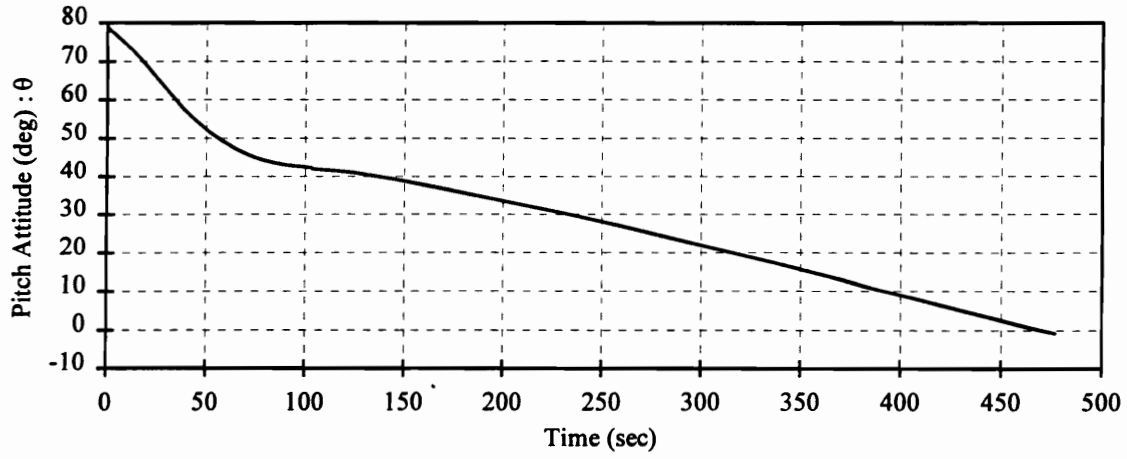

Figure 4.6: Point Mass Solution - Pitch Attitude History

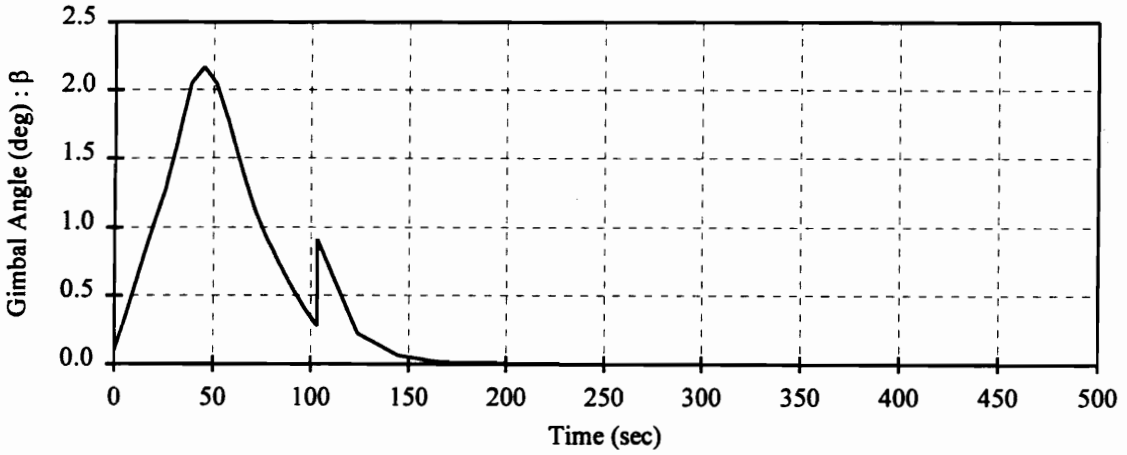

Figure 4.7: Point Mass Solution - Gimbal Angle History

Figure 4.8 shows the thrust history of the vehicle. During the first portion of stage one, the thrust is increasing as a result of the decreasing atmospheric pressure at the exhaust nozzles with increasing altitude. At staging, the thrust decreases when the number of engines decrease from ten to three.

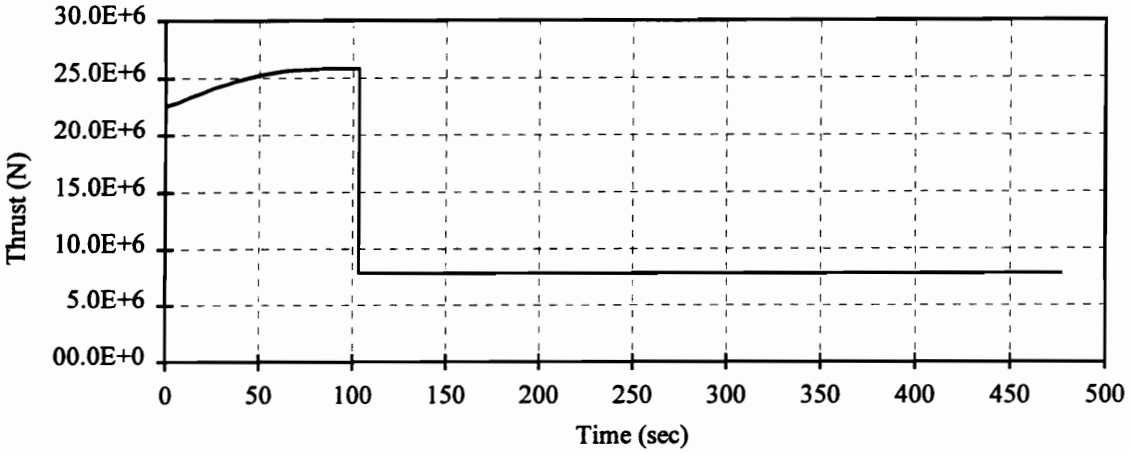

Figure 4.8: Point Mass Solution - Thrust History

Figure 4.9 shows the angle of attack, α, of the vehicle during the launch trajectory. The angle of attack and gimbal angle are being used to provide a force normal to the vehicle flight path in order to assist in raising the vehicle into orbit. During the first stage this normal force is being created by both the angle of attack, which results in aerodynamic lift, and the gimbal angle which directs a portion of the engine thrust normal to the flight path. As the vehicle moves out of the atmosphere the gimbal angle must tend to zero to maintain moment equilibrium and the angle of attack is used to orient some of the thrust normal to the flight path.

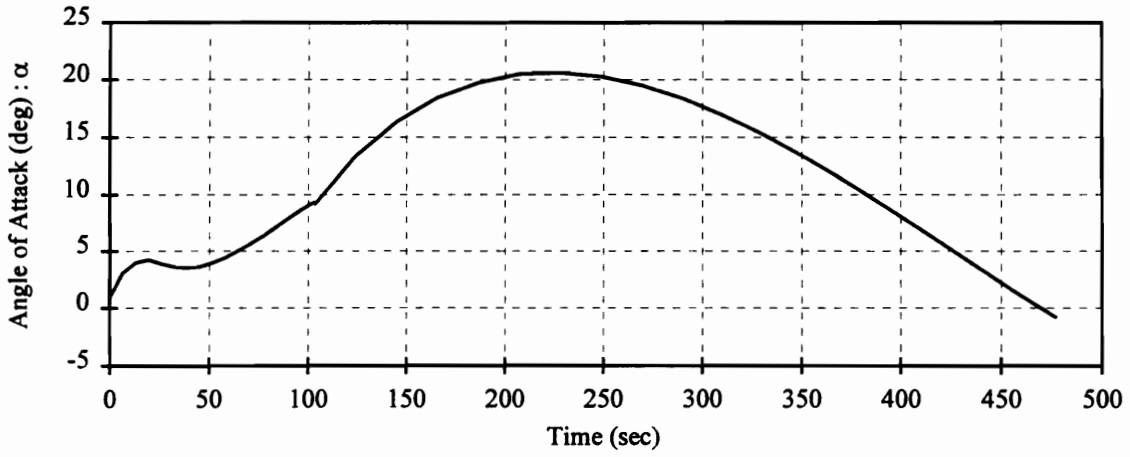

Figure 4.9: Point Mass Solution - Angle of Attack History

Figure 4.10 shows the dynamic pressure imposed on the vehicle during flight. As seen in the figure, most of the second stage is flown in negligible dynamic pressure.

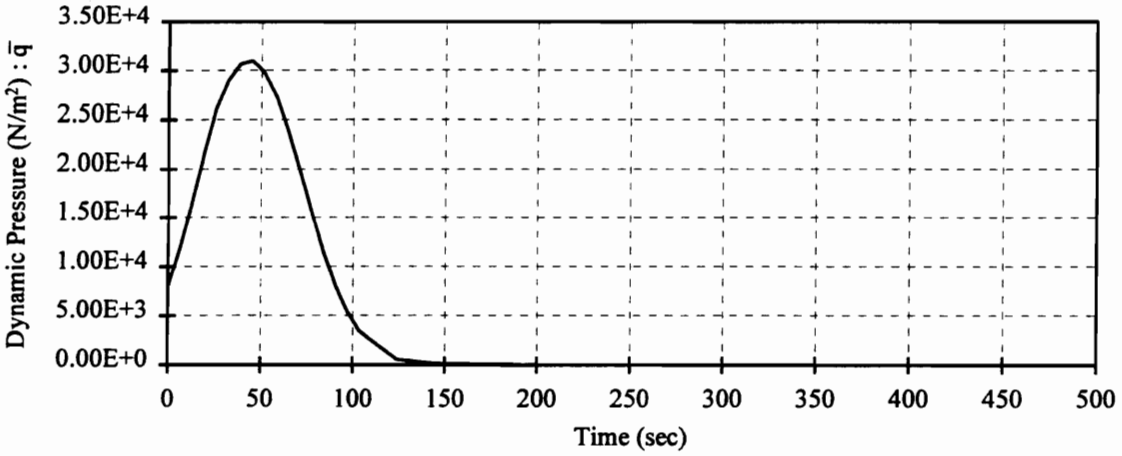

Figure 4.10: Point Mass Solution - Dynamic Pressure History

Figures 4.11 and 4.12 show the semi-major axis, a, and the orbit eccentricity, e, respectively. At terminal time the semi-major axis has obtained the desired value of approximately 1.03 Re and the orbit eccentricity has obtained its desired value of approximately 0.01.

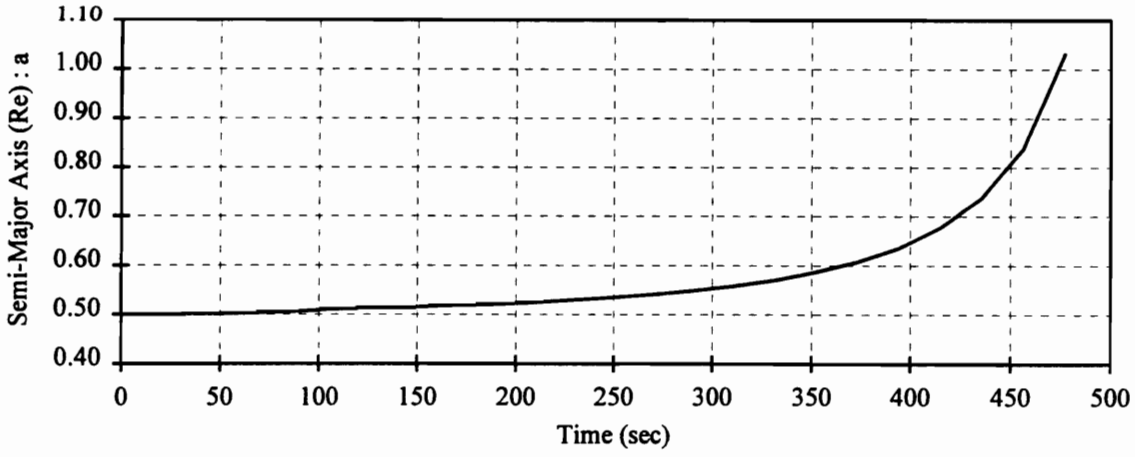

Figure 4.11: Point Mass Solution - Semi-Major Axis History

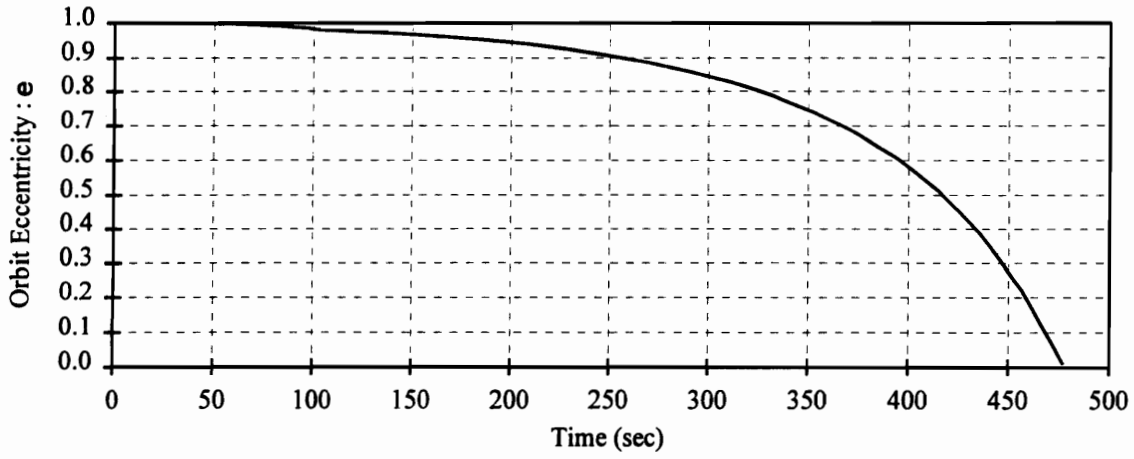

Figure 4.12: Point Mass Solution - Orbit Eccentricity History

The terminal conditions for the obtained point mass trajectory are shown in Table 4.1. The desired perigee is 148.164 km and the desired apogee is 277.813 km.

Table 4.1: Point Mass Solution Terminal Conditions

Final Time (sec)	477.20
Final Mass (kg)	1.4992×10^{5}
Semi-major Axis (Re)	1.0334
Orbit Eccentricity	9.8354×10^{-3}
Perigee (km)	148.164
Apogee (km)	277.813

5.0 APPROXIMATING THE FULL ORDER PROBLEM

In Section 3.1, Singular Perturbation Theory was introduced and a singular perturbation parameter, ε, was defined. This parameter was set to zero in the reduced order (point mass) problem that was then solved. The assumption is that the reduced order problem serves as a good approximation to the full order problem except where point conditions are imposed on the *fast* elements of the state vector. These point conditions were lost in the reduced order problem. The goal is now to make corrections to the reduced order solution in the areas of the lost point conditions by including the effects of the rigid body dynamics. This composite solution will be an improved approximation to the full order problem.

5.1 Corrections for Point Conditions

Define Outer and Inner Problem

In order to discuss the corrections it would be helpful to define two terms; "outer problem" and "inner problem". The outer problem is the reduced order problem to which we have already obtained a solution. For our problem, this solution can be thought of as the control law which provides the path guidance for the vehicle. The inner problem can be thought of as the control law which provides orientation of the vehicle. In the outer problem solution, we obtained a nominal history or profile of the *slow* and *fast* elements of the state vector. The inner problem will provide deviations in the *fast* elements from this nominal profile in order to match the boundary conditions on the *fast* elements of the state vector.

Our intent is to investigate the behavior of the *fast* elements in the region near the lost boundary conditions. If we introduce a new time variable defined in Equation 5.1, we can investigate the dynamics of the *fast* elements near the point conditions at initial time

t_i. Note that in a feedback sense, the current time can be considered the initial time for the remainder of the trajectory and the current state the initial boundary condition. Therefore, the formulation to follow can be applied at any time along the trajectory.

$$\tau_1 = (t - t_i) / \varepsilon \tag{5.1}$$

This new time variable, τ_1, "stretches" time for small values of ε. We can use this definition to change the independent variable of our system equations. The state/costate equations with respect to τ_1 are shown in Equation 5.2.

$$\frac{dx}{d\tau_1} = \varepsilon \cdot f(x,y,u) \tag{5.2a}$$

$$\frac{d\lambda_x}{d\tau_1} = -\varepsilon \cdot \frac{\partial H}{\partial x} \tag{5.2b}$$

$$\frac{dy}{d\tau_1} = g(x,y,u,\varepsilon) \tag{5.2c}$$

$$\frac{d\lambda_y}{d\tau_1} = -\frac{\partial H}{\partial y} \tag{5.2d}$$

On inspection of Equations 5.2a and 5.2b. we can see that as ε approaches zero the *slow* elements of the state vector, x, and their corresponding costate elements, λ_x, become constants with respect to the stretched time τ_1. We will use this fact by again taking the zeroth order approximation and setting ε to zero in obtaining a solution to Equations 5.2c and 5.2d. Note that the values of the *fast* elements obtained in the outer problem are equilibrium values since the conditions $g(x,y,u,0)=0$ and $\frac{\partial H}{\partial y} = 0$ were imposed.

Stability Considerations

The system of equations for our inner problem with $\varepsilon=0$ are given in Equation 5.3.

$$\frac{d\theta}{d\tau_1} = q \tag{5.3a}$$

$$\frac{dq}{d\tau_1} = \frac{M - T \cdot \ell \cdot \sin\beta}{I_{yy} \cdot M_{ref}} \tag{5.3b}$$

$$\frac{d\lambda_\theta}{d\tau_1} = \lambda_V \cdot \left[\frac{T \cdot \sin(\theta - \gamma + \beta) + \frac{\partial D}{\partial \theta}}{m} \right] - \lambda_\gamma \cdot \left[\frac{T \cdot \cos(\theta - \gamma + \beta) + \frac{\partial L}{\partial \theta}}{m \cdot V} \right] - \lambda_q \cdot \left[\frac{\frac{\partial M}{\partial \theta}}{I_{yy} \cdot M_{ref}} \right] \tag{5.3c}$$

$$\frac{d\lambda_q}{d\tau_1} = -\lambda_\theta \tag{5.3d}$$

The key idea we use from Singular Perturbation Theory is a notion of stability.[13] The solution is to be approximated as a sum of an "outer" and an "inner" term, where the "inner" term is non-zero only in local regions near a boundary point. Thus, the "inner" term must decay to zero as we move away from the boundary points. In our case these boundary points are the initial time (current time in a feedback implementation), the staging time, and possibly the terminal time. In fact, our terminal conditions do not involve any of the *fast* state elements and there is no terminal boundary layer.

The system expressed by Equation 5.3 represents a fourth-order nonlinear dynamic model. As noted above, the "outer" values of the fast variables are necessarily an equilibrium point for the system. However, equilibrium points for state/costate systems, such as Equation 5.3, are never stable in the usual sense. This is due to the state/costate structure which requires that if some components decay other components must grow. This will be further discussed later in this chapter. There will be special initial conditions such that the "growing" components remain zero. The locus of such conditions forms a stable surface with the property that initial points exactly on this surface will evolve to the equilibrium point.

On might think of the inverted pendulum problem as an example. With special initial values of displacement and velocity, those that make the total energy just right, the pendulum will move to the unstable inverted equilibrium point.

Unfortunately for a nonlinear system, such as given by Equation 5.3, it is difficult to describe this two dimensional stable surface in the four dimensional space. We will approximate this nonlinear surface through linearization. This approximation will lead to a stable subspace that is tangent to the stable surface. In the vicinity of the equilibrium point the subspace will serve to approximate the surface.

Linearization of Inner Problem

First the system will be linearized using small perturbation analysis. If we let

$$\theta = \theta^{\circ} + \Delta\theta$$

$$q = q^{o} + \Delta q$$

$$\lambda_{\theta} = \lambda_{\theta}{}^{\circ} + \Delta\lambda_{\theta}$$

$$\lambda_{q} = \lambda_{q}{}^{\circ} + \Delta\lambda_{q}$$

$$\beta = \beta^{\circ} + \Delta\beta$$

$$D = D^{\circ} + \left[\frac{\partial D}{\partial\theta}\right]^{\circ} \cdot \Delta\theta$$

$$L = L^{\circ} + \left[\frac{\partial L}{\partial\theta}\right]^{\circ} \cdot \Delta\theta$$

$$M = M^{\circ} + \left[\frac{\partial M}{\partial\theta}\right]^{\circ} \cdot \Delta\theta$$

$$\frac{\partial M}{\partial\theta} = \left[\frac{\partial M}{\partial\theta}\right]^{\circ} + \left[\frac{\partial^{2} M}{\partial\theta^{2}}\right]^{\circ} \cdot \Delta\theta$$

where the superscript "o" denotes the value obtained in the outer zeroth order solution of our problem. Substituting these expressions back into Equation 5.3, we obtain the linear system shown by Equation 5.4.

$$\frac{d\Delta\theta}{d\tau_{1}} = \Delta q \qquad (5.4a)$$

$$\frac{d\Delta\theta}{d\tau_1} = \Delta q \tag{5.4a}$$

$$\frac{d\Delta q}{d\tau_1} = Q_\theta \cdot \Delta\theta + Q_\beta \cdot \Delta\beta \text{ where} \tag{5.4b}$$

$$Q_\theta = \frac{\left[\frac{\partial M}{\partial \theta}\right]^\circ}{I_{yy}{}^\circ \cdot M_{ref}}$$

$$Q_\beta = -\frac{T^\circ \cdot \ell \cdot \cos\beta^\circ}{I_{yy}{}^\circ \cdot M_{ref}}$$

$$\frac{d\Delta\lambda_\theta}{d\tau_1} = LT_\theta \cdot \Delta\theta + LT_{\lambda_q} \cdot \Delta\lambda_q + LT_\beta \cdot \Delta\beta \text{ where} \tag{5.4c}$$

$$LT_\theta = \lambda_V{}^\circ \cdot \left(\frac{T^\circ \cdot \cos(\theta^\circ - \gamma^\circ + \beta^\circ) + \left[\frac{\partial^2 D}{\partial \theta^2}\right]^\circ}{m^\circ} \right)$$

$$+\lambda_\gamma{}^\circ \cdot \left(\frac{T^\circ \cdot \sin(\theta^\circ - \gamma^\circ + \beta^\circ) + \left[\frac{\partial^2 L}{\partial \theta^2}\right]^\circ}{m^\circ \cdot V^\circ} \right)$$

$$-\lambda_q{}^\circ \cdot \left(\frac{\left[\frac{\partial^2 M}{\partial \theta^2}\right]^\circ}{I_{yy}{}^\circ \cdot M_{ref}} \right)$$

$$LT_{\lambda_q} = -\frac{\left[\frac{\partial M}{\partial \theta}\right]^\circ}{I_{yy}{}^\circ \cdot M_{ref}}$$

$$LT_\beta = \lambda_V{}^\circ \cdot \left(\frac{T^\circ \cdot \cos(\theta^\circ - \gamma^\circ + \beta^\circ)}{m^\circ} \right)$$

$$+\lambda_\gamma{}^\circ \cdot \left(\frac{T^\circ \cdot \sin(\theta^\circ - \gamma^\circ + \beta^\circ)}{m^\circ \cdot V^\circ} \right)$$

$$\frac{d\Delta\lambda_q}{d\tau_1} = -\Delta\lambda_\theta \tag{5.4d}$$

We will use this linear system and the linearized form of the necessary condition $\frac{\partial H}{\partial \beta} = 0$ to obtain the control perturbation $\Delta\beta$ which will be used to solve the inner problem. Recall from Chapter 3;

$$\frac{\partial H}{\partial \beta} = -\lambda_V \cdot \left[\frac{T \cdot \sin(\theta - \gamma + \beta)}{m}\right] + \lambda_\gamma \cdot \left[\frac{T \cdot \cos(\theta - \gamma + \beta)}{m \cdot V}\right] - \lambda_q \cdot \left[\frac{T \cdot \ell \cdot \cos\beta}{I_{yy} \cdot M_{ref}}\right] = 0$$

This equation will be linearized and solved for $\Delta\beta$ in terms of $\Delta\theta$, Δq, $\Delta\lambda_\theta$, $\Delta\lambda_q$ as shown in Equation 5.5.

$$\Delta\beta = -\frac{B_\theta}{B_\beta} \cdot \Delta\theta + B_{\lambda_q} \frac{B_{\lambda_q}}{B_\beta} \cdot \Delta\lambda_q \text{ where} \tag{5.5}$$

$$B_\theta = -\lambda_V{}^\circ \cdot \left(\frac{T^\circ \cdot \cos(\theta^\circ - \gamma^\circ + \beta^\circ)}{m^\circ}\right) - \lambda_\gamma{}^\circ \cdot \left(\frac{T^\circ \cdot \sin(\theta^\circ - \gamma^\circ + \beta^\circ)}{m^\circ \cdot V^\circ}\right)$$

$$B_{\lambda_q} = -\frac{T^\circ \cdot \ell \cdot \cos\beta^\circ}{I_{yy}{}^\circ \cdot M_{ref}}$$

$$B_\beta = -\lambda_V{}^\circ \cdot \left(\frac{T^\circ \cdot \cos(\theta^\circ - \gamma^\circ + \beta^\circ) + \left[\frac{\partial^2 D}{\partial \theta^2}\right]^\circ}{m^\circ}\right) - \lambda_\gamma{}^\circ \cdot \left(\frac{T^\circ \cdot \sin(\theta^\circ - \gamma^\circ + \beta^\circ) + \left[\frac{\partial^2 L}{\partial \theta^2}\right]^\circ}{m^\circ \cdot V^\circ}\right) + \lambda_q{}^\circ \cdot \left(\frac{T^\circ \cdot \ell \cdot \sin\beta^\circ}{I_{yy}{}^\circ \cdot M_{ref}}\right)$$

We can see that this Equation 5.5 can form the basis of a feedback control law where

$$\Delta\theta = \theta - \theta^\circ$$

and

$$\Delta\lambda_q = \lambda_q - \lambda_q{}^\circ .$$

The value of θ is the current pitch angle and is assumed measurable by sensors on the vehicle. However, the value of λ_q is not known and will be solved for based on the stability of the linear system.

The expression for Δβ, Equation 5.5, will then be used in Equation 5.4 to obtain the closed loop linear system shown in Equation 5.6.

$$\begin{bmatrix} \frac{d\Delta\theta}{d\tau_1} \\ \frac{d\Delta q}{d\tau_1} \\ \frac{d\Delta\lambda_\theta}{d\tau_1} \\ \frac{d\Delta\lambda_q}{d\tau_1} \end{bmatrix} = \begin{bmatrix} 0 & 1 & 0 & 0 \\ A_{21} & 0 & 0 & A_{24} \\ A_{31} & 0 & 0 & A_{34} \\ 0 & 0 & -1 & 0 \end{bmatrix} \cdot \begin{bmatrix} \Delta\theta \\ \Delta q \\ \Delta\lambda_\theta \\ \Delta\lambda_q \end{bmatrix} \tag{5.6}$$

where

$$A_{21} = Q_\theta - Q_\beta \cdot \frac{B_\theta}{B_\beta}$$

$$A_{24} = -Q_\beta \cdot \frac{B_{\lambda_q}}{B_\beta}$$

$$A_{31} = LT_\theta - LT_\beta \cdot \frac{B_\theta}{B_\beta}$$

$$A_{34} = LT_{\lambda_q} - LT_\beta \cdot \frac{B_{\lambda_q}}{B_\beta}$$

We can analyze the stability of this system by examining its characteristic equation.

$$\lambda^4 + (A_{34} - A_{21})\lambda^2 + (A_{24}A_{31} - A_{21}A_{34}) = 0$$

This system has Hamiltonian structure, therefore the eigenvalues will appear in pairs symmetric not only about the real axis but also about the imaginary axis.[8,13,14] Solving this equation for λ^2 we obtain,

$$\lambda^2 = \tfrac{1}{2}\left[-(A_{34} - A_{21}) \pm \sqrt{(A_{34} - A_{21})^2 - 4(A_{24}A_{31} - A_{21}A_{34})}\right]$$

Upon investigating the expressions for A_{34} and A_{21}, we find that A_{21}=-A_{34}. In fact, it is shown in Bryson[7] that the 2x2 submatrix in the lower right hand corner of matrix A is the negative transpose of the 2x2 in the upper left hand corner. In addition, the submatricies in the upper right corner and the lower left corner are symmetric. Matricies of this form are said to have Hamiltonian structure and are guaranteed to have eigenvalues symmetric about the origin. Hence, this relation between A_{21} and A_{34} will always be true. Using this result to simplify the equation for λ_2 we obtain,

$$\lambda^2 = -A_{34} \pm \sqrt{-A_{24}A_{31}}$$

Assuming that $A_{34} < 0$ (it is for our problem), there are four cases to be considered. Case 1; if the term $A_{24}A_{31}$=0, the eigenvalues appear as repeated real roots at $\pm\sqrt{|A_{34}|}$. Case 2; if $A_{24}A_{31}$>0, the eigenvalues appear as four complex roots symmetric about both the real and imaginary axes. Case 3; if $A_{24}A_{31}$<0 and $-A_{34} > \left|\sqrt{-A_{24}A_{31}}\right|$, the eigenvalues will appear as four distinct real roots with symmetry about the imaginary axis. Case 4; if $A_{24}A_{31}$<0 and $-A_{34} \leq \left|\sqrt{-A_{24}A_{31}}\right|$, two of our eigenvalues will be either zero or purely imaginary. If case 4 occurs, our stability argument breaks down and the proposed method of obtaining an inner loop control will not work. Fortunately for our problem we obtain non-zero real components for all of the eigenvalues.

Since the eigenvalues have symmetry about the imaginary axis, two will indicate stable modes of the system while two will indicate unstable modes. We wish to construct a feedback control law that will negate any deviations in the *fast* state elements about the reference values without exciting their unstable modes.

Inner Problem Feedback Gains

From the two stable eigenvalues previously obtained we need to calculate the associated eigenvectors $v^{[1]}$ and $v^{[2]}$. These eigenvectors will be used to construct an initial

condition vector that will allow a return to equilibrium in a stable manner. Equation 5.7 gives the form of the initial condition vector,

$$\begin{bmatrix} \Delta\theta \\ \Delta q \\ \Delta\lambda_\theta \\ \Delta\lambda_q \end{bmatrix} = \alpha_1 \cdot v^{[1]} + \alpha_2 \cdot v^{[2]} \tag{5.7}$$

where α_1 and α_2 are yet unknown and $v^{[1]}$ and $v^{[2]}$ are expressed as;

$$v^{[1]} = \begin{bmatrix} v_1^{[1]} \\ v_2^{[1]} \\ v_3^{[1]} \\ v_4^{[1]} \end{bmatrix} \qquad v^{[2]} = \begin{bmatrix} v_1^{[2]} \\ v_2^{[2]} \\ v_3^{[2]} \\ v_4^{[2]} \end{bmatrix}.$$

The idea is to pick the values of $\Delta\lambda_\theta$ and $\Delta\lambda_q$ such that the initial condition vector can be constructed from the stable eigenvectors of the system. If the costates are continuously chosen in this manner the control which is a function of $\Delta\lambda_q$ will drive the system back to equilibrium. In order to obtain the values of $\Delta\lambda_\theta$ and $\Delta\lambda_q$, the known elements $\Delta\theta$ and Δq are used to solve for α_1 and α_2 in terms of $v^{[1]}$ and $v^{[2]}$. The eigenvectors are obtained from the relation;

$$(\lambda_i I - A)v^{[i]} = 0$$

where λ_i are the forward time stable eigenvalues.

If the eigenvalues λ_i are distinct real eigenvalues, then two distinct eigenvectors can be obtained from the above equation. If the eigenvalues, λ_i, are repeated reals, the first eigenvector $v^{[1]}$ can be obtained using the above relation and the second vector $v^{[2]}$ will be a generalized eigenvector obtained using the relation;

$$(\lambda_2 I - A)v^{[2]} = v^{[1]}.$$

If complex eigenvalues are obtained, the first relation can be solved for a complex eigenvector v. This eigenvector can be used such that $v^{[1]}$ is the real part of v and $v^{[2]}$ is

the imaginary part of v. Once $v^{[1]}$ and $v^{[2]}$ are determined, expressions for α_1 and α_2 can be obtained by solving the following equations.

$$\Delta\theta = \alpha_1 \cdot v_1^{[1]} + \alpha_2 \cdot v_1^{[2]}$$
$$\Delta q = \alpha_1 \cdot v_2^{[1]} + \alpha_2 \cdot v_2^{[2]}$$

We can then solve for $\Delta\lambda_\theta$ and $\Delta\lambda_q$ in terms of the forward time stable eigenvectors and the expressions for α_1 and α_2 in terms of $\Delta\theta$ and Δq. The expression for $\Delta\lambda_q$ can then be substituted back into Equation 5.5 to obtain the feedback expression shown in Equation 5.8.

$$\Delta\beta = K_{\beta_\theta} \cdot \Delta\theta + K_{\beta_q} \cdot \Delta q \tag{5.8}$$

5.2 Numerical Values of Feedback Gains

As noted above, any point on the zeroth-order outer solution provides an equilibrium point for the zeroth-order inner system given by Equation 5.3. Accordingly, the gain calculations described above can be carried out at any point along the outer solution. For our problem, this calculation leads to the following results for the gain history as shown in Figures 5.1a - 5.1b.

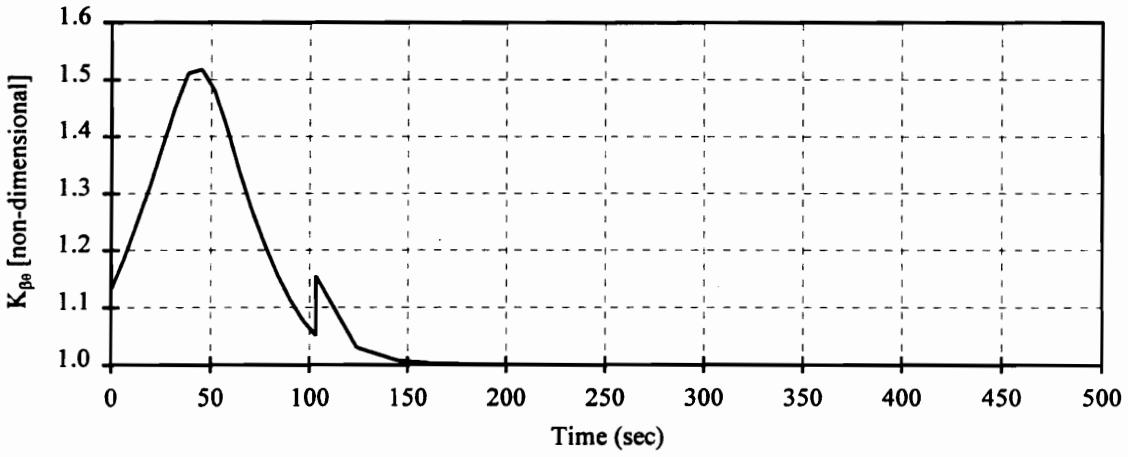

Figure 5.1a: Time History of Inner Problem Feedback Gain - K_{β_θ}

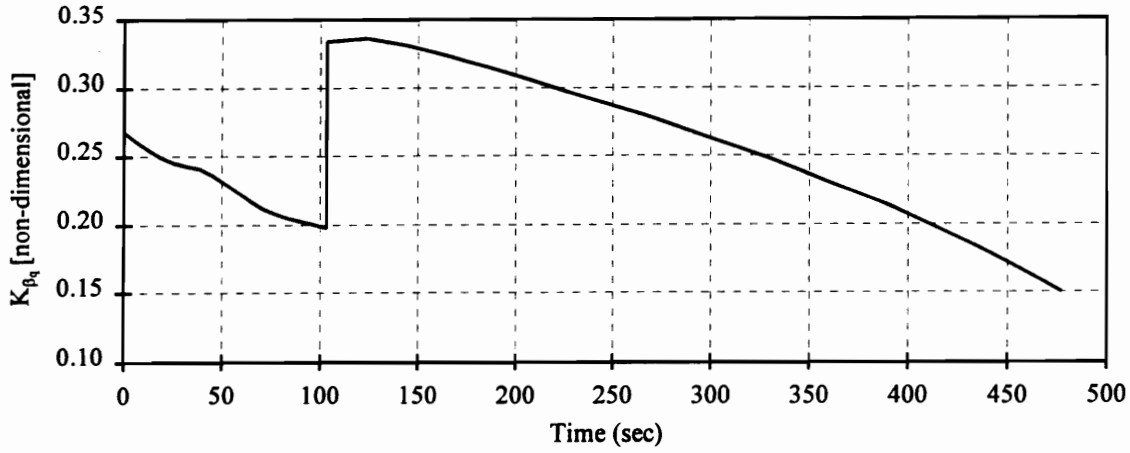

Figure 5.1b: Time History of Inner Problem Feedback Gain - K_{β_q}

Boundary Layer Corrections

The feedback law obtained for calculating the deviation in the gimbal angle, $\Delta\beta$, about the reference gimbal angle in terms of $\Delta\theta$ and Δq provides a means of tracking the equilibrium values θ^o and q^o along the trajectory. In addition, it also provides a means of recovering the point conditions on the *fast* state elements. For example, at initial time ($t=t_0$), the non-dimensional feedback gains K_{β_θ} and K_{β_q} are calculated as,

$$K_{\beta_\theta} = 1.1335$$

$$K_{\beta_q} = 0.2684$$

If the initial perturbations on θ and q are $\Delta\theta$=1 degree and Δq=0, Figure 5.2 shows how the *fast* state element perturbation $\Delta\theta$ tracks, as modeled by the linear system, to the equilibrium value of the reference trajectory. The correction to the reduced order problem near a point condition is termed a boundary layer correction.[14] Note that the time constant for this system is on the order of the time scale, τ_p (~6 sec), for the *fast* state elements. While there is no sharp relation between the time constant of the inner

closed-loop dynamics and the time scale for the *fast* state elements, one does expect that they will be on the same order of magnitude.

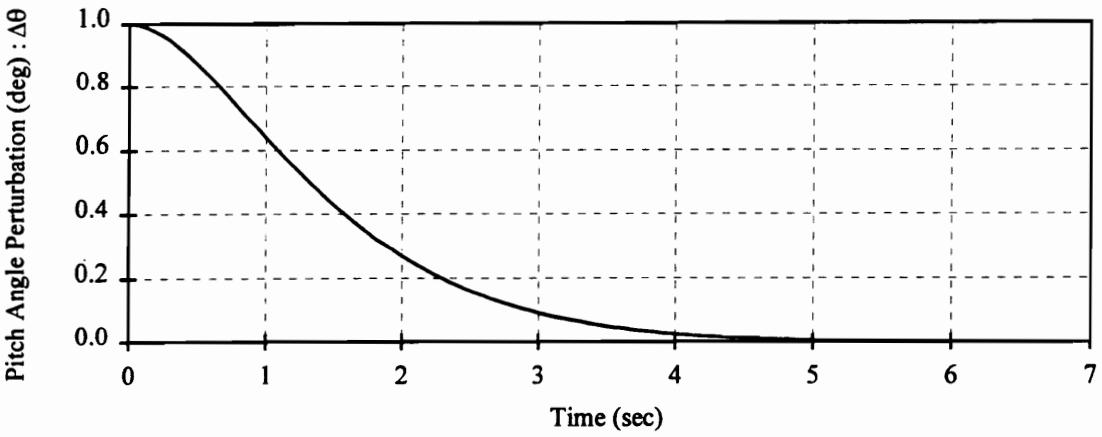

Figure 5.2 Example of Boundary Layer Correction at Time t_0

In addition to providing corrections to match the initial conditions on the *fast* state elements at time $t=t_0$, the staging condition of a zero angle of attack can also be incorporated. As the staging time is approached, a boundary layer correction, called a terminal layer, will be used to move the fast state elements off of the outer problem solution in order to meet the staging condition of zero angle of attack.[14] The backward stable gains are computed in the same manner as the initial layer feedback with the exception that the backward time stable eigenvectors are used in the gain calculation. If we then compute a boundary layer correction starting at the staging conditions and time $t = t_s^-$ and move backward in time, the fast elements will go to the equilibrium values of the outer problem solution.

Calculating the non-dimensional feedback gains at $t = t_s^-$ for the terminal layer, we obtain;

$$K_{\beta_0} = 1.0506$$

$$K_{\beta_q} = -0.1980$$

Note that upon comparing these gains with the forward time stable gains, we see that;

$$K_{\beta_\theta} \text{ (forward stable)} = K_{\beta_\theta} \text{ (backward stable)}$$

$$K_{\beta_q} \text{ (forward stable)} = -K_{\beta_q} \text{ (backward stable)}$$

Figure 5.3 shows an example of the terminal boundary layer correction for $\Delta\theta$ where the staging condition forces a correction in θ and q of $\Delta\theta=1$ and $\Delta q=0$.

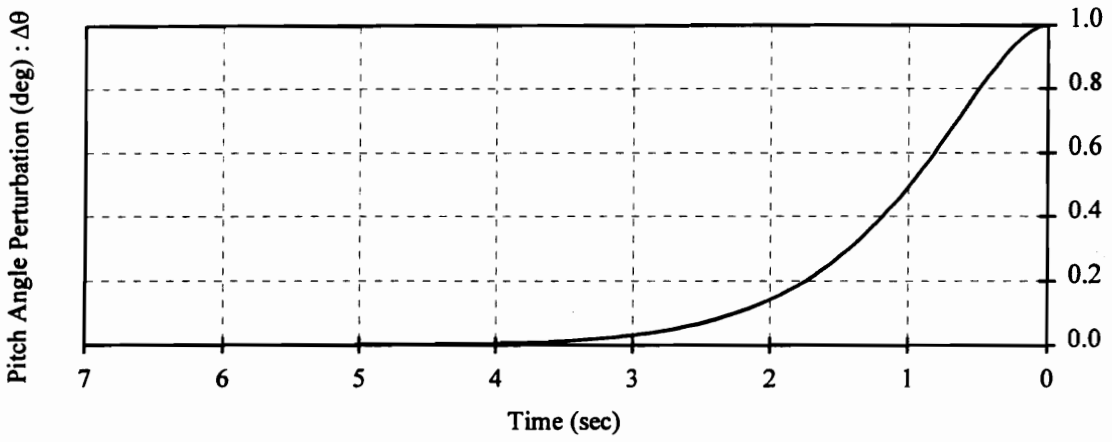

Figure 5.3 Example of Boundary Layer Correction at Time t_s^-

Just after staging, another boundary layer correction will be present to move from the staging conditions back to the equilibrium values of the reference trajectory. This correction is implemented in the same manner as the initial boundary layer correction at time $t=t_o$.

For our problem, we wish to simulate the launch of the trajectory in forward time from initial time, t_o, to final time, t_f. There is a problem in implementing the terminal boundary layer just before staging which is forward time unstable. In order to implement

the effects of the terminal boundary layer, we modify the correction process to use the forward time stable gains. The terminal boundary layer is then accomplished by switching the reference θ, that we are attempting to track, from θ^o obtained in the zeroth order outer solution, to γ^o at a time just before staging. The feedback will then drive $\alpha=\theta-\gamma$ to zero for staging. Just after staging, the reference θ for tracking will be switched back to θ^o obtained in the zeroth order outer solution. An example of the pitch angle, θ, and the angle of attack, α, near staging can be seen in Figures 5.4 and 5.5.

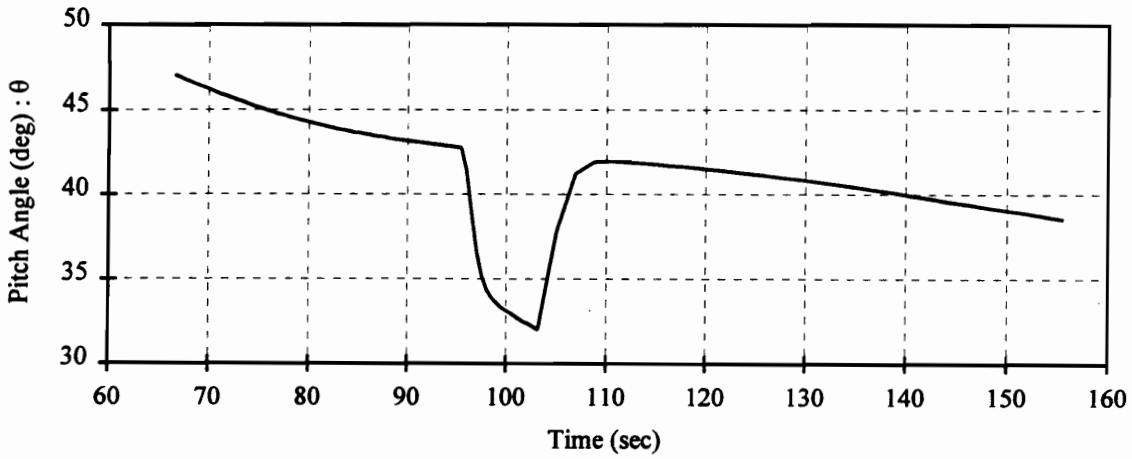

Figure 5.4: Example of Imposing Angle of Attack Constraint at Staging (Pitch Angle History)

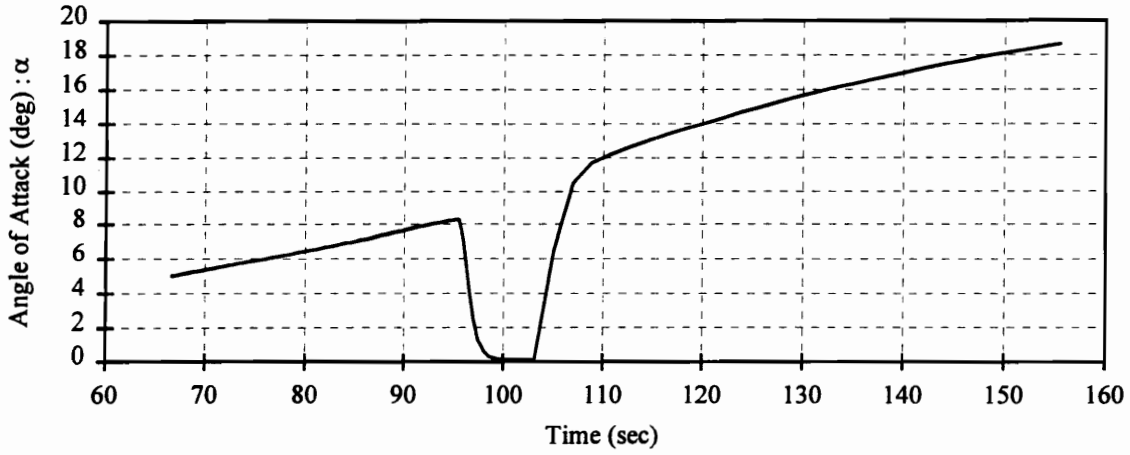

Figure 5.5 Example of Imposing Angle of Attack Constraint at Staging (Angle of Attack History)

Note that the angle of attack was not driven all the way to zero due to a reference pitch rate of zero. The fact that the reference pitch rate is zero causes a tracking error to be present throughout the trajectory as the control attempts to track a changing pitch orientation while attempting to keep the pitch rate at zero.

6.0 NEIGHBORING OPTIMAL CONTROL

Now that a method has been constructed to account for perturbations and point constraints on the *fast* state elements, we need to investigate correcting for perturbations in the *slow* state elements. With feedback for the *fast* state elements only, perturbations in the *slow* state elements will not be corrected and the launch vehicle may move away from the desired launch trajectory. In order to construct a feedback system for the *slow* state elements, neighboring optimal control theory will be used.

The idea behind neighboring optimal control is to look at the optimal solution already obtained as one solution in a family of optimal solutions.[7] This idea can be explained with the use of Figure 6.1 which shows a family of optimal trajectories.

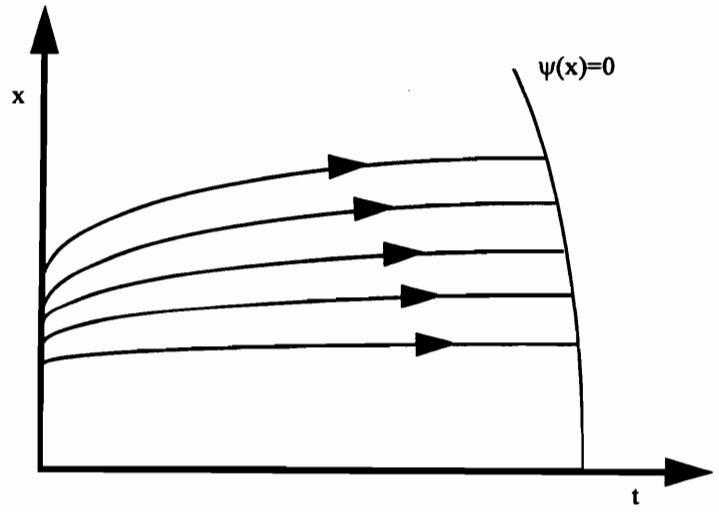

Figure 6.1: Neighboring Optimal Control Illustration

Associated with each value of x, where $x \in R^n$, is a control u such that x will proceed along its optimal path to the terminal condition $\psi(x)$. If there is a perturbation in x at an arbitrary time, there will be a new optimal path and associated $u(\bullet)$ along which x can

proceed to the terminal condition $\psi(x)$. The idea of neighboring optimal control is to determine how the associated control $u(\bullet)$ changes with perturbations in x. Note that with a perturbation in x we obtain a new control $u(\bullet)$ that will move x along a new optimal path to the terminal condition $\psi=0$ and not attempt to return x to its initial reference trajectory.

First Order Expansion of Control Structure

With the solution of the reduced order optimization problem, the control functions $u^{o}(t)$ are obtained. These functions are open loop controls and will not account for perturbations off the corresponding optimal trajectory. Hence, if uncertainties in the initial conditions or flight environment are encountered the trajectory flown using the control function $u^{o}(t)$ will deviate from the desired path. In order to alleviate this problem a method of correcting for perturbations in the trajectory must be implemented. This can be accomplished by feeding back information about the present trajectory and comparing it with the reference or nominal trajectory. If a difference exists between the present and reference trajectory then the control input can be modified in an attempt to correct for the perturbation in the trajectory.

We want to have the ability to correct for perturbations in the *slow* state elements: r, V, γ, and m. We do not need to correct for perturbations in ϕ since it does not appear in the right hand side of any of the differential equations or in any of the constraints. If a Taylor series expansion is carried out to first order on the control functions with respect to the *slow* states elements, we obtain:

$$\beta(t) = \beta^{o}(t) + \sum \frac{\partial \beta}{\partial x_i}(t) \cdot \Delta x_i(t)$$

$$\theta(t) = \theta^{o}(t) + \sum \frac{\partial \theta}{\partial x_i}(t) \cdot \Delta x_i(t) \qquad \text{where } x_i = [r, V, \gamma, m].$$

The control $q(t)$=0 results from all trajectories due to the imposed algebraic constraints and hence does not require expansion. The partial derivatives, $\frac{\partial \beta}{\partial x_i}$ and $\frac{\partial \theta}{\partial x_i}$, of the control with respect to the *slow* state elements are about the reference trajectory and the state perturbations are defined as $\Delta x_i = x - x^\circ$.

Feedback Gain Calculation

For our example a numerical approximation to the partial derivatives will be calculated. A numerical approximation is one of the reasons for using an indirect method, with its greater accuracy, to obtain a solution to the outer problem. The simplest method for obtaining the numerical approximation is to perturb the initial conditions one at a time about the reference trajectory initial conditions and resolve the optimization problem. The forward difference approximation for the partial derivative can then be expressed as follows:

$$\frac{\partial u}{\partial x_i} = \frac{u - u^\circ}{x - x^\circ}.$$

Although this method is straight-forward, the optimization problem must be resolved for each state perturbation. In addition, this method only results in the partial derivative approximation valid at the initial time. To obtain approximations for other points along the trajectory, the perturbations about the reference trajectory must be made at different points along the path. The optimization problem must then be resolved for each perturbation from the time of the perturbation to the end of the trajectory. For example, if the problem being solved has four state variables and the partial derivatives are desired at ten points along the trajectory, then forty optimal solutions must be solved in addition to that of the reference trajectory.

An alternate method, and the one used for our problem, is to obtain partial derivative approximations along the entire trajectory using trajectories perturbed only at the initial point.[17] For any arbitrary point in the trajectory, we can expand the perturbation in control from the nominal trajectory as follows.

$$\Delta u = \frac{\partial u}{\partial r}\Delta r + \frac{\partial u}{\partial V}\Delta V + \frac{\partial u}{\partial \gamma}\Delta\gamma + \frac{\partial u}{\partial m}\Delta m$$

At this point we note an additional modification to the neighboring optimal approach. In lieu of introducing perturbations at a given value of time and computing the required change in u(t), we instead will use the vehicle mass as the independent variable. Since the mass is monotonically decreasing, it is suitable for use as an independent variable. Thus we have

$$\begin{aligned}\Delta u(m) &= \frac{\partial u}{\partial r}\Delta r + \frac{\partial u}{\partial V}\Delta V + \frac{\partial u}{\partial \gamma}\Delta\gamma \\ &= \mathrm{K}_{u_r}\Delta r + \mathrm{K}_{u_V}\Delta V + \mathrm{K}_{u_\gamma}\Delta\gamma\end{aligned}$$

where the gains are now indexed by the mass of the vehicle and $\frac{\partial u}{\partial m}$ does not need to be calculated.

This selection of mass as the new independent variable is not an arbitrary choice. In order to calculate the numerical approximation to the partial derivative a method of indexing trajectories for comparison must be set. It has been shown by Kelley[18], that comparisons based on cost remaining to the expected final cost as given by the performance index is the best method. It is not a good idea to use the time since launch since some perturbations may move us along the nominal trajectory. Figure 6.2 illustrates this point. Suppose at an arbitrary time $\hat{t}$ we are at point A, $\mathrm{x} = \mathrm{x}(\hat{t})$, on a neighboring extremal to our nominal trajectory. It is a better to choice to use point C on the nominal trajectory as the reference point as opposed to point B, $\mathrm{x} = \mathrm{x}^{\circ}(\hat{t})$. This type

of comparison is termed a transverse comparison and compares the trajectories based upon lines of equal cost to go.

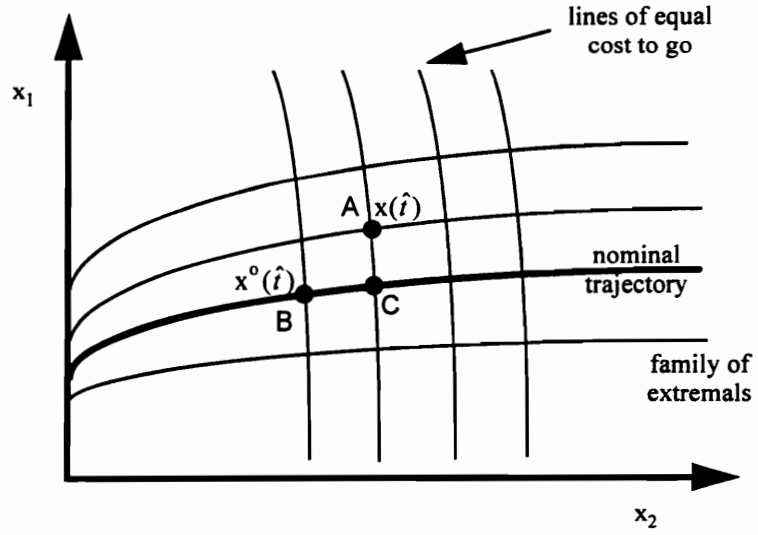

Figure 6.2: Transverse Comparison Illustration

For our problem, the cost is the negative of the final mass. Therefore, during the second stage of flight for our problem, the value of mass-to-go is used to index trajectories for comparison and calculating the approximation to the partial derivative. During the first stage of flight the trajectories will be compared based on the value of mass-to-staging. This method of comparison was selected since staging occurs at a specified value of the mass. For trajectories that have mass perturbations that take them outside the range of mass of the reference trajectory, the reference trajectory values are extrapolated.

If we perturb each of the remaining states, either one at a time or in three differing combinations, and reoptimize to obtain three trajectories, we will have a system of three equations and three unknowns at each point along the trajectory. In principle, this system can be solved for an approximation to each of the partial derivatives if all of the state perturbations are non-zero throughout the trajectory. To avoid the difficulties with

encountering a zero perturbation, additional trajectories can be included in the solution process. This process will produce an overdetermined system of linear equations that will be solved for using a least squares approximation to the partial derivatives.[17] For our example problem, we computed eight perturbed trajectories listed in Table 6.1.

Table 6.1: Trajectory Perturbations for Example Problem

Perturbed Trajectory	Δr	ΔV	$\Delta\gamma$
1	+ 1 % in alt.	+ 1 %	+ 1 %
2	+ 1 % in alt.	+ 1 %	- 1 %
3	+ 1 % in alt.	- 1 %	+ 1 %
4	- 1 % in alt.	+ 1 %	+ 1 %
5	- 1 % in alt.	- 1 %	+ 1 %
6	- 1 % in alt.	+ 1 %	- 1 %
7	+ 1 % in alt.	- 1 %	- 1 %
8	- 1 % in alt.	- 1 %	- 1 %

In addition, care must be taken to handle the possibility that the numerical approximation "blows up" near the terminal constraint. This problem occurs because the respective values of some of the state elements in the different trajectories converge to the same value at the terminal time as required by the boundary conditions. When this convergence happens the denominator of the numerical approximation goes to zero and the gain "blows up".

This numerical problem did occur while calculating the gains for the orbital insertion problem. The problem was handled by limiting the gains near terminal time such that the gains were linearly extrapolated from a point before divergence.

Slow State Element Feedback Gains

The *slow* state feedback gains obtained for this problem are shown in Figures 6.3 - 6.8, as scheduled as a function of mass. Note that the gap in the plots is due to the discontinuity in mass which occurs at staging.

The numerical problem with the gain calculation can be seen in Figures 6.6 and 6.8 where the gains are beginning to show the divergent behavior as the mass approaches its minimum value. Remember that as time progresses forward in the trajectory the plots should be read right to left.

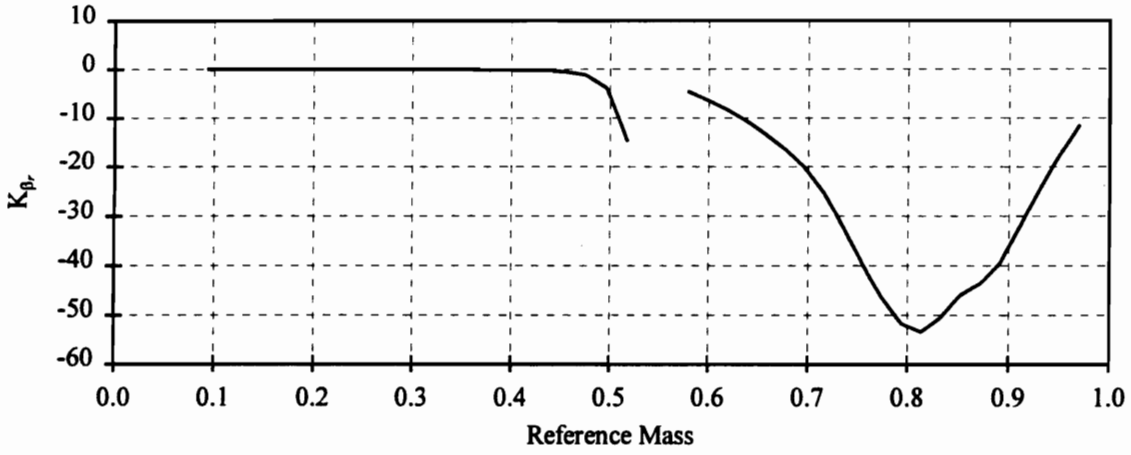

Figure 6.3: Neighboring Optimal Control Gain - K_{β_r}

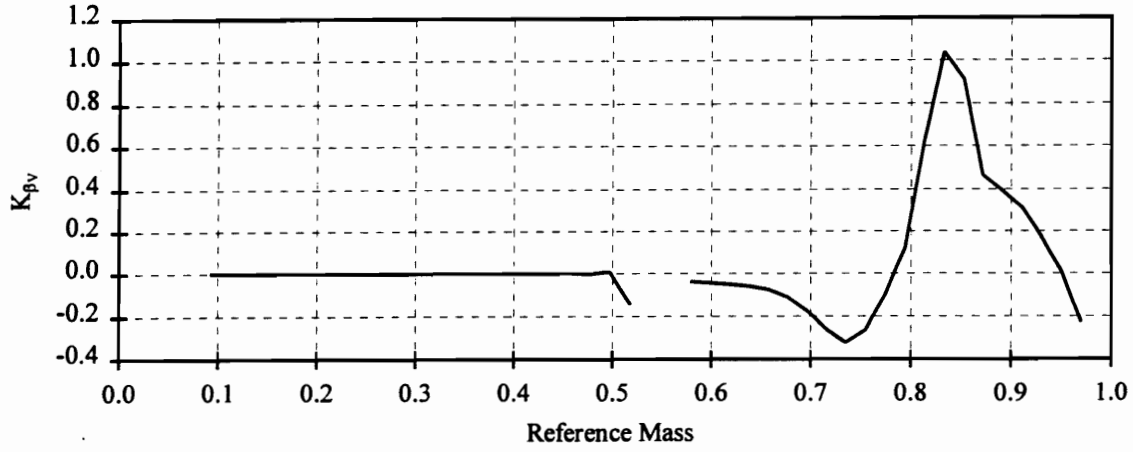

Figure 6.4: Neighboring Optimal Control Gain - K_{β_v}

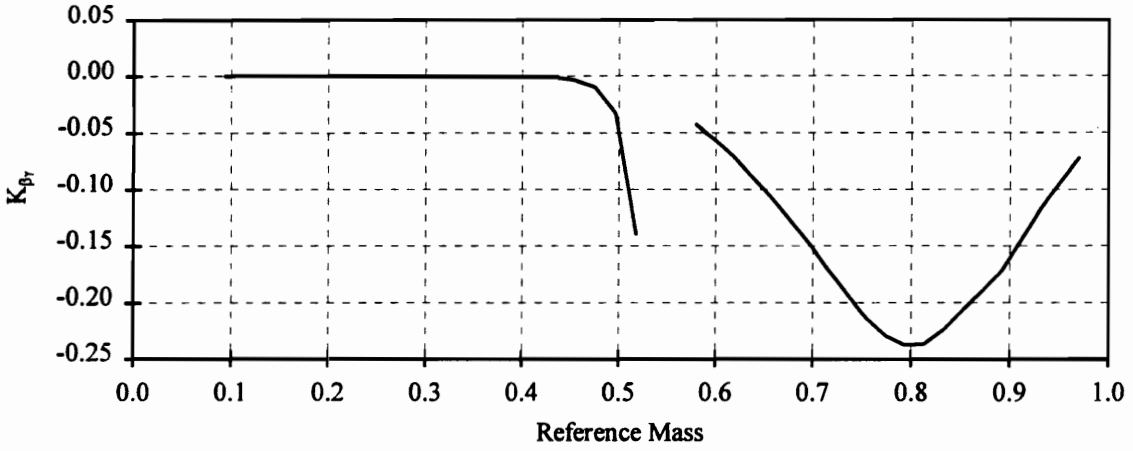

Figure 6.5: Neighboring Optimal Control Gain - K_{β_γ}

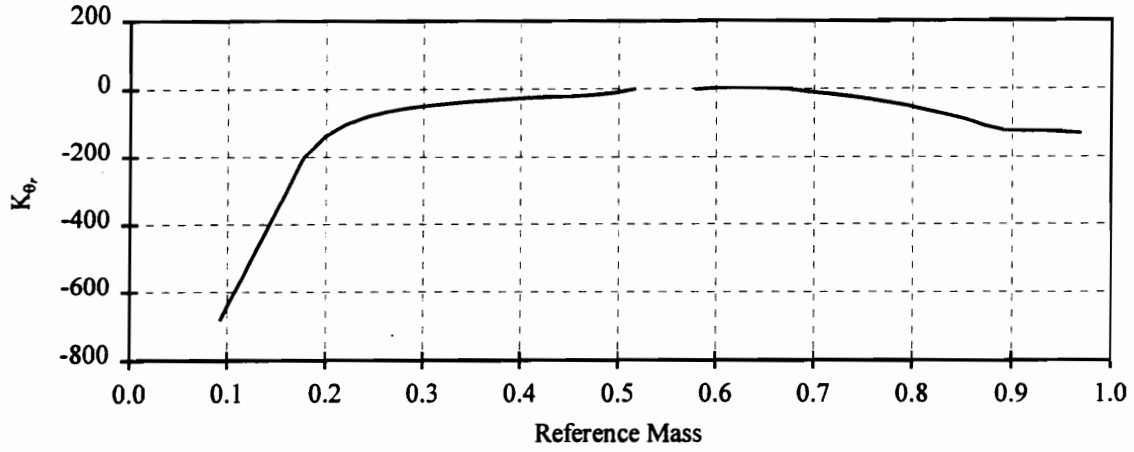

Figure 6.6: Neighboring Optimal Control Gain - K_{θ_r}

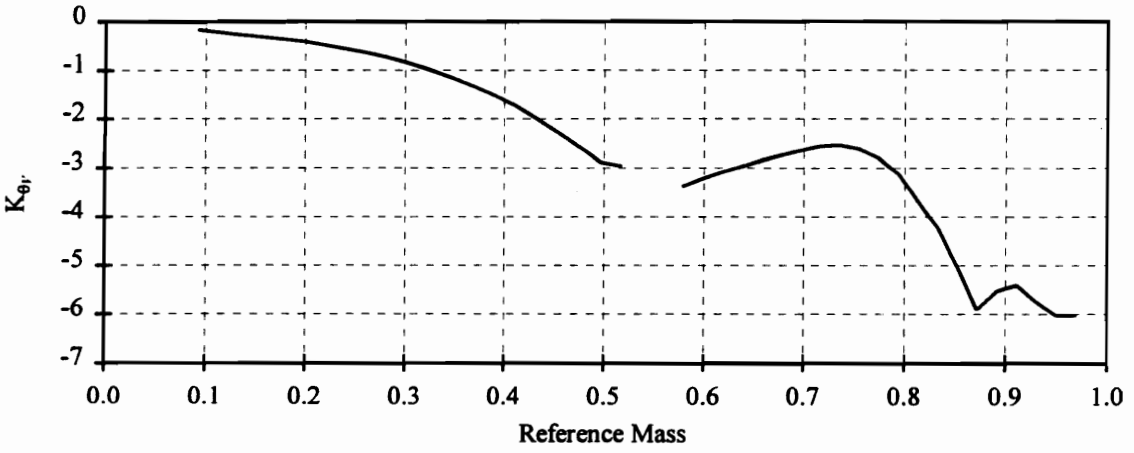

Figure 6.7: Neighboring Optimal Control Gain - K_{θ_v}

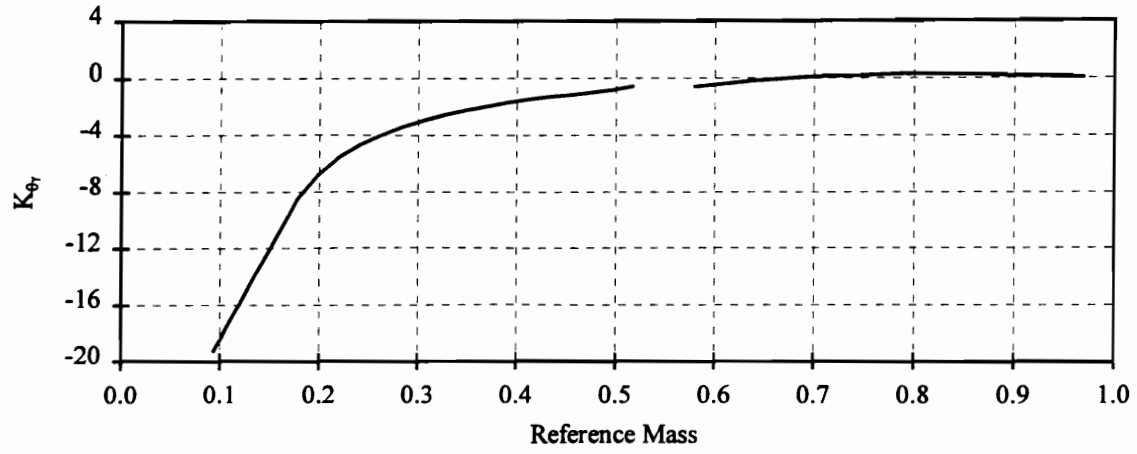

Figure 6.8: Neighboring Optimal Control Gain - K_{θ_γ}

The *fast* state element feedback gains are also scheduled as a function of mass and are shown in Figure 6.9 and 6.10.

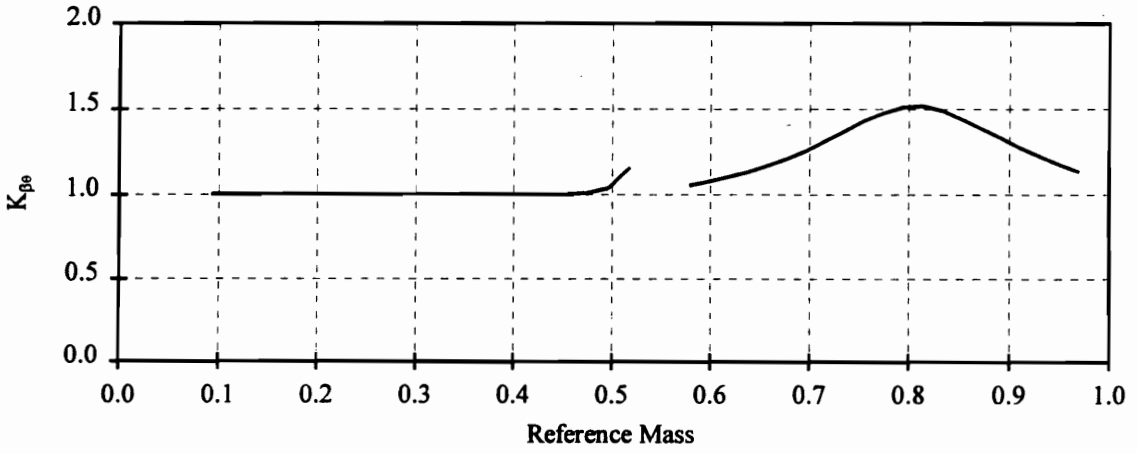

Figure 6.9: Singular Perturbation Control Gain - K_{β_θ}

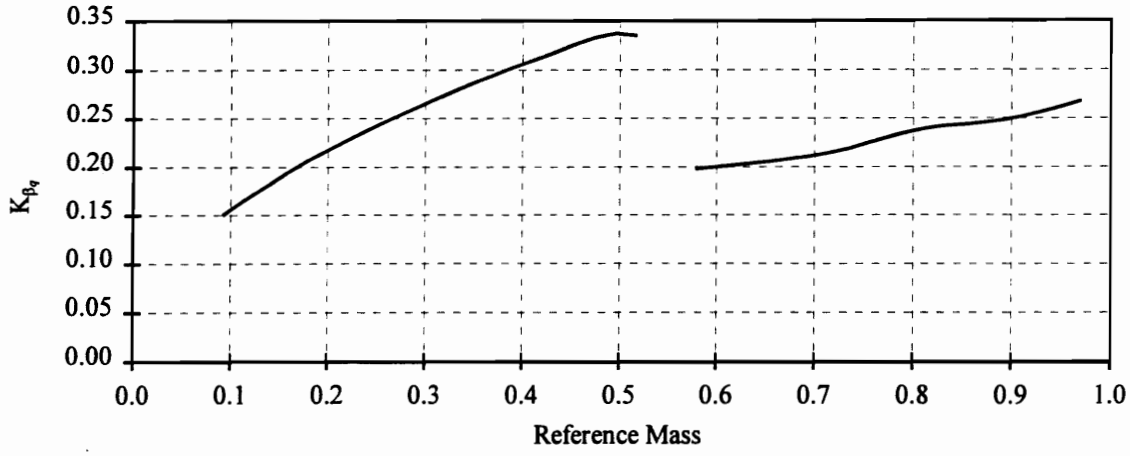

Figure 6.10: Singular Perturbation Control Gain - K_{β_q}

7.0 FEEDBACK RESULTS

7.1 Formulated Control Structure

In order to launch the vehicle into a desired orbit, a method of setting the vehicle controls must be determined. In Chapter 3 we outlined a procedure to obtain an optimal control history based on a point mass model of the vehicle. Then, in Chapter 4, the control histories β°, θ°, and q° were presented. In Chapter 5, using ideas of Singular Perturbation Theory the controls θ and q were elevated back to state variables to describe the pitch dynamics of the vehicle. A feedback implementation was then developed to provide deviations to the control $\beta^{\circ}(t)$ in order to have the state elements $\theta(t)$ and $q(t)$ track their reference values presented in Chapter 4.

$$\beta(t) = \beta^{\circ}(t) + K_{\beta_\theta} \cdot [\theta - \theta^{\circ}(t)] + K_{\beta_q} \cdot [q - q^{\circ}(t)]$$

In Chapter 6, the ideas of neighboring optimal control were used in order to provide a feedback implementation for vehicle guidance based on perturbations in the outer problem initial conditions. The independent variable used was also changed from time to mass in order to compare different trajectories and numerically calculate feedback gains. In addition to the deviation to the control $\beta^{\circ}(m)$, deviations to $\theta^{\circ}(m)$ and $q^{\circ}(m)$ were also obtained. The resulting control structure obtained after applying the ideas of both Singular Perturbation Theory and neighboring optimal control is;

$$\begin{aligned}\beta(m,r,V,\gamma,\theta,q) = \beta^{\circ}(m;r,V,\gamma) &+ K_{\beta_\theta}(m) \cdot [\theta - \theta^{\circ}(m;r,V,\gamma)] \\ &+ K_{\beta_q}(m) \cdot [q - q^{\circ}(m;r,V,\gamma)]\end{aligned}$$

where

$$\beta^{\circ}(m;r,V,\gamma) = \beta^{\circ}(m) + K_{\beta_r}(m)\cdot[r - r^{\circ}(m)] + K_{\beta_V}(m)\cdot[V - V^{\circ}(m)] + K_{\beta_\gamma}(m)\cdot[\gamma - \gamma^{\circ}(m)]$$

$$\theta^{\circ}(m;r,V,\gamma) = \theta^{\circ}(m) + K_{\theta_r}(m)\cdot[r - r^{\circ}(m)] + K_{\theta_V}(m)\cdot[V - V^{\circ}(m)] + K_{\theta_\gamma}(m)\cdot[\gamma - \gamma^{\circ}(m)]$$

$$q^{\circ}(m;r,V,\gamma) \equiv 0 \qquad \text{[due to the algebraic constraints]}$$

As can be seen, in order to implement this control structure we need:

1) The nominal state and control histories obtained by the solution of the outer problem; $r^{\circ}(m)$, $V^{\circ}(m)$, $\gamma^{\circ}(m)$, $\beta^{\circ}(m)$, $\theta^{\circ}(m)$, and $q^{\circ}(m)$; given in Chapter 4,
2) The singular perturbation feedback gains; $K_{\beta_\theta}(m)$ and $K_{\beta_q}(m)$; given in Chapter 5.
3) The neighboring optimal control gains; $K_{\beta_r}(m)$, $K_{\beta_V}(m)$, $K_{\beta_\gamma}(m)$, $K_{\theta_r}(m)$, $K_{\theta_V}(m)$, and $K_{\theta_\gamma}(m)$; given in Chapter 6.

7.2 Implementation of Control Structure

Using a FORTRAN simulation the feedback implementation of the orbital insertion problem was modeled. This simulation modeled the vehicle as described in Chapter 2 with the control, β, calculated based on the feedback structure previously developed. Figures 7.1 through 7.13 show the resulting feedback trajectory without imposing the angle of attack constraint at staging along with the point mass model trajectory shown for reference.

Figure 7.1a shows that the feedback trajectory flies a slightly higher profile than the reduced order (point mass) model. Shown in Figure 7.1b is the difference in the two altitude profiles. This difference is due to the reference inertial pitch rate of zero which

causes a tracking error as the vehicle attempts to pitch over while keeping a zero pitch rate. As a result of this conflict, the pitch orientation lags behind the reference model and the vehicle flies a higher profile. This effect is also seen in Figures 7.4 and 7.6.

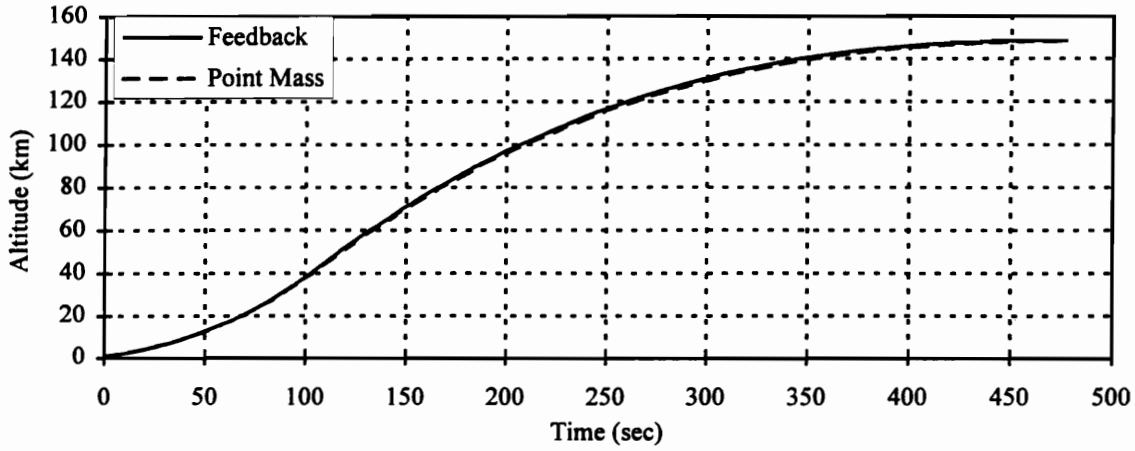

Figure 7.1a: Altitude Comparison between Feedback Trajectory without Alpha Constraint and Point Mass Reference Trajectory

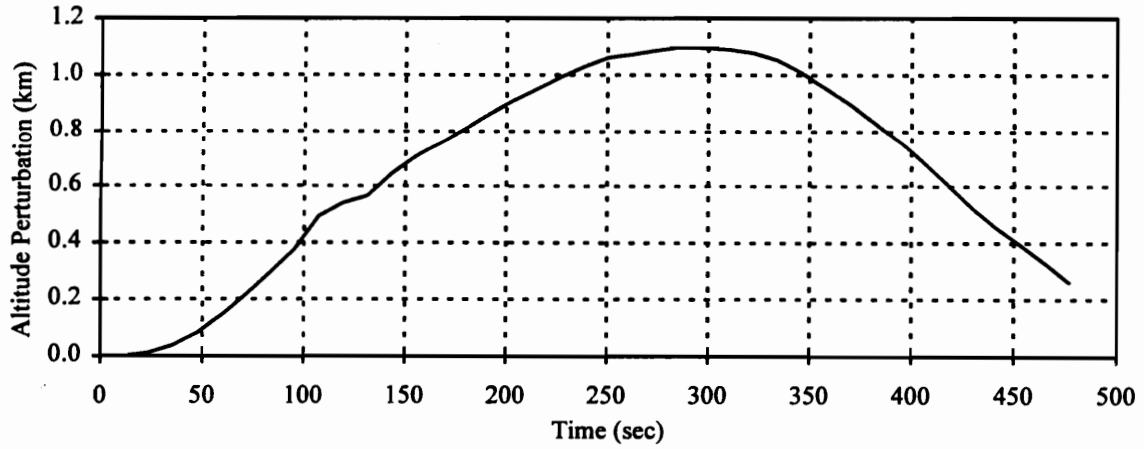

Figure 7.1b: Altitude Perturbation of Feedback Trajectory without Alpha Constraint from Point Mass Reference Trajectory

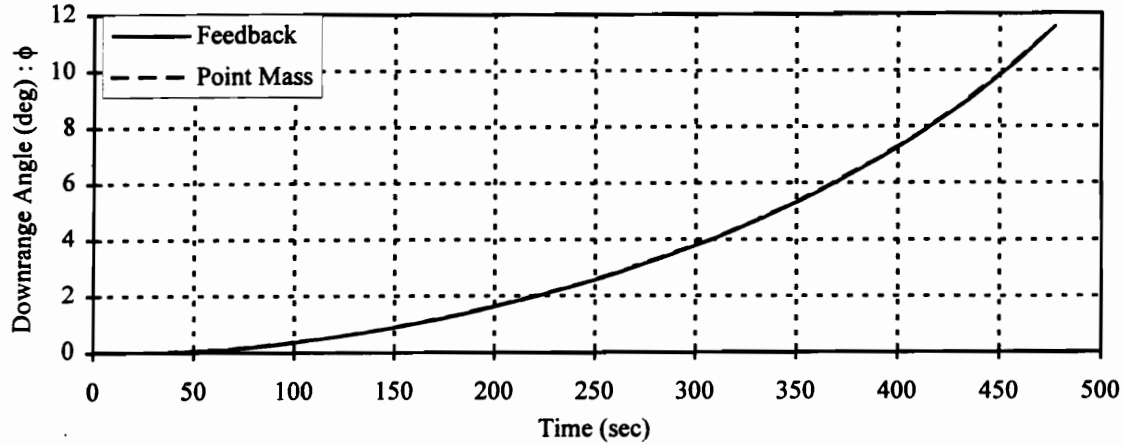

Figure 7.2: Downrange Angle Comparison between Feedback Trajectory without Alpha Constraint and Point Mass Reference Trajectory

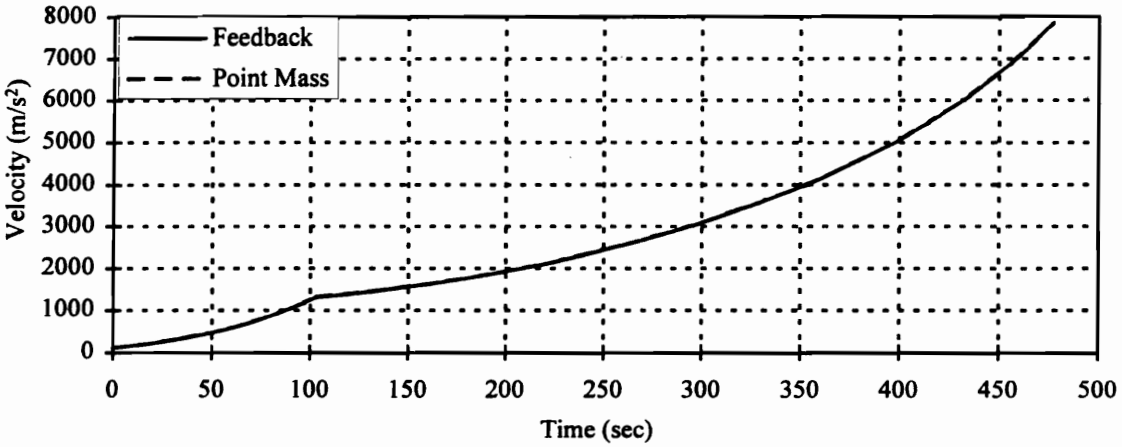

Figure 7.3: Velocity Comparison between Feedback Trajectory without Alpha Constraint and Point Mass Reference Trajectory

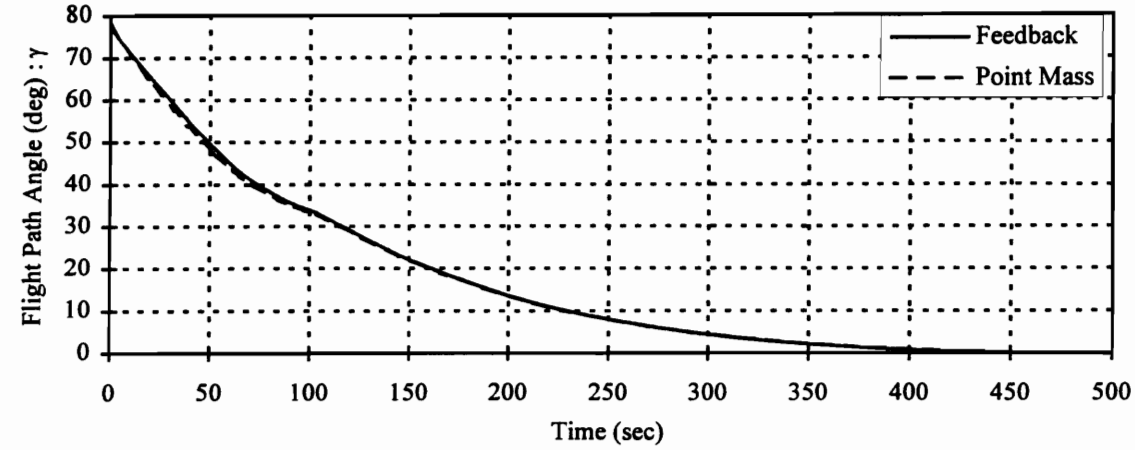

Figure 7.4: Flight Path Angle Comparison between Feedback Trajectory without Alpha Constraint and Point Mass Reference Trajectory

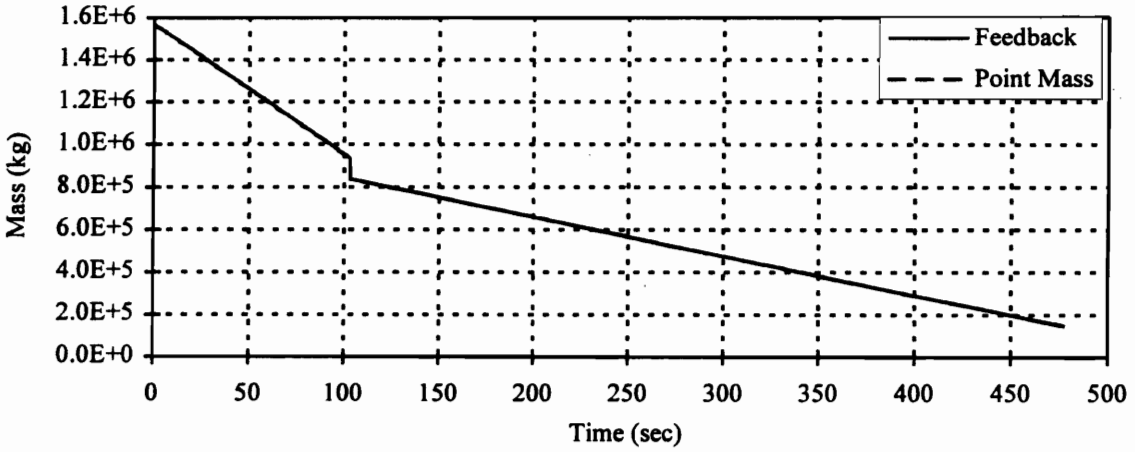

Figure 7.5: Mass Comparison between Feedback Trajectory without Alpha Constraint and Point Mass Reference Trajectory

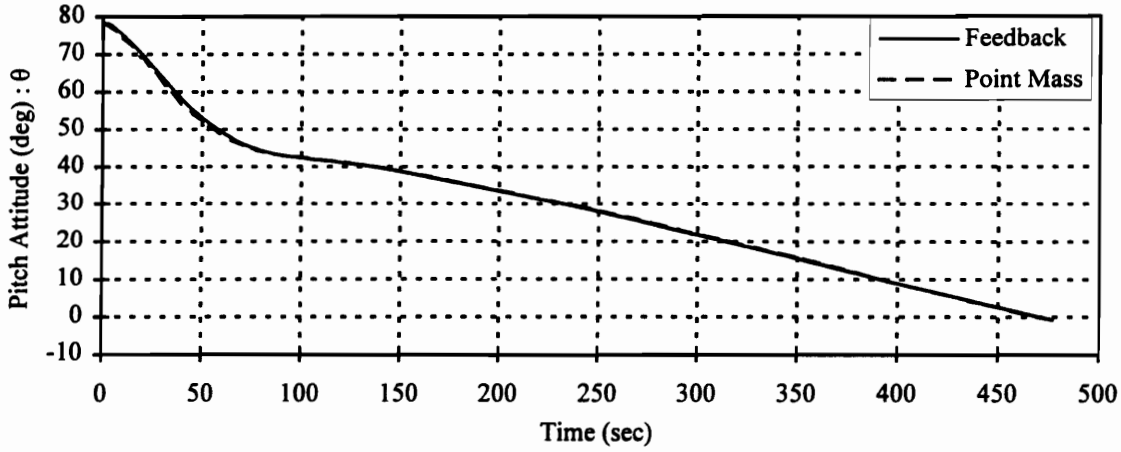

Figure 7.6: Pitch Attitude Comparison between Feedback Trajectory without Alpha Constraint and Point Mass Reference Trajectory

In Figure 7.7, we see the pitch rate of the feedback and point mass models. The pitch rate calculated by the point mass model can be seen to be identically zero due to the imposed algebraic constraint. The pitch rate for the feedback model is initially positive as the vehicle makes an initial boundary layer correction to obtain a positive angle of attack and then begins pitching over. At staging the pitch rate dips as the vehicle attempts to track the reference pitch attitude that has a discontinuity at staging.

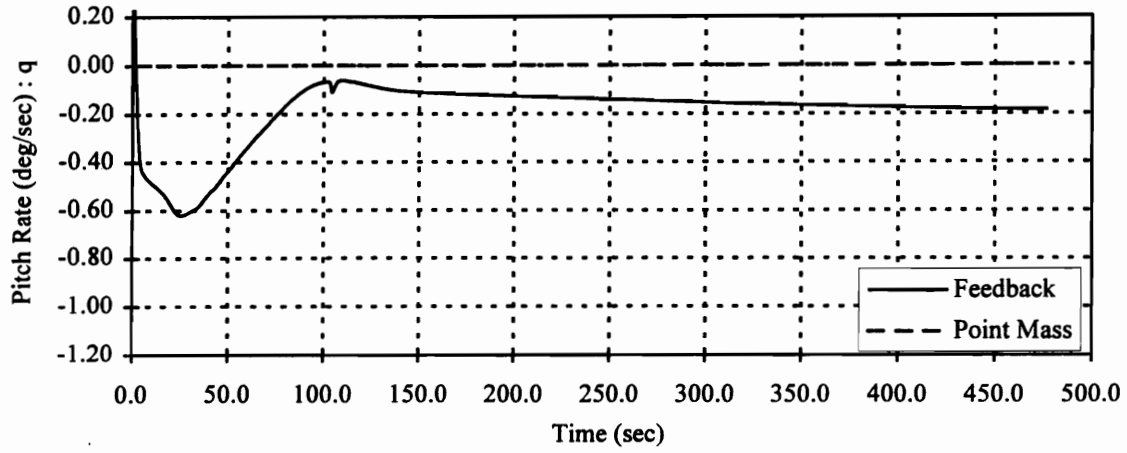

Figure 7.7: Pitch Rate Comparison between Feedback Trajectory without Alpha Constraint and Point Mass Reference Trajectory

Differences can also be seen in the engine gimbal angle shown in Figure 7.8. The difference is partially due to the tracking errors previously mentioned and partially due to the allowance of an external moment on the vehicle by the feedback trajectory.

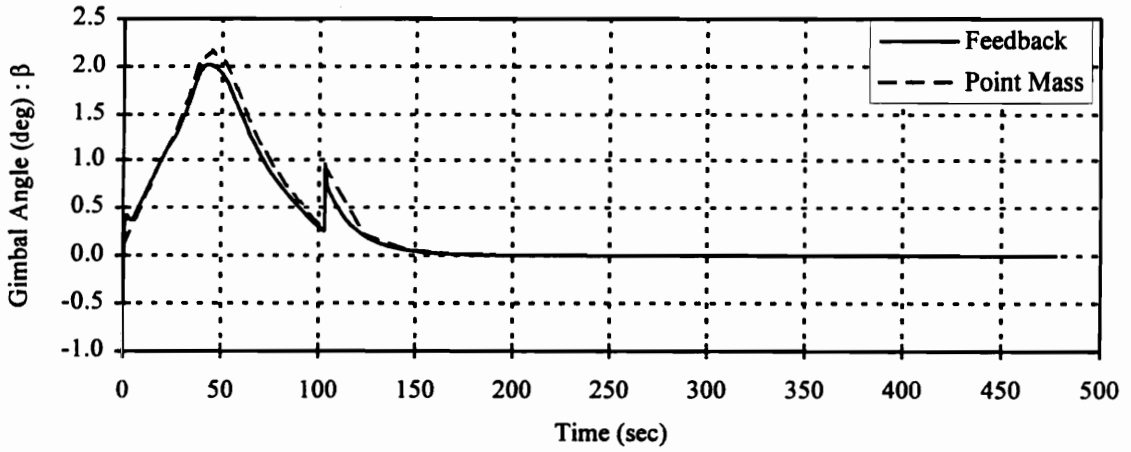

Figure 7.8: Gimbal Angle Comparison between Feedback Trajectory without Alpha Constraint and Point Mass Reference Trajectory

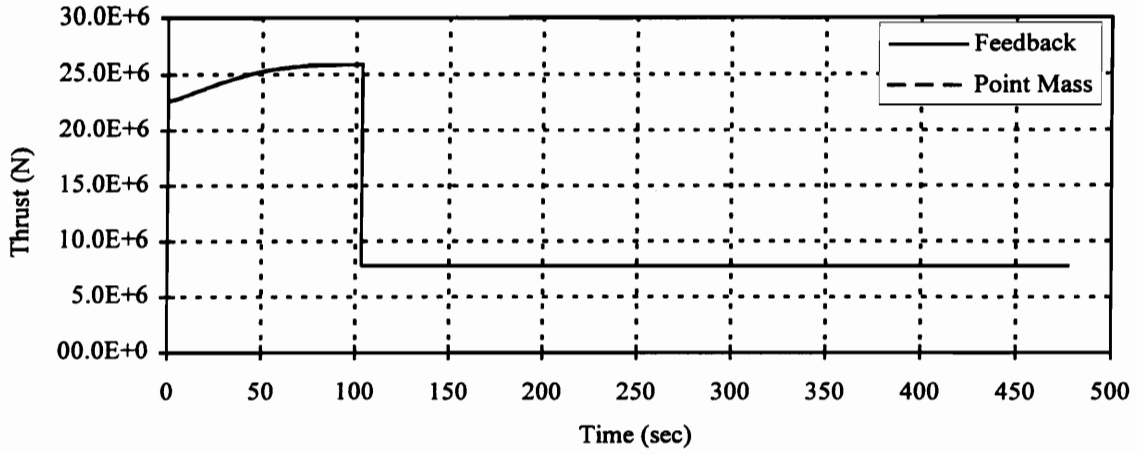

Figure 7.9: Thrust Comparison between Feedback Trajectory without Alpha Constraint and Point Mass Reference Trajectory

In Figure 7.10 the angle of attack history for the two models can be seen. The differences in the histories is attributed to the tracking of the reference pitch orientation. It is interesting to note the correspondence between the differences seen in the angle of attack plots and the gimbal angle plots. Notice that when the angle of attack for the feedback trajectory is above that of the point mass model (during the first 25 seconds) the gimbal angle for the feedback trajectory is also above that of the point mass model. During the middle portion of the flight, the feedback angle of attack and gimbal angle are both below that of the point mass model. This correspondence is a result of the relation between the moments produced as a result of the angle of attack and the gimbal angle. The vehicle is aerodynamically unstable in pitch, thus a positive gimbal angle is needed to counter a positive angle of attack. During the final portion of the flight the aerodynamic moment approaches zero due to the thin atmosphere, noted by the dynamic pressure profile shown in Figure 7.11, and thus the correspondence between the gimbal angle and the angle of attack diminishes.

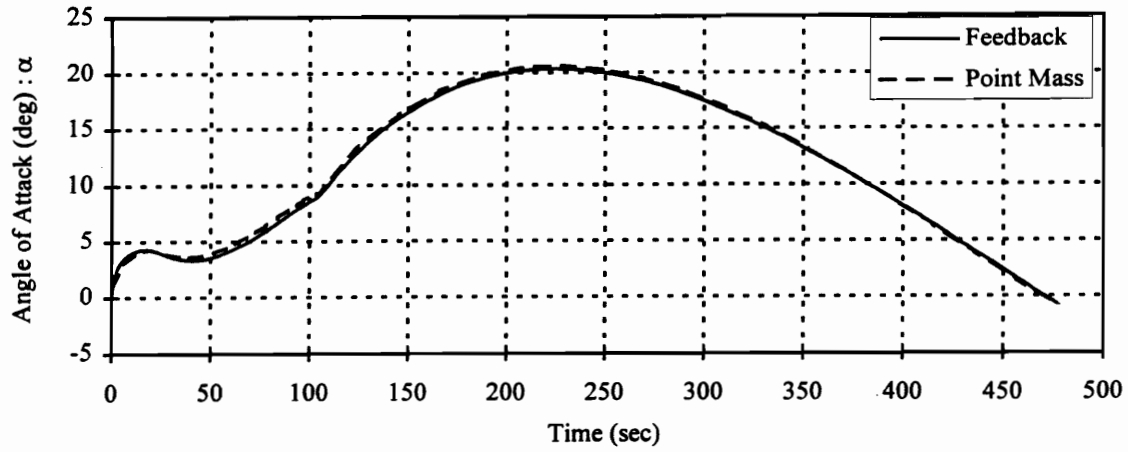

Figure 7.10: Angle of Attack Comparison between Feedback Trajectory without Alpha Constraint and Point Mass Reference Trajectory

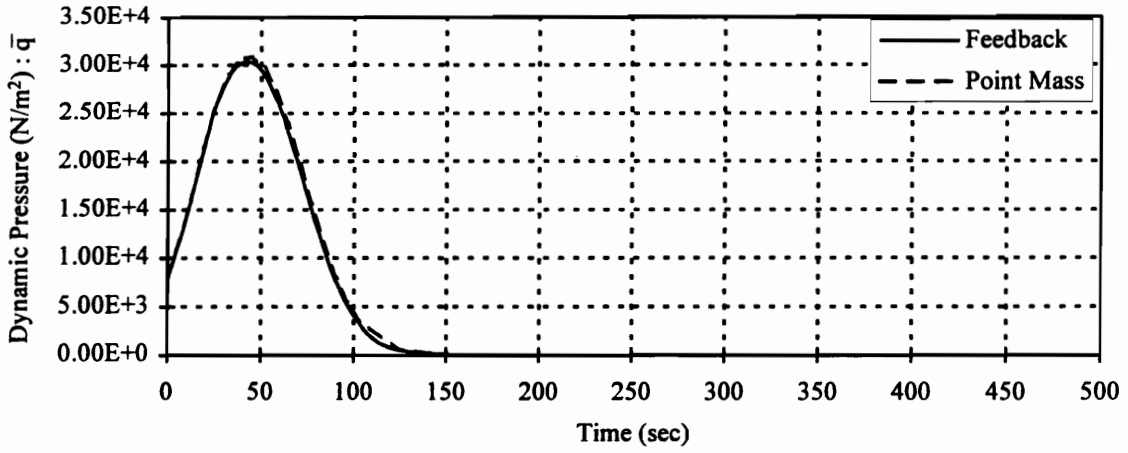

Figure 7.11: Dynamic Pressure Comparison between Feedback Trajectory without Alpha Constraint and Point Mass Reference Trajectory

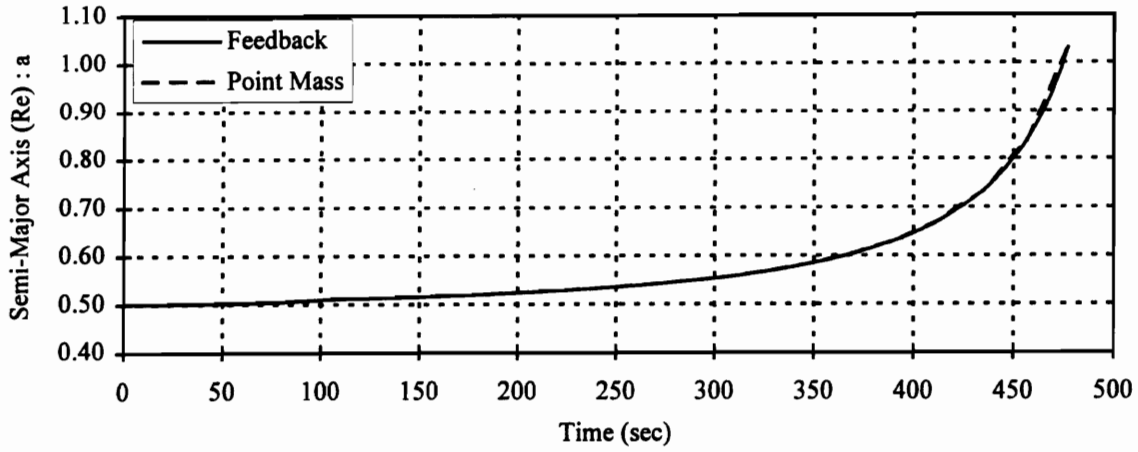

Figure 7.12: Semi-Major Axis Comparison between Feedback Trajectory without Alpha Constraint and Point Mass Reference Trajectory

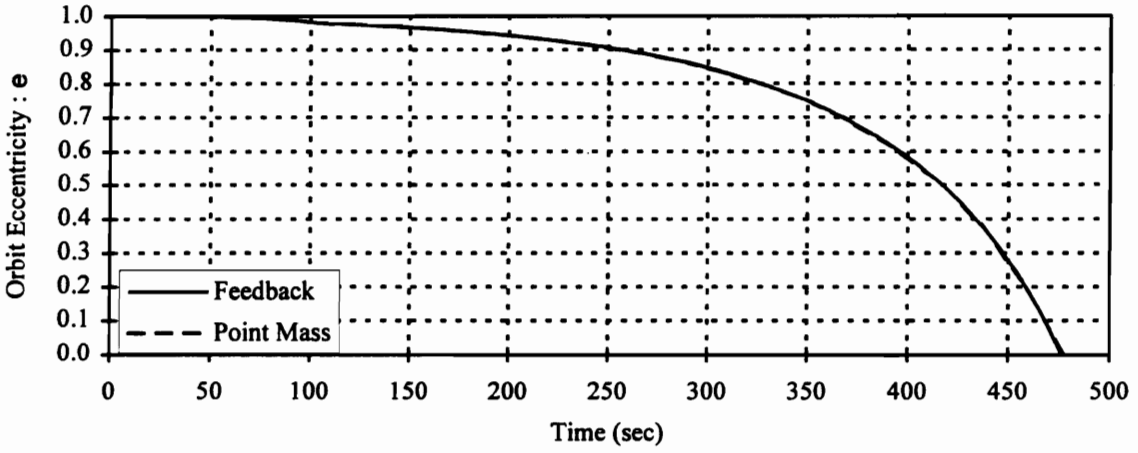

Figure 7.13: Orbit Eccentricity Comparison between Feedback Trajectory without Alpha Constraint and Point Mass Reference Trajectory

Table 7.1 shows the terminal conditions for the point mass and feedback trajectories. The feedback trajectories were considered to have reached terminal conditions when the desired semi-major axis was reached. As can be seen the feedback trajectory is slightly less efficient due to the errors in tracking the nominal trajectory. Recall that the desired perigee and apogee of the orbit are 148.164 km and 277.813 km respectively.

Table 7.1 :

	$a(t_f)$ (Re)	$e(t_f)$	Perigee (km)	Apogee (km)	$m(t_f)$ (kg)	t_f (sec)
Point Mass	1.0334	0.98354×10^{-2}	148.164	277.813	0.14992×10^{6}	477.20
Feedback	1.0334	0.98498×10^{-2}	148.069	277.908	0.14988×10^{6}	477.22

7.3 Perturbations in Initial Conditions

The initial conditions were then perturbed to see the effects on the feedback trajectories. The perturbations were made large enough to make these effects visible. Table 7.2 shows the terminal condition for these trajectory runs. As expected the initial positive perturbations in altitude and velocity resulted in less fuel being used. The initial perturbation in flight path angle did not result in a significant difference in fuel consumption but did effect the orbit eccentricity the most. The trajectory with the mass perturbation had the longest time of flight and hence burnt the most fuel as a result of having more mass to boost into orbit.

Table 7.2 :

Perturbation	$a(t_f)$ (Re)	$e(t_f)$	Perigee (km)	Apogee (km)	$m(t_f)$ (kg)	t_f (sec)
+ 5% in altitude; Δr	1.0334	0.97167×10^{-2}	148.946	277.031	0.14998×10^{6}	477.17
+ 5% ΔV	1.0334	0.97182×10^{-2}	148.937	277.040	0.15041×10^{6}	476.93
+ 5% $\Delta\gamma$	1.0334	0.97017×10^{-2}	149.045	276.932	0.14988×10^{6}	477.22
+ 2% Δm	1.0334	0.98781×10^{-2}	147.883	278.094	0.15301×10^{6}	480.64

7.4 Angle of Attack Constraint at Staging

The angle of attack constraint at staging is now imposed. This constraint forces the angle of attack to zero at staging in order to reduce the aerodynamic loads on the vehicle at this point. As discussed in Chapter 5, this constraint is included by switching the commanded pitch attitude from the reference pitch attitude obtained by the point mass model and modified by the neighboring optimal control feedback gains, to the flight path angle. The feedback will then attempt to drive the angle of attack to zero. The switch occurs at a point at which 95% of the first stage flight is completed. At staging, the commanded pitch attitude is switched back from the flight path angle to the modified reference pitch attitude.

Figures 7.14 through 7.26 show the resulting feedback trajectory with the angle of attack constraint imposed along with the point mass model trajectory shown for reference.

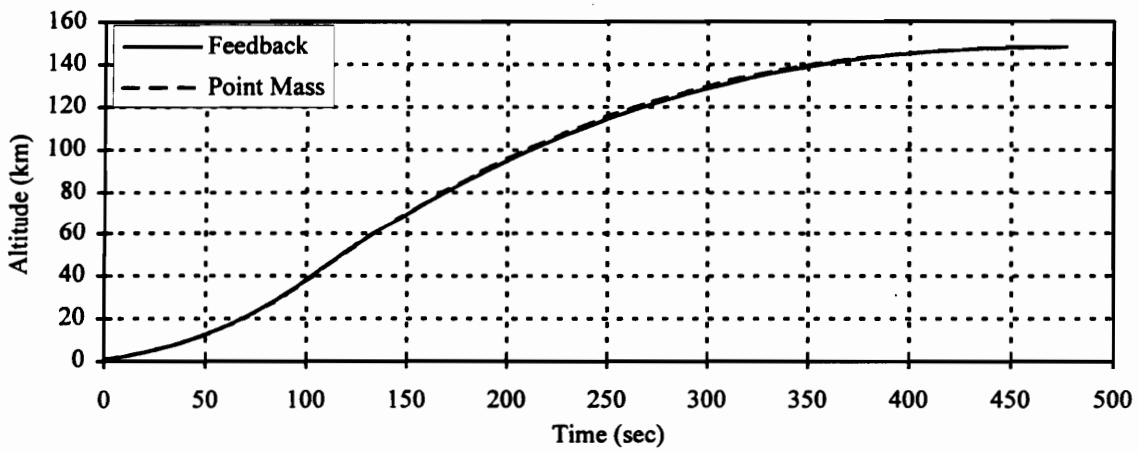

Figure 7.14: Altitude Comparison between Feedback Trajectory with Alpha Constraint and Point Mass Reference Trajectory

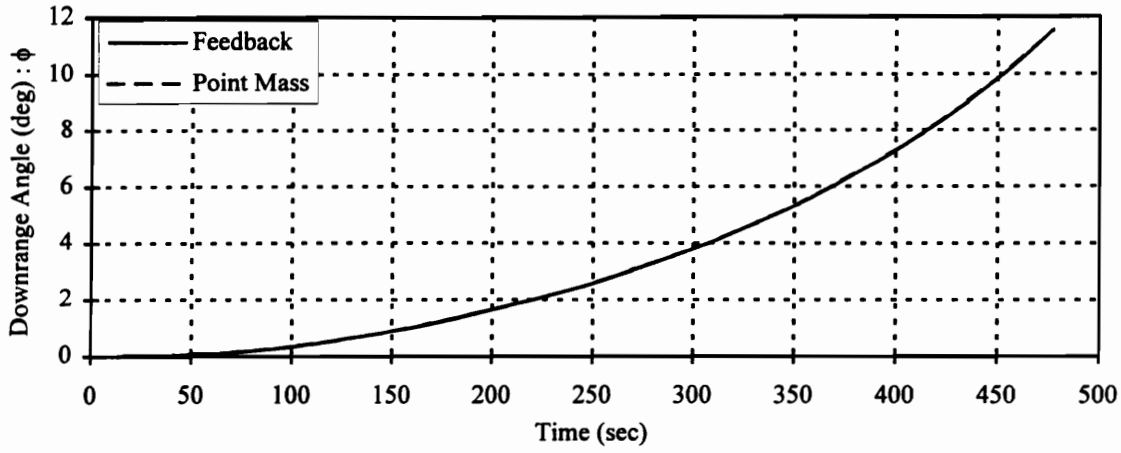

Figure 7.15: Downrange Angle Comparison between Feedback Trajectory with Alpha Constraint and Point Mass Reference Trajectory

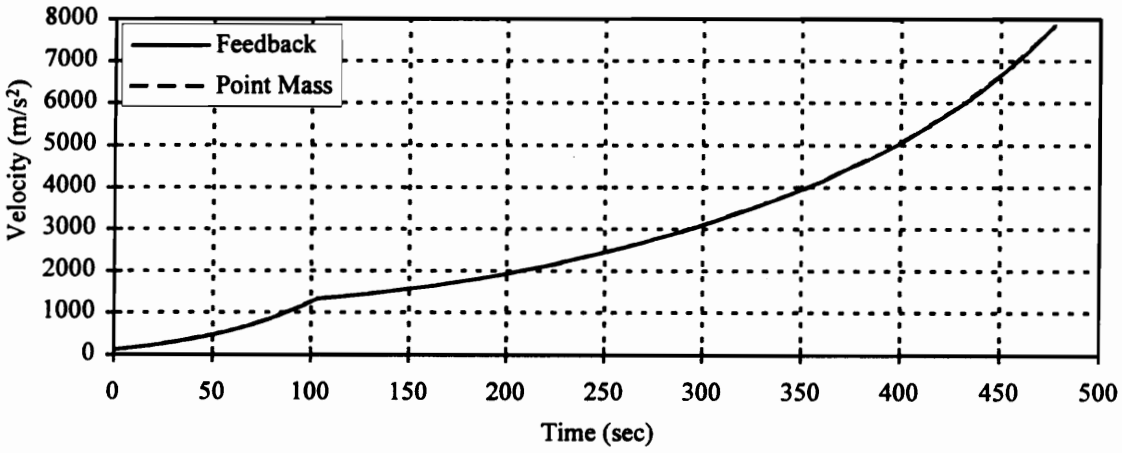

Figure 7.16: Velocity Comparison between Feedback Trajectory with Alpha Constraint and Point Mass Reference Trajectory

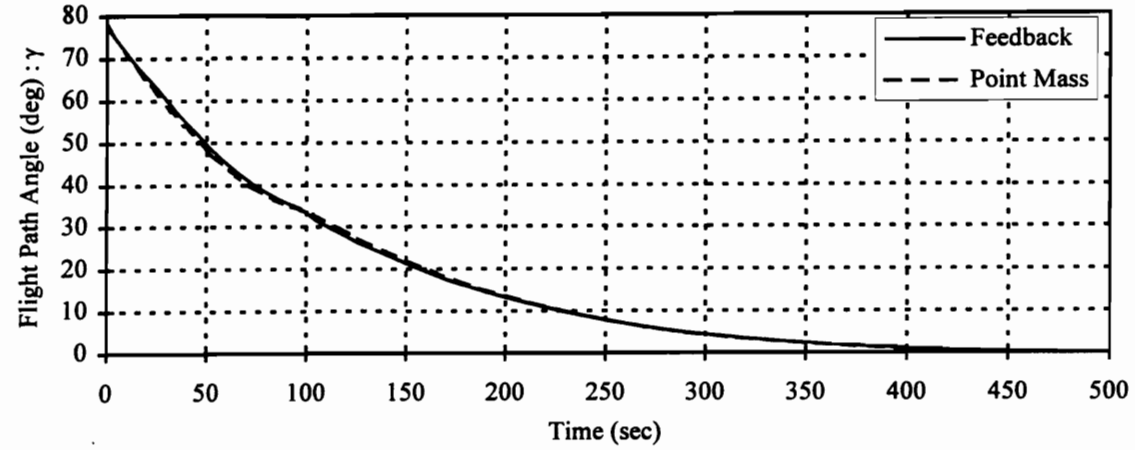

Figure 7.17: Flight Path Angle Comparison between Feedback Trajectory with Alpha Constraint and Point Mass Reference Trajectory

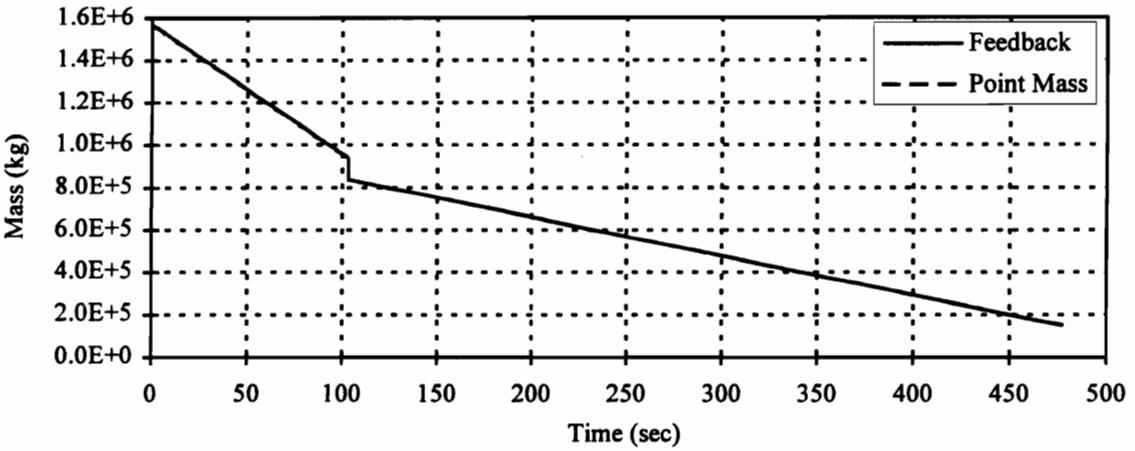

Figure 7.18: Mass Comparison between Feedback Trajectory with Alpha Constraint and Point Mass Reference Trajectory

The effects of modeling the angle of attack constraint can be clearly seen in Figure 7.19 which shows the pitch orientation of the vehicle. It can be seen where the pitch attitude tracks the flight path angle just before staging.

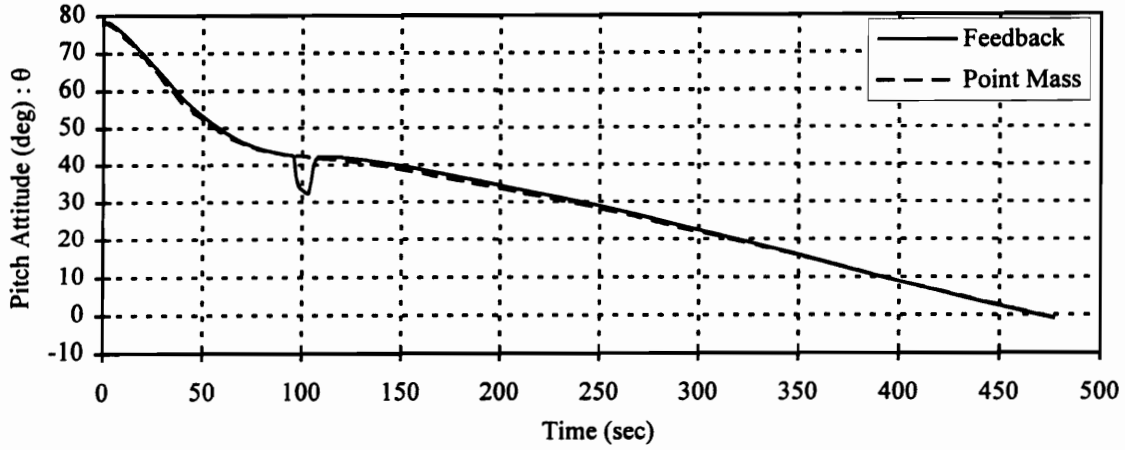

Figure 7.19: Pitch Attitude Comparison between Feedback Trajectory with Alpha Constraint and Point Mass Reference Trajectory

Figures 7.20 and 7.21 show the fast dynamics that occur near staging. The achieved pitch rate just before and after staging is close to an order of magnitude greater than that present elsewhere in the trajectory. These fast pitch dynamics are lost in the point mass model. The gimbal angle deflections are also much greater near staging. This type of information could be of great importance in estimating loads experienced by the vehicle.

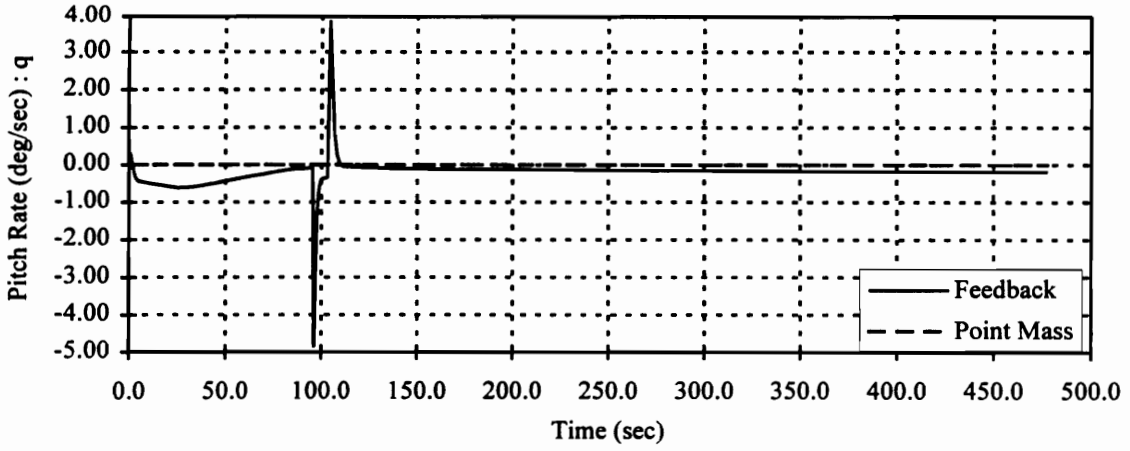

Figure 7.20: Pitch Rate Comparison between Feedback Trajectory with Alpha Constraint and Point Mass Reference Trajectory

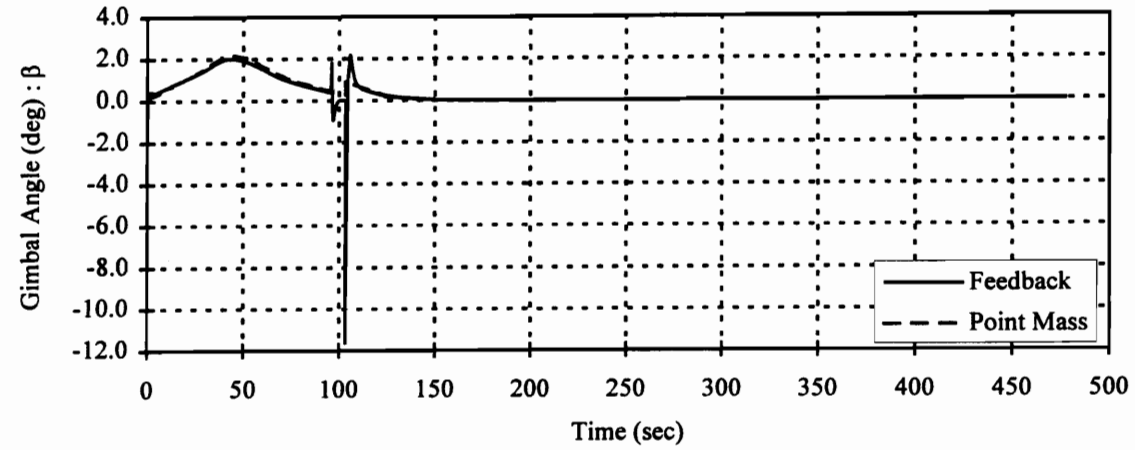

Figure 7.21: Gimbal Angle Comparison between Feedback Trajectory with Alpha Constraint and Point Mass Reference Trajectory

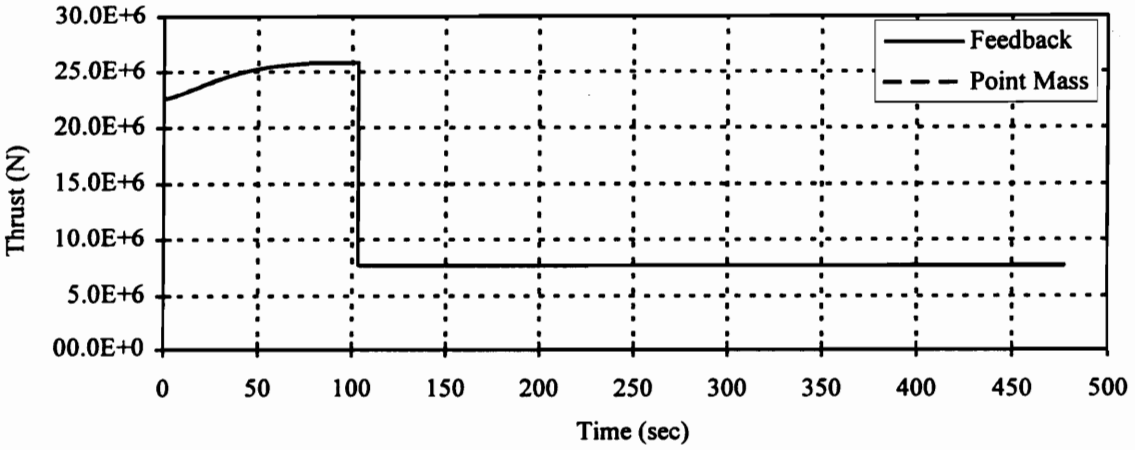

Figure 7.22: Thrust Comparison between Feedback Trajectory with Alpha Constraint and Point Mass Reference Trajectory

The angle of attack plot, Figure 7.23, clearly shows the effect of the angle of attack constraint. At staging the angle of attack has been driven to zero. It can also be seen how the angle of attack is greater than that of the point mass model for a period after staging. During this portion of flight the vehicle is generating more lift than in the point mass

model in order to increase the flight path angle and hence altitude rate in an attempt to "close in" on the point mass model altitude profile.

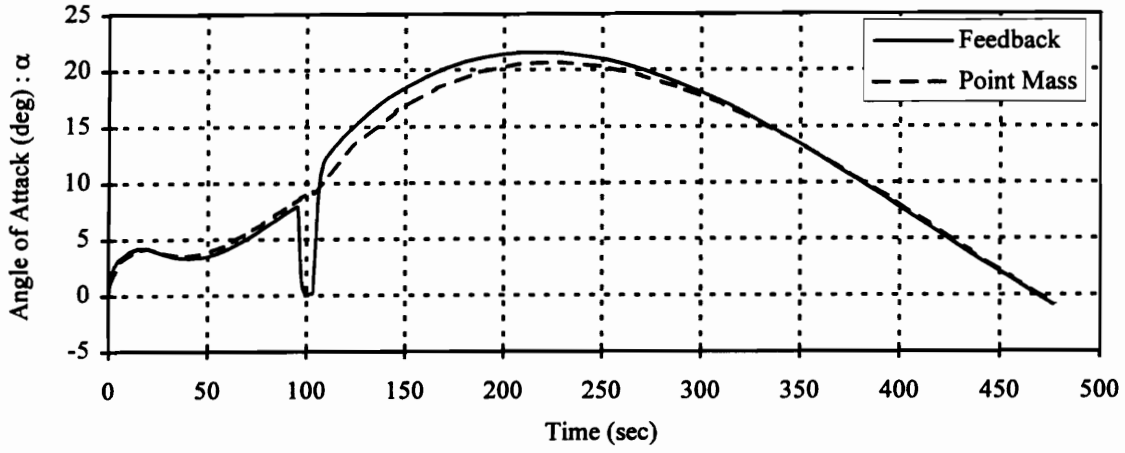

Figure 7.23: Angle of Attack Comparison between Feedback Trajectory with Alpha Constraint and Point Mass Reference Trajectory

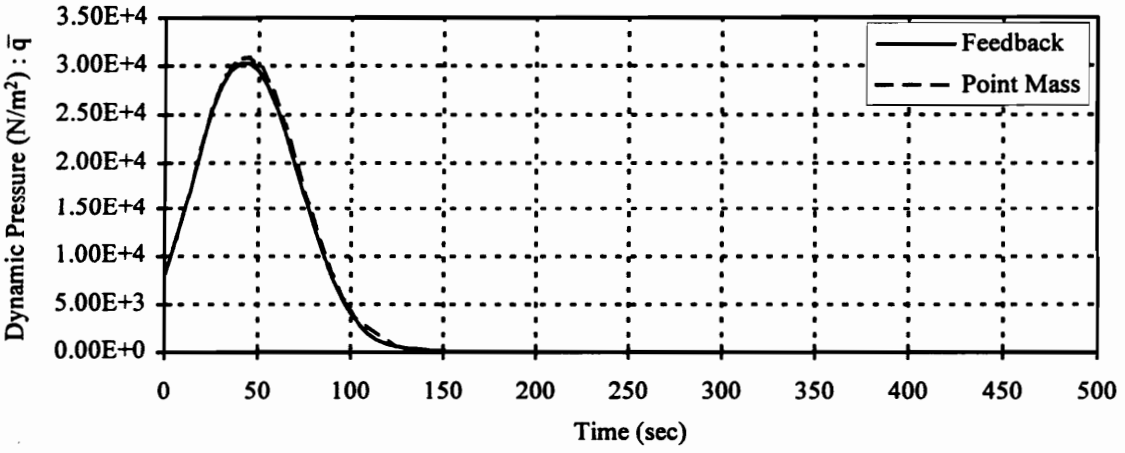

Figure 7.24: Dynamic Pressure Comparison between Feedback Trajectory with Alpha Constraint and Point Mass Reference Trajectory

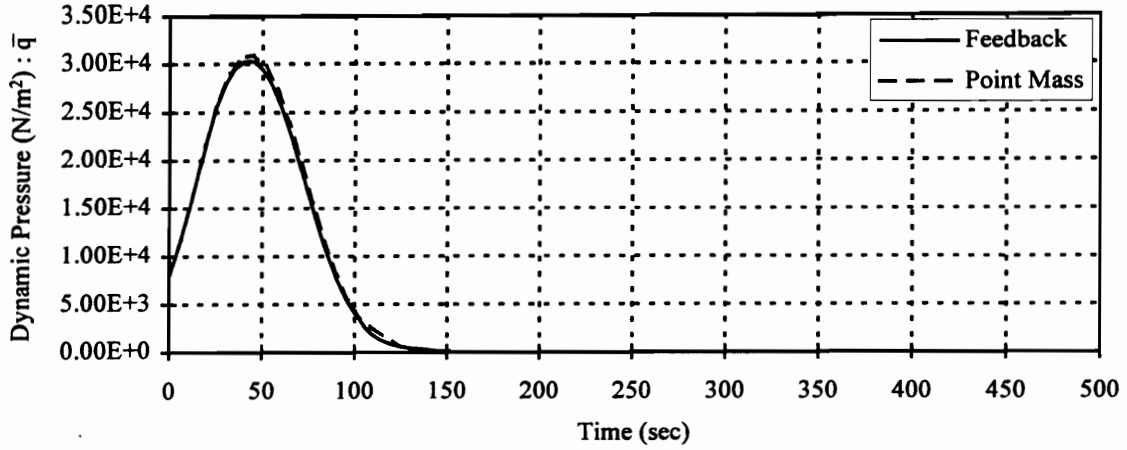

Figure 7.25: Semi-Major Axis Comparison between Feedback Trajectory with Alpha Constraint and Point Mass Reference Trajectory

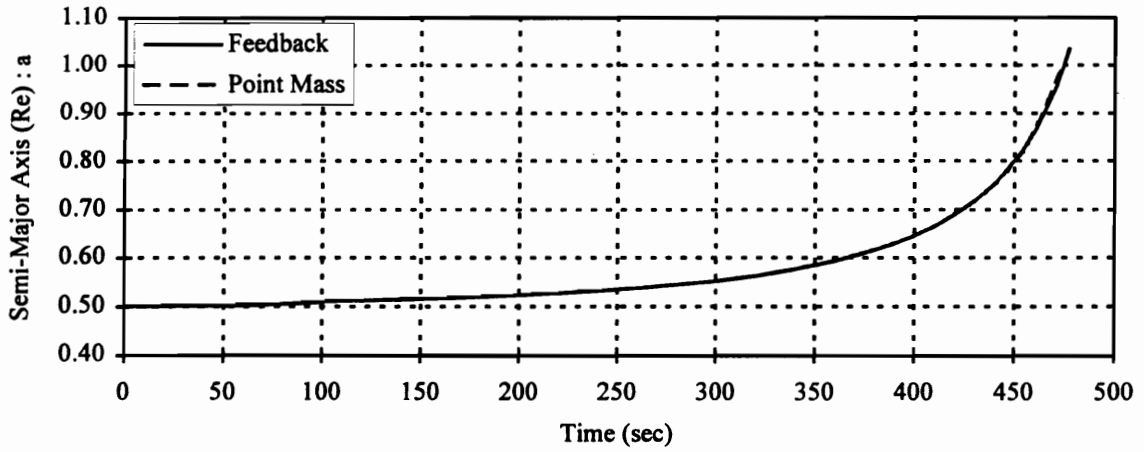

Figure 7.26: Orbit Eccentricity Comparison between Feedback Trajectory with Alpha Constraint and Point Mass Reference Trajectory

Table 7.3 shows the terminal conditions of the feedback trajectories both with and without the angle of attack constraint modeled. As can be seen there is not a large difference in the terminal condition of the two trajectories.

Table 7.3 :

	$a(t_f)$ (Re)	$e(t_f)$	Perigee (km)	Apogee (km)	$m(t_f)$ (kg)	t_f (sec)
Without α constraint	1.0334	0.98498×10^{-2}	148.069	277.908	0.14988×10^{6}	477.22
With α constraint	1.0334	0.98994×10^{-2}	147.742	278.235	0.14972×10^{6}	477.31

7.5 Variations in the Singular Perturbation Parameter

The next step is to vary the singular perturbation parameter ε. Since this parameter was based on physical parameters, it will be varied in a physically meaningful manner. Recall from Chapter 3 that;

$$\varepsilon = \sqrt{\frac{I_{yy_{ref}}}{M_{ref}}} \Big/ \sqrt{\frac{Re}{g_0}}.$$

The pitch moment of inertia will be used to vary ε since this has a physical significance to the vehicle and has a large impact on the pitch dynamics. Two variations in the moment of inertia were used. First the moment of inertia was decreased by a factor of 10. This has the effect of decreasing ε by a factor of $\sqrt{10}$. Next the moment of inertia was increased by a factor of 10 which increased ε by a factor of $\sqrt{10}$. The two additional feedback trajectories were then run and the results are shown in Figures 7.27 through 7.32. Only the plots of variables that showed distinguishable differences have been included.

Figure 7.27 shows the altitude history of the three different feedback trajectories along with the point mass model. It can be seen that the altitude for both the baseline ε value, ε_b, and the reduced ε value are below the altitude of the point mass model. This

difference in altitude is due to the reduction of angle of attack near staging that results in a lower trajectory. However, with the higher ε value, the vehicle is slow to respond to the staging condition and does not reach a zero angle of attack, as seen in Figure 7.32. This slow response in combination with the tracking error previously discussed results in an altitude profile that is above that of the point mass model.

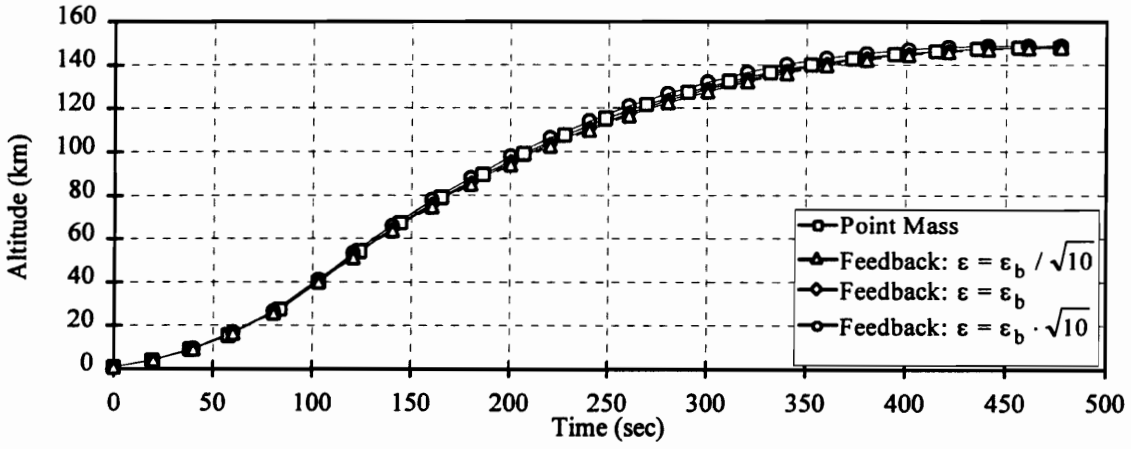

Figure 7.27: Altitude History with Variations in the Singular Perturbation Parameter

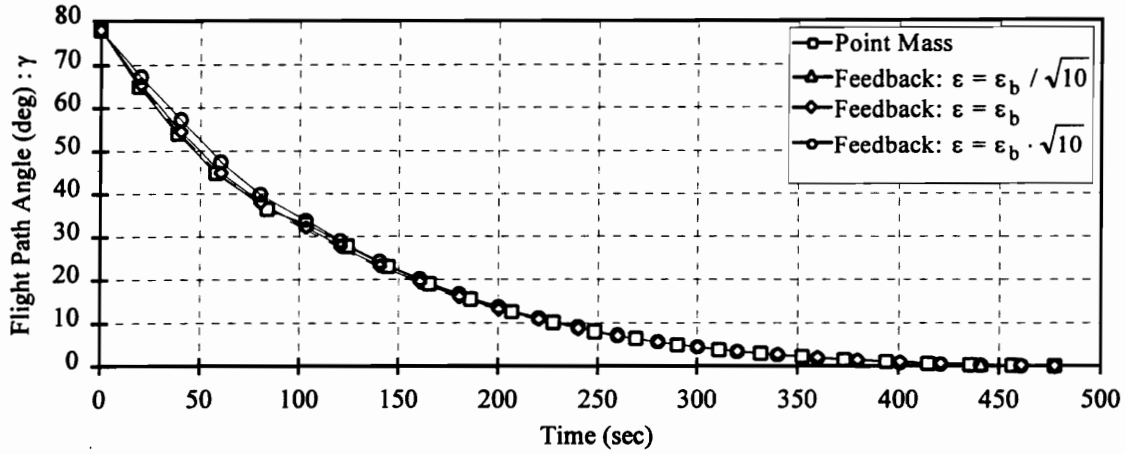

Figure 7.28: Flight Path Angle History with Variations in the Singular Perturbation Parameter

The differences in the pitch attitude can be seen in Figure 7.29. As expected the vehicle with the lowest pitch moment of inertia has the fastest dynamics. It can also be seen in conjunction with the angle of attack profile in Figure 7.32 that the vehicles with the lower moment of inertia values are more successful at meeting the angle of attack constraint at staging.

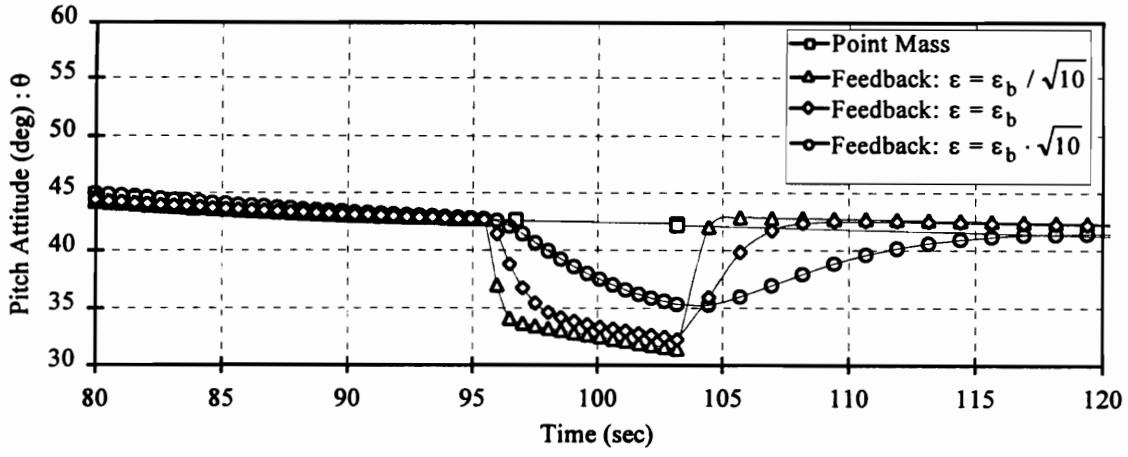

Figure 7.29: Pitch Attitude History with Variations in the Singular Perturbation Parameter

In Figure 7.30 the pitch rate can be seen. As expected the vehicles with the lower moment of inertia values are able to achieve the higher pitch rates.

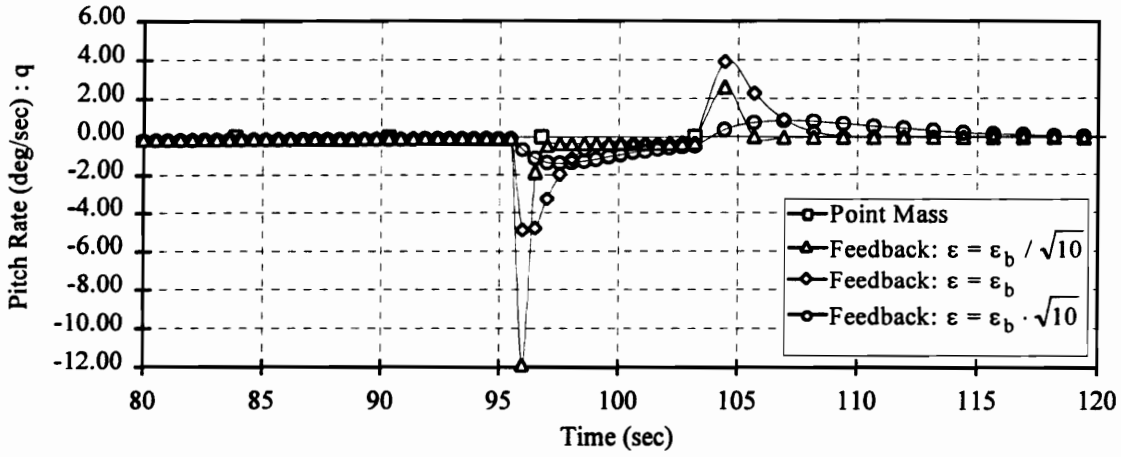

Figure 7.30: Pitch Rate History with Variations in the Singular Perturbation Parameter

Figure 7.31 shows the gimbal angle history of the different trajectories. As expected, it can be seen that the vehicle with the largest pitch moment of inertia requires the longest duration of gimbal deflection to impose a pitch rate on the vehicle. Note that the gimbal angle is discontinuous at staging.

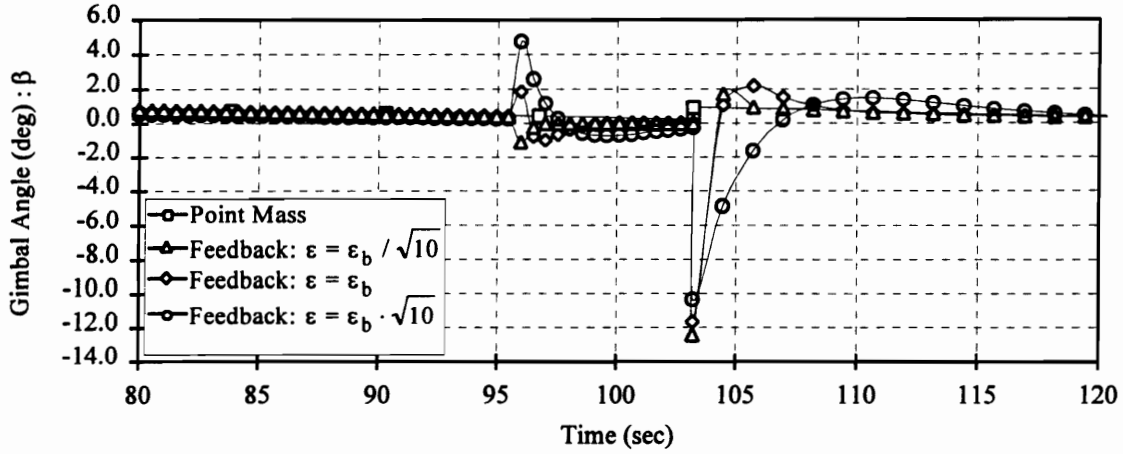

Figure 7.31: Gimbal Angle History with Variations in the Singular Perturbation Parameter

The angle of attack histories can be seen in Figures 7.32. This figure best illustrates the differences in the variations in the singular perturbation parameter ε. As can be seen the vehicle with the lowest moment of inertia responds the fastest to the implementation of the angle of attack constraint while the vehicle with the largest moment of inertia responds sluggishly as compared with the other ε values. Note that the vehicle with the smallest moment of inertia is able to meet the angle of attack constraint the best.

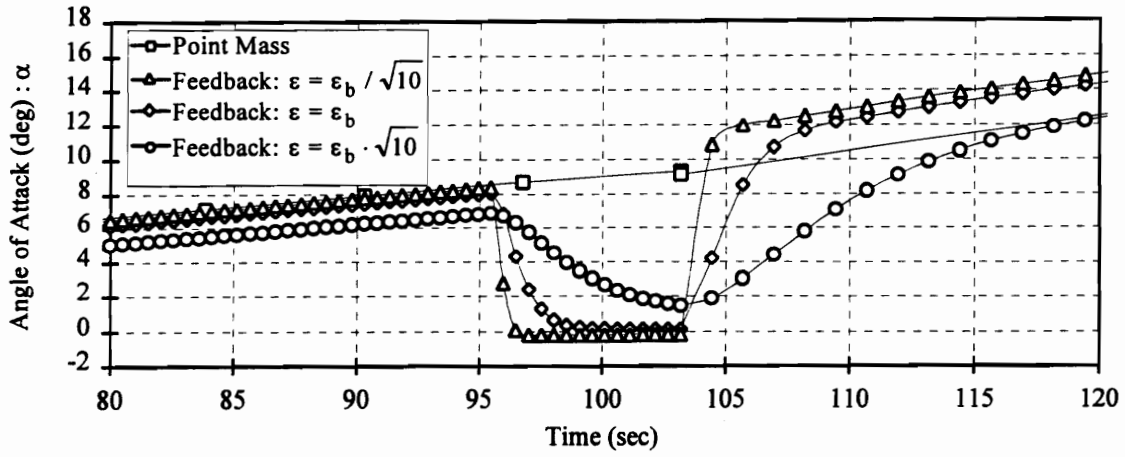

Figure 7.32: Angle of Attack History with Variations in the Singular Perturbation Parameter

Tables 7.4 shows the terminal conditions achieved by the different values of the singular perturbation parameter ε. Note that there are not large differences in the terminal conditions between the different values of ε.

Table 7.4 :

	$a(t_f)$ (Re)	$e(t_f)$	Perigee (km)	Apogee (km)	$m(t_f)$ (kg)	t_f (sec)
$\varepsilon_b / \sqrt{10}$	1.0334	0.99374×10^{-2}	147.492	278.484	0.14971×10^{6}	477.32
ε_b	1.0334	0.98994×10^{-2}	147.742	278.235	0.14972×10^{6}	477.31
$\varepsilon_b \times \sqrt{10}$	1.0334	0.99058×10^{-2}	147.700	278.276	0.14965×10^{6}	477.35

8.0 CONCLUSION

It has been shown that Singular Perturbation Theory and Neighboring Optimal Control provide a means to extend the generally used point mass model to include the pitch dynamics of the vehicle. By including the pitch dynamics a new reference trajectory can be obtained which will be closer to the full order problem by including the effects of constraints involving the orientation of the vehicle. This new reference trajectory can be used as a baseline for performance studies.

It has also been shown that the system equations can be normalized in a manner such that the singular perturbation parameter, ε, evolves naturally in the problem. By letting ε evolve naturally in the normalization, the locations of ε in the differential equations also occurred naturally and did not need to be selected in an ad hoc manner.

As seen in the trajectory comparisons the feedback trajectory has problems tracking the point mass trajectory due to its zero pitch rate with changing pitch orientation. Alleviating this problem would provide a better feedback model and is recommended as an area for future research. This may be accomplished by an alternate formulation of the state variables that describe the pitch dynamics or a higher order expansion of the singular perturbation parameter.

REFERENCES

1. Seywald, H., Cliff, E.M., "Goddard Problem in Presence of a Dynamic Pressure Limit", *Jounal of Guidance, Control, and Dynamics*, Vol. 16, No. 4, July-August 1993, pp.776-781.

2. Tsien, H.S., and Evans, R.C., "Optimal Thrust Programming for a Sounding Rocket", *Journal of American Rocket Society*, Vol. 21, No 5, 1951.

3. Tsiotras, P., Kelley, H.J., "Goddard Problem with Constrained Time of Flight", *Journal of Guidance, Control, and Dynamics*, Vol. 15, No. 2,1992, pp. 289-296.

4. Hibbs, A.R., "Optimum Burning Program for Horizontal Flight", *American Rocket Society*, July-August 1952, pp. 204-212.

5. Cicala, P., Miele, A., "Generalized Theory of the Optimum Thrust Programming for the Level Flight of a Rocket-Powered Aircraft", *Jet Propulsion*, June 1956, pp. 443-469.

6. Bryson, A.E., Ross, S.E., "Optimum Rocket Trajectories With Aerodynamics Drag", *Jet Propulsion*, July 1958.

7. Bryson, A.E., Ho, Y.C., *Applied Optimal Control*, Hemisphere Publishing Corporation, Washington D.C., 1975

8. Cliff, E.M., "A Singular Perturbation Approach to Pitch-Loop Design", *Proceedings of the American Automatic Control Conference*, San Diego, CA, May 1990, pp. 1819-1823..

9. Bushong, P.M., *A Multi-Loop Guidance Scheme using Singular Perturbation and Linear Quadratic Regulator Techniques Simultaneously*, (Ph.D. dissertation, Virginia Polytechnic Institute and State University, 1991.)

10. Pamadi, B., Spacecraft Control Branch, NASA Langley Research Center, Hampton, VA, (Fax communication to E.M. Cliff)

11. Seywald, H., Cliff, E.M., "A Feedback Control for the Advanced Launch System", *Proceedings of the 1991 Guidance, Navigation, and Control Conference.* AIAA 1991.

12. Bless, R., Seywald, H., Cliff, E.M., "Hodograph Analysis in Aircraft Trajectory Optimization", *Proceedings of the AIAA Guidance, Navigation, and Control Conference.* 1993 (AIAA Paper 93-3742).

13. Kelley, H.J., "Aircraft Maneuver Optimization by Reduced-Order Approximation", *Control and Dynamic Systems*, Leondes, C.T. (ed.), Volume 10, Academic Press, New York, 1973, pp. 131-177.

14. O'Malley, R.E. Jr., *Singular Perturbation Methods for Ordinary Differential Equations*, Springer-Verlag, New York, 1991.

15. Ardema, M.D., "An Introduction to Singular Perturbations", *Singular Perturbations in Systems and Control*, Springer-Verlag, New York, 1983.

16. Pierre, D.A., *Optimization Theory with Applications*, Dover Publications, New York, 1969.

17. Hartman, R.D., *Optimal Maneuver Guidance with Sensor Line of Sight Constraint*, (Ph.D. dissertation, Virginia Polytechnic Institute and State University, 1992.)

18. Kelley, H.J., "Guidance Theory and Extremal Fields", *IRE Transactions on Automatic Control*, October 1962, pp. 75-82.

19. Bate, R.R., Mueller, D.D., White, J.E., *Fundamentals of Astrodynamics*, Dover Publications, New York, 1971.

20. Gill, P.E., Murray, W., Wright, M.H., *Practical Optimization*, Academic Press, San Diego, CA., 1989.

21. Ewing, G.E., *Calculus of Variations with Applications*, Dover Publications, New York, 1985.

22. Kelley, H.J., "An Optimal Guidance Approximation Theory", *IEEE Transactions on Automatic Control*, Volume AC-9, Number 4, October 1964, pp. 288-293.

23. Lu, P., "Trajectory Optimization and Guidance for an Advanced Launch Vehicle", January 1992, (AIAA Paper 93-0732).

24. Lu, P. "Nonlinear Trajectory Tracking Guidance with Application to a Launch Vehicle", *Journal of Guidance, Control, and Dynamics*, Vol. 19, No. 1, January-February 1996, pp. 99-106.

25. Seywald, H., Cliff, E.M., "Neighboring Optimal Control Based Feedback Law for the Advanced Launch System", *Journal of Guidance, Control, and Dynamics*, Vol. 17, No. 6, November-December 1994, pp. 1154-1162.

26. Feeley, T. S., Speyer, J.L., "Techniques for Developing Approximate Optimal Advanced Launch System Guidance", *Journal of Guidance, Control, and Dynamics*, Vol. 17, No. 5, September-October 1994, pp. 889-896.

27. Calise, A.J., "On the Use of Singular Perturbation Methods in the Solution of Variational Problems", *Proceedings of Joint Automatic Control Conference*, June 1973, pp. 184-192.

28. Tsiotras, P., Kelley, H.J., "Drag Law Effects in the Goddard Problem", IFAC Optimization Workshop, Tblisi, Georgia, USSR, June 21-25, 1988.

APPENDIX A - DESCRIPTION OF SIMULATION MODELS

Appendix A will give details on the atmospheric, aerodynamic, and propulsive models used in the numerical simulations. These models are intended to provide a realistic representation of the real world yet be simple to implement. The atmospheric and propulsion models are believed to be identical to those used by Seywald[11], while the aerodynamic models have been modified in order to provide a smooth surface fit to the data. The purpose of presenting these numerical models is to enable others to compare results is so desired.

Atmospheric Models

The modeling of the atmosphere is comprised of three components; a speed of sound model, a density model, and an atmospheric pressure calculation.

Speed of Sound

The speed that sound will travel through the atmosphere is given by a sixth order polynomial with altitude as the independent variable. The result is used to calculate the vehicle Mach number which feeds into the calculation of the aerodynamic coefficients. The speed of sound, a, is given by Equation A.1 where h is the vehicle altitude in kilometers, a is the resulting speed of sound in meters/second, and the polynomial coefficients are given in Table A-1.

$$\mathrm{a} = a_0\left(c_0 + c_1 \cdot \mathrm{h} + c_2 \cdot \mathrm{h}^2 + c_3 \cdot \mathrm{h}^3 + c_4 \cdot \mathrm{h}^4 + c_5 \cdot \mathrm{h}^5 + c_6 \cdot \mathrm{h}^6\right) \qquad \text{(A.1)}$$

Table A-1: Speed of Sound Polynomial Coefficients

Coefficient	Value
a_0	$0.3329494352 \times 10^{3}$
c_0	$0.102207711387 \times 10^{1}$
c_1	$-0.262500934305 \times 10^{-1}$
c_2	$0.142474099963 \times 10^{-2}$
c_3	$-0.298404907679 \times 10^{-4}$
c_4	$0.274897035390 \times 10^{-6}$
c_5	$-0.109152741878 \times 10^{-8}$
c_6	$0.147617851753 \times 10^{-11}$

The calculated speed of sound for altitudes up to 160 kilometers is shown in Figure A-1.

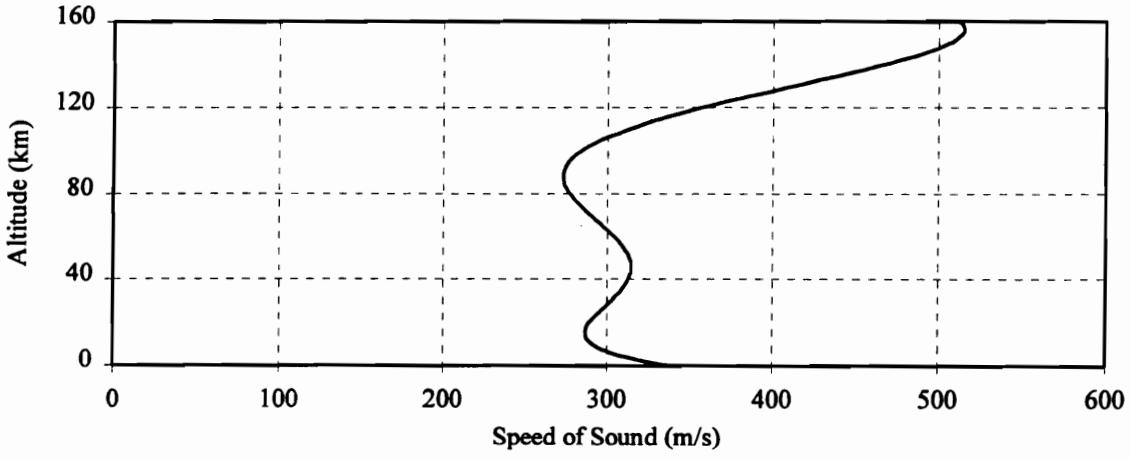

Figure A-1: Modeled Speed of Sound Profile

Atmospheric Density

The density of the atmosphere is modeled as a function of altitude. Equation A-2 gives the density, ρ, in kg/m^3 where h is in kilometers and the coefficients are given in Table A-2. A plot of the calculated density up to altitudes of forty kilometers is shown in Figure A.2.

$$\rho = b_3 \cdot e^{\alpha_1}$$
$$\text{where } \alpha_1 = -b_1 - b_2 h + b_1 \cdot e^{\alpha_2} \qquad \text{(A.2)}$$
$$\text{and } \alpha_2 = -\left(a_1 h + a_2 h^2 + a_3 h^3 + a_4 h^4\right)$$

Table A-2: Density Function Coefficients

Coefficient	Value
a_1	-3.48643241 x 10^{-2}
a_2	3.50991865 x 10^{-3}
a_3	-8.33000535 x 10^{-5}
a_4	1.15219733 x 10^{-6}
b_1	1.02280550
b_2	0.12122693
b_3	1.22500000

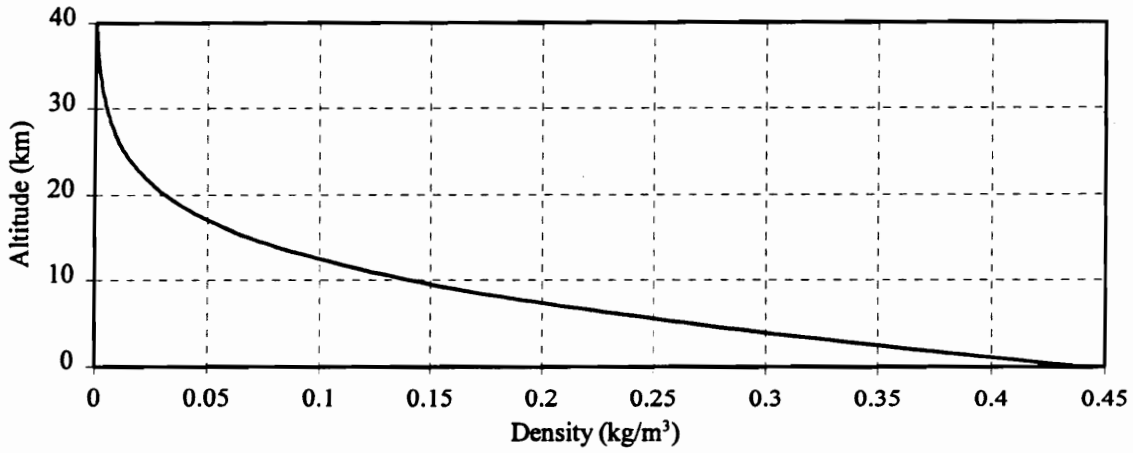

Figure A-2: Modeled Density Profile

Atmospheric Pressure

The atmospheric pressure is calculated based on the relation for an ideal gas

$$p = \frac{\rho \cdot a^2}{\gamma}$$

where the density, ρ, and speed of sound, a, are calculated as previously discussed. The variable γ is the ratio of specific heats and is modeled with a constant value of 1.4.

where the density, ρ, and speed of sound, a, are calculated as previously discussed. The variable γ is the ratio of specific heats and is modeled with a constant value of 1.4.

Aerodynamic Models

The aerodynamic models necessary for the problem discussed are lift, drag, and pitching moment models. The value of dynamic pressure, $\bar{q}$, used by the models is calculated by the expression $\bar{q} = \frac{1}{2}\rho V^2$.

The density, ρ, is given by the atmospheric model and V is the vehicle total velocity. Also required are the aerodynamic reference area, S, and reference length, $\bar{c}$.

$$S = 131.306369 \text{ m}^2$$

$$\bar{c} = 84.205877 \text{ m}$$

The reference area S represents the total base area of the vehicle core and booster, while the reference length represents the total length of the core vehicle.

The non-dimensional lift coefficient (C_L), drag coefficient (C_D), an pitching moment coefficient (C_M) are functions of the vehicle Mach number, M, and angle of attack, α, As a result of the need to have smooth derivatives of the aerodynamic forces and moments with respect to the states and controls, the tabular data available on the ALS vehicle was functionally surface fit in order to obtain differentiable expressions for the aerodynamics in terms of M and α. The following subsections outline the calculation of the lift, drag, and pitching moment on the vehicle.

In an actual vehicle the aerodynamic coefficients can change significantly at staging. However, this change is not modeled in this study. In order to keep the model simple the lift and pitching moment coefficient models are the same for stage one and stage two of the vehicle. The drag coefficient model is changed such that the calculated drag coefficient for stage two is one half that of stage one at the same Mach number and angle

of attack. This simplification should have negligible effect on the results since the aerodynamic forces and moments drop significantly due to the low dynamic pressure in this region of flight. In addition, the purpose of this work is not to obtain a specific trajectory for this vehicle but to show the techniques and effects of using a singular perturbation model to include the pitch dynamics in the vehicle model.

Lift

The vehicle lift is given by Equation A.4 where α is expressed in radians and the function coefficients are given in Table A-3.

$$L = \bar{q} \cdot S \cdot C_L(\mathrm{M},\alpha) \tag{A.4}$$

$$C_L = (L_0 + L_1 \cdot \mathrm{M}) \cdot \alpha$$

The surface fit for the lift coefficient C_L is shown in Figure A-3. Note that in the figure α is shown in units of degrees.

Table A-3: C_L Function Coefficients

Coefficient	Value
L_0	0.043
L_1	1.625×10^{-3}

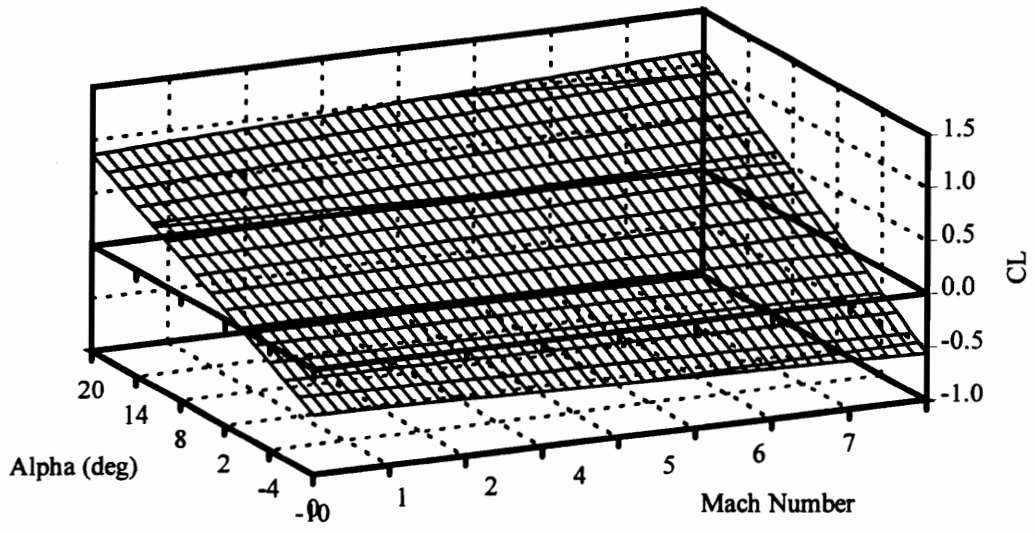

Figure A-3: Lift Coefficient

Drag

The vehicle drag is given by Equation A.5 where α is expressed in radians and the function coefficients are tabulated in Table A-4.

$$D = \bar{q}(\rho, V) \cdot S \cdot C_D(M, \alpha) \tag{A.5}$$

$$C_D = C_{D0}(M) + k(M) \cdot (\alpha \cdot \tfrac{180}{\pi})^2$$

$$C_{D_0} = D_0 + \left(D_1 + D_2 \cdot \tan^{-1}\left(D_3 \cdot (M - D_4)\right)\right) \cdot \left(1 + D_5 \cdot e^{\left(D_6 \cdot (M - D_7)^2\right)}\right)$$

$$k = k_1 \cdot M + k_2$$

The complication in the C_{D_0} expression is a result of the usual drag behavior near Mach=1. The surface fit for the drag coefficient C_D is shown in Figure A-4. Note that in the figure α is shown in units of degrees.

Table A-4: C_D Function Coefficients

Coefficient	Value
D_0	0.160
D_1	0.215
D_2	0.129
D_3	10.00
D_4	0.850
D_5	0.814
D_6	-0.800
D_7	0.750
k_1	-3.125×10^{-5}
k_2	1.300×10^{-3}

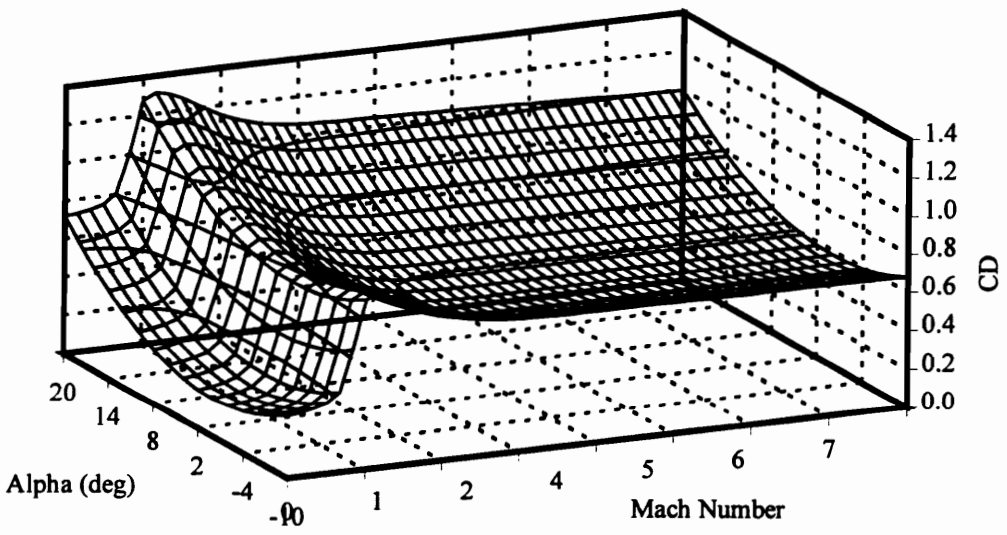

Figure A-4: Drag Coefficient

Pitching Moment

The vehicle pitching moment is given by Equation A.6 where α is expressed in radians and the function coefficients are tabulated in Table A-5.

$$M = \bar{q}(\rho, V) \cdot S \cdot \bar{c} \cdot C_M(M, \alpha) \tag{A.6}$$

$$C_M = C_{M_1}(\mathrm{M},\alpha) + C_{M_2}(\mathrm{M},\alpha)$$

$$C_{M_1} = L_1 \cdot \mathrm{M} \cdot (\alpha \cdot \tfrac{180}{\pi}) + L_2 \cdot (\alpha \cdot \tfrac{180}{\pi}) + L_3 \cdot \mathrm{M} + L_4$$

$$C_{M_2} = (E_1 \cdot (\alpha \cdot \tfrac{180}{\pi}) + E_2) \cdot \mathrm{e}^{-\left[\frac{(\mathrm{M}-M_0)\frac{1}{\pi}\left(M_1 - \tan^{-1}(M_2 \cdot (\mathrm{M}-M_0))\right)}{\omega_n}\right]}$$

The surface fit for the pitching moment coefficient C_M is shown in Figure A-5. Note that in the figure α is shown in units of degrees. Again the complication in C_{M_2} arises from the transonic behavior.

Table A-5: C_M Function Coefficients

Coefficient	Value
L_1	-0.27101094838599 x 10^{-3}
L_2	0.11682570862606 x 10^{-1}
L_3	0.16851032948609 x 10^{-2}
L_4	0.35751730216124 x 10^{-2}
M_0	1.3713067220255
M_1	1.5
M_2	0.1 x 10^{7}
E_1	0.31816920579938 x 10^{-2}
E_2	0.35019268019610 x 10^{-1}
ω_n	0.84593773937827

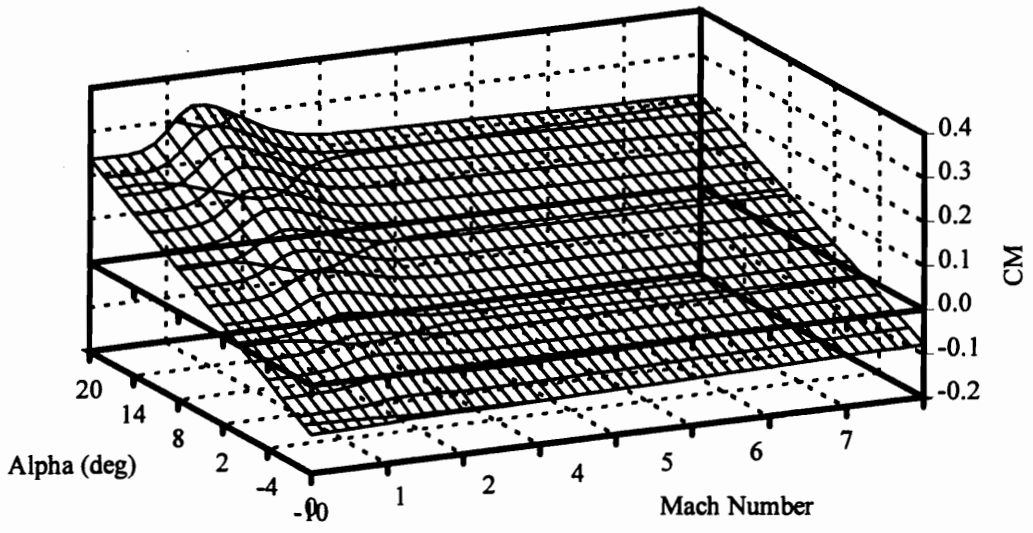

Figure A-5: Pitch Moment Coefficient

Propulsion Model

The vehicle modeled has ten engines during the first stage of flight with three engines continuing through the second stage. All engines are modeled identically with the thrust generated given by Equation A.7.

$$T = T_{vac} - p \cdot A \tag{A.7}$$

The vacuum-thrust, T_{vac} is modeled as a constant, T_{vac} = 2,585,879 Newtons and the atmospheric pressure, p, is calculated as previously discussed. The engine exit plane area, A = 3.751467368 square meters.

VITA

William Michael Waldron was born on December 30, 1964 in Nashville, Tennessee and graduated from Warren County High School, Front Royal, Virginia in 1983. As an undergraduate, he studied Aerospace and Ocean Engineering at Virginia Polytechnic Institute and State University receiving his Bachelor of Science Degree in 1987. He was employed in private industry as an aerospace engineer until 1990 when he returned to Virginia Polytechnic Institute and State University to continue his education. In 1993, he completed his course work and returned to private industry while continuing his research studies. He was married to Betty Jo Thompson in 1992 and has one child, Emily Rachel Waldron.